Hydrodynamics and sediment transport in the Duwamish River Estuary

Margaret A. McKeon

A dissertation

submitted in partial fulfillment of the

requirements for the degree of

Doctor of Philosophy

University of Washington

2020

Reading Committee:

Alexander Horner-Devine, Chair

Sarah Giddings

Jim Thomson

Program Authorized to Offer Degree:

Civil and Environmental Engineering

University of Washington

Abstract

Hydrodynamics and sediment transport in the Duwamish River Estuary

Margaret A. McKeon

Chair of the Supervisory Committee:
Professor Alexander Horner-Devine
Civil and Environmental Engineering

Nearly two-thirds of the world's major cities have been built around estuaries. As populations have grown, many estuaries have been modified, impacting their hydrodynamic regime. Urbanized estuaries, which are typically among the most highly modified, are also often contaminated due to the proximity of intense industrial activity, motivating the need to better understand their hydrodynamic and transport processes in order to better inform current management and future modifications. This study focuses on hydrodynamics and sediment transport in the Duwamish River estuary, a highly engineered and contaminated tidal salt wedge estuary located next to downtown Seattle, WA.

Hydrographic measurements of salt wedge structure and dynamics spanning a 20-fold range of river discharges are used to investigate the seasonal variability in the strongly stratified Duwamish River estuary. The effect of river discharge on salt wedge length, stratification, pycnocline thickness, and intratidal differences in salinity structure are evaluated. The salt wedge decreases in length and becomes more stratified as river discharge increases. The ebb and flood responses to increasing discharge are markedly different; the flood phase structure shows little seasonal

dependence, while the ebb structure changes due to an internal hydraulic response that is strongest at two severe lateral constrictions. This response varies with the net barotropic forcing, which is controlled by river discharge. The asymmetry between the flood and ebb structure is explained using a two-layer hydraulic framework, although spatially, tidally, and seasonally variable vertical mixing also modifies the structure. As a result of the persistent stratification and dominance of hydraulic dynamics, channel constrictions influence circulation and transport during ebb tides. These dynamics also generate a flood/ebb asymmetry in salt wedge structure and circulation that is modulated seasonally through discharge. We hypothesize that these dynamics lead to a seasonally modulated residual circulation.

In 2001 the lower Duwamish Estuary was added to the national list of Superfund Sites. A Record of Decision was issued in 2014 recommending a $342 million remedial plan for the remaining 412 ac, 57% (235 ac) of which relies on the burial of contaminated sediment by cleaner sediment originating from upstream. We re-examine existing total suspended sediment load data to understand the magnitude and timing of suspended sediment delivery to the estuary. We use three existing datasets, with data ranging from 1966 to 2019, and develop new rating curves using a piecewise approach. The new rating curves have improved R^2 values compared with previous attempts. A combined-fit rating curve accurately estimates 1960s and 2010s annual loads, whereas no single rating curve generated here or previously is appropriate for the entire period from 1961 to present. Using the combined-fit, we find that most of the $11.7 \pm 4.8 \times 10^4$ mt/year long term mean annual load occurs from November-May during high discharge events. There is evidence that modern annual load estimates may be closer to $9.4 \pm 4.4 \times 10^4$ mt/year, down from a 1960s annual load of $16.2 \pm 5.5 \times 10^4$ mt/year. Estimates of fine and coarse loads derived from modern data indicate that 70% of the average annual total load is composed of fine sediment.

We present new measurements of SSC throughout the estuary from 2011-2013 in the form of transects and bottom-mounted moorings, which we use to investigate sediment sources in the estuary, transport pathways, the role of local resuspension, and relevant timescales. Upstream sediment is delivered to the estuary in only a handful of storm events that last on the order of days. Gravitational settling transfers upstream sediment to the salt wedge during loading events. As the salt wedge retreats during ebb, retained material is resuspended and re-entrained into the upper

layer. The upper layer exports some material seaward, but some re-settles into the salt wedge. The flooding salt wedge re-entrains and transports fluffy material landward. Our measurements show that retained material is reworked in the estuary for three to four months after a delivery event until it is depleted through seaward export and consolidation.

TABLE OF CONTENTS

LIST OF FIGURES

LIST OF TABLES

ACKNOWLEDGEMENTS

First, I would like to acknowledge that the Duwamish River runs through the ancestral lands of the Duwamish Indian Tribe, and honor the traditional land and water of the Coast Salish Peoples on which this work took place.

The draw of this project was the opportunity to work on a scientifically interesting problem with very real-world consequences. One unexpected side-effect was that we were perpetually underfunded—it turned out to be hard to convince funding agencies that we had anything useful to add to a ten-year Superfund Site Remedial Investigation. As a result, this project was held together by electrical tape, hose clamps, and the generosity of many, many people.

I struggled long and hard throughout this process. Beyond all expectation, and very possibly reason, my advisor Alex stuck with me through it all. I'll never be able to thank you enough Alex, and words cannot express how deeply grateful I am for your singular blend of kindness and intelligence.

This dissertation would not have been possible without the unwavering support and excellent guidance of my committee. Sarah, Jim, and Andrea, thank you for being such brilliant scientists and generous human beings. I was often lost in the trees and you helped me see the forest.

I am so grateful to the many volunteers who provided help in the field, in particular, P. Clayton, J. Wilson, the UW EFM group, and thirty-six ambitious undergraduate fluid dynamics students. I also thank the 2012 FHL Estuarine and Coastal Fluid Dynamics class, in particular P. MacCready, W.R. Geyer, K. Arnott, J. Lopez, A. Tabatabai, S. Warner, and M. Williams. Many thanks to A. Ogston, C. Nittrouer, J. Thompson, A. Jessup, and Gravity Environmental LLC for the use of

vessels and equipment, and the South Park Marina and Shumate Family for the use of their facilities.

This research was supported by the University of Washington Royalty Research Fund, the Sea-Bird Electronics Student Equipment Loan Program, Gravity Environmental LLC, and the Amherst College Graduate School Fellowship Program.

Last but not least, thanks to my family and friends for their support throughout this process. Abby and Maureen, I could not have done this without you.

DEDICATION

For ALM, MSM, and KLS who lacked the opportunities than I have had,

and for GNS and EAL, may they have even more.

Chapter 1. Introduction

Nearly two-thirds of the world's major cities have been built around estuaries (Ross 1995). As populations have grown, many estuaries have been modified, impacting their hydrodynamic regime. Urbanized estuaries, which are typically among the most highly modified, are also often contaminated due to the proximity of intense industrial activity, motivating the need to better understand their hydrodynamic and transport processes in order to better inform current maintenance and future modifications. This study focuses on the Duwamish River Estuary, a highly engineered and contaminated tidal salt wedge estuary located next to downtown Seattle, WA.

1.1 SALT WEDGE HYDRODYNAMICS

Estuarine regimes are often characterized in terms of their salinity structure because the degree of stratification controls vertical turbulent diffusion of momentum, salt, sediment, and pollutants (Hansen and Rattray 1966). Estuaries with strong vertical stratification are classified as "salt wedge" estuaries. In salt wedge estuaries saline water intrudes from the ocean in a wedge-like layer along the bottom and remains distinct from overlying riverine water because strong vertical stratification at the density interface inhibits vertical mixing. This estuary type typically arises from a combination of high river discharge and weak tides (Schijf and Schonfeld 1953). Salt wedge estuaries can also occur with moderate to strong tidal forcing provided there is sufficient river input, and are termed "tidal salt wedge" estuaries (Geyer and Ralston 2011). Unlike their microtidal cousins, tidal salt wedge estuaries are marked by intratidal variability (Geyer and Farmer 1989; Giddings et al. 2011; Partch and Smith 1978; Ralston et al. 2010a), and since these systems are typically "short" (i.e. the salinity intrusion length is on the same order as the tidal excursion), they are also highly spatially variable. Unlike well- and partially-mixed estuaries whose longitudinal salinity gradients span large distances and do not deviate significantly from the tidal mean, the longitudinal salinity gradient in a tidal salt wedge estuary is concentrated at the landward tip of the salt wedge, or toe, and is advected with the tide. Thus, unlike more well-mixed estuaries, intratidal variations in salinity structure in tidal salt wedge estuaries tend to be more important dynamically than the tidal mean salinity structure. This has been shown both in

theoretical analyses (Burchard and Baumert 1998; Jay and Smith 1990a) and observations (Chawla et al. 2008; de Nijs et al. 2011; Giddings et al. 2011; Jay 1987; Jay and Smith 1990b).

Thus, tidal salt wedge estuaries present an observational challenge and most studies have focused on understanding the complex intratidal processes (de Nijs et al. 2011; Geyer and Smith 1987; Geyer and Farmer 1989; Partch and Smith 1978). Several studies have investigated fortnightly to monthly timescales (Giddings et al. 2011; Ralston et al. 2010a; Ralston et al. 2010b), but only Chawla et al. (2008) have captured the full seasonal variability in a strongly stratified estuary. Their study drew on a battery of measurements from over one year in the Columbia River Estuary, and determined that residual circulation in the Columbia depends on whether the system is strongly or partially stratified. Stratification there varies fortnightly and seasonally with the spring-neap cycle and the river hydrograph.

1.2 SUSPENDED SEDIMENT TRANSPORT IN SALT WEDGE ESTUARIES

Estuaries support a diverse array of industries and biological activity, and are often also in close proximity to urban populations (Ross 1995). The fate and transport of locally generated sediment and sediment from upstream is important for managing local ecosystems, exposure to contaminants, and coastal erosion. Estuarine sediment transport is controlled by the complex interactions of geometry, tides, riverflow, stratification, bottom sediment availability, and upstream sediment load (Geyer 1993). In many partially-stratified estuaries, this interplay often gives rise to one or more estuarine turbidity maxima (ETMs) that move with the salinity intrusion and can also be associated with geographic features (Burchard et al. 2018). In highly stratified estuaries with strong tidal currents, or tidal salt wedge estuaries, the interaction of tidal currents, strong vertical stratification, and suspended sediment is less well-studied.

In unstratified tidal flow, resuspension and erosion occur in a predictable cycle. Bed stress increases with velocity until a critical shear stress is exceeded (Shields 1936). Bed sediment is mobilized and entrained into the water column where it is held in suspension according to a balance between the vertical diffusion of bottom-generated turbulence and its own propensity to succumb to gravity and fall out of suspension. While in suspension, sediment is advected with the mean velocity and can travel some distance before it falls out of suspension and is deposited. As velocity

decreases, so too does bottom-generated turbulence. Bed stress falls below the critical threshold and sediment is no longer brought into suspension. There is less turbulence diffused into the water column and the balance maintaining sediment in suspension tilts towards gravitational settling and deposition. This cycle is repeated with tidally oscillating currents according to the availability of bed sediment and may be modified by upstream loading.

Strong vertical stratification in the salt wedge interrupts this cycle in several important ways. Sharp vertical stratification, as is typical in the salt wedge, effectively divides the water column into two regions: the fresh upper fresh layer, isolated from bed-generated turbulence and not in contact with the bed, and the saline lower layer. In the lower layer, stratification caps the vertical progression of bottom-generated turbulence and thereby inhibits bed stress (Fugate and Chant 2005; Geyer 1993). The lower layer therefore has a decreased capacity to both suspend sediment and to maintain it in suspension. The saline and reduced-turbulence conditions are also favorable for flocculation. Moreover, strong stratification limits the entrainment of bottom-generated sediment into the upper layer where mean flow is more strongly seaward, thereby reducing its potential for seaward transport. The upper layer, which generally carries sediment generated upstream, is isolated from bottom-generated turbulence, and is increasingly unable to maintain sediment in suspension (Kostaschuk 2002). The entrainment of salinity into the upper layer can also induce floc formation and increase gravitational settling into the lower layer.

The landward extent of vertical stratification, or the toe of the salt wedge, is the boundary between unstratified, high bedstress tidal flow and two-layered tidal flow. The location of the toe varies daily with the tides and seasonally with river discharge. In the Fraser, increased deposition was found during the salt wedge advance and enhanced resuspension was associated with the toe during retreat (Kostaschuk 2002; Kostaschuk and Luternauer 1989). Several studies have found that the tidal excursion of the salt wedge toe tends to be associated with trapping, in a tidally averaged sense (Geyer 1993; Jaeger and Nittrouer 1995). A study conducted in the Hudson found this to also be true of regions within the salt wedge that tend to form salinity fronts due to sharp changes in width and depth (Ralston et al. 2012). The ultimate fate of sediment trapped at the toe and within the salt wedge can also vary on longer timescales, as was also shown in the Hudson, where

sediment tends to accumulate near the mouth during the freshet and is subsequently transported slowly landward with the salt wedge as riverflow drops (Woodruff et al. 2001).

The vertical structure of estuarine bed sediment can also play an important role in sediment transport. The surface of the bed is often covered by a very thin (2mm) "fluff layer" composed of loosely aggregated material that is easily remobilized and entrained into the water column (Maa et al. 1998; Scully and Friedrichs 2007). Beneath the fluff layer, the bed may be either unconsolidated or settled (Mehta et al. 1989). Unconsolidated bed material has a higher porosity and can be resuspended when bed stress exceeds a critical value (Mehta et al. 1989). This material is also referred to as a "mobile pool" and is generally much thicker than the fluff layer (Geyer and Ralston 2018). Over time, hydrostatic pressure squeezes pore water from interstitial gaps and the material becomes consolidated and much harder to resuspend (Mathew and Winterwerp 2017; Mehta et al. 1989).

Consolidation is a complex process that is influenced by biological, chemical, and physical conditions (Winterwerp 2011). Very generally, and for a purely mud layer, consolidation time scales with the square of the layer thickness (Winterwerp 2011) and laboratory experiments have shown that the presence of sand increases consolidation rate (Torfs et al. 1996). Pure mud solutions in laboratory settings without external forcing of the flow can consolidate in 48 hr (Parker and Lee 1981) and Parchure and Mehta (1985) suggest that a muddy deposit a few centimeters thick might take a week to consolidate under moderate tidal forcing conditions. These timescales are on the order of the fortnightly neap-spring cycle and imply that consolidation must be considered in estuarine environments.

Some insight into consolidation timescales may be gained by considering modeling efforts. There are a variety of frameworks that may be employed (Winterwerp 2011), however observations of bed density showed an exponential approach to an equilibrium density (Hayter and Mehta 1986) and modeling consolidation empirically as a first-order relaxation has yielded good results (Sanford 2008). Using e-folding consolidation times of 1-3 days, the Sanford model (2008) showed that intratidal variations in bottom stress yield enough consolidation during and after slack to generate a small net deposit. This pattern is modified fortnightly by neap-spring variations in

erosion, and is consistent with observations from the upper Chesapeake Bay (Sanford 2008) and Hudson River Estuary (Traykovski et al. 2004).

1.3 UPSTREAM SUSPENDED SEDIMENT LOADING

Historically, direct measurements of total suspended sediment load are challenging to acquire and while recently the technology required for continuous monitoring has become relatively inexpensive, installation, calibration, and maintenance can all be quite costly. Thus, use of a rating curve is still widespread. A rating curve uses sparse estimates of total suspended sediment load, L, and river discharge, Q, to develop a relationship that can be applied to a continuous time series of discharge or a flow frequency table. Typically the form of this relationship is $L = aQ^b$, where a and b are coefficients from a log-space regression (Campbell and Bauder 1940). Variations on this traditional form include taking a piecewise approach to accommodate slope breaks (Ryan and Porth 2007; Templeton and Jay 2013), developing separate rating curves for rising and falling limbs of the hydrograph (Glysson 1987), and developing separate rating curves for each season (Walling 1974). Although rating curves are widely used, there are drawbacks. While rating curves generally capture mean loads well, scatter in the load estimates used for the regression can result in significant error when estimating instantaneous loads.

1.4 STUDY SITE DESCRIPTION

The Duwamish River Estuary is fed by the Green River and empties into the Puget Sound at Elliott Bay near Seattle, WA, USA. It is a highly stratified estuary, made even more so as a result of channel modifications. The current highly engineered estuary state is a consequence of its proximity to Seattle and the rich history of the city's evolution in response to growing anthropogenic pressure. In the context of this study there are two facts that are relevant to the system's hydrodynamics. First, in the early 1900s the lower 10 km were channelized and straightened for improved navigation, thereby shortening the channel and increasing the bed slope by a factor of three or more relative to the natural slope. Second, throughout the early to mid 20th century untreated industrial waste was discharged into the waterway. Toxic hydrocarbons preferentially sorbed onto sediment particles, leaving the bed sediments laden with very slowly decaying contaminants such as PCBs, PAHs, and PDBEs among others (LDWG 2010). In 2001

the Environmental Protection Agency (EPA) named the lower 10 km of the estuary a Superfund Site. Many of the most highly contaminated locations have been remediated, but final site-wide remediation will continue for the next several years and will be monitored closely for decades. Over a decade later, in December of 2014, a Record of Decision was issued recommending a remedial plan for the remaining 412 ac costing $342 million. While 177 ac will be actively remediated through some combination of dredging and capping, 57% (235 ac) relies on "monitored natural recovery", or the passive reliance on the burial of contaminated sediment by cleaner sediment originating from upstream of the estuary. From 2017-2019 data was collected to re-establish baseline contamination in the estuary, which may have changed in the intervening years since the Remedial Investigation. In 2019 the process of finalizing details for the remediation plan issued in 2014 was begun. Implementing the remediation plan is expected to take several years, and monitoring with be ongoing for many years after that.

Three studies in the late 1960s and early 1970s provided initial information about the salinity structure in the Duwamish. They noted that it is two-layered in nature throughout the year (Dawson and Tilley 1972), with the salt wedge intruding as far as 16 km up-estuary (Santos and Stoner 1972), and remaining below river kilometer (RK) 12.5 for flows over 28 m^3s^{-1} (roughly half a typical water year) (Stoner 1967). Sediment loads were measured by the United States Geological Survey (USGS) from 1963 to 1966 and were determined to have an exponential relationship to mean daily discharge for loads exceeding 500 tons/day (Harper-Owes 1981). Using this analysis and flow frequencies dating back to 1961, the annual sediment load was estimated to be 172,000-205,000 mt/year, with 70-95% remaining in the estuary, primarily between RK 8 and the Turning Basin (Harper-Owes 1983). To the author's knowledge, Harper-Owes (1983) is the only published study of suspended sediment transport in the Duwamish.

1.5 RESEARCH OBJECTIVES AND DOCUMENT ORGANIZATION

The objective of this dissertation is to increase understanding of the fate and transport of suspended sediment and associated contaminants in strongly stratified, urbanized estuaries, and in particular, the Duwamish River estuary. Specific research goals are (1) to investigate seasonal salt wedge dynamics is an important first step towards understanding seasonal and longer-term transport of contaminated bed sediment, (2) to analyze and quantify existing upstream loading data to the

estuary, and (3) to describe suspended sediment in the estuary and identify sediment sources in the estuary, transport pathways, local resuspension, and relevant timescales.

Field campaigns carried out in the Duwamish from 2011 to 2013 are presented and analyzed in Chapters 2 and 4. Chapter 2 uses hydrodynamic measurements collected over a 20-fold range of river discharge to understand seasonal salt wedge dynamics in the context of two-layer theory. Chapter 3 re-examines existing suspended sediment load data, presents existing ratings curves, and develops new ratings curves to better quantify upstream suspended sediment delivery to the estuary. Chapter 4 uses SSC and hydrodynamics measurements form 2011-2013 fieldwork to describe suspended sediment transport patterns and pathways within the estuary. These chapters were written for standalone publication in peer-reviewed journals. Chapter 2 was published in *Estuaries and Coasts* as McKeon et al. (2020). Chapters 3 and 4 are in preparation for publication. Research conclusions and recommendations are presented in Chapter 5.

Chapter 2. Seasonal changes in structure and dynamics in an urbanized salt wedge estuary

2.1 INTRODUCTION

Nearly two-thirds of the world's major cities have been built around estuaries (Ross 1995). As populations have grown, many estuaries have been modified, impacting their hydrodynamic regime. Urbanized estuaries, which are typically among the most highly modified, are also often contaminated due to the proximity of intense industrial activity, motivating the need to better understand their hydrodynamic and transport processes in order to better inform current maintenance and future modifications. This study focuses on the Duwamish River Estuary, a highly engineered and contaminated tidal salt wedge estuary located next to downtown Seattle, WA.

Estuarine regimes are often characterized in terms of their salinity structure because the degree of stratification controls vertical turbulent diffusion of momentum, salt, sediment, and pollutants (Hansen and Rattray 1966). Estuaries with strong vertical stratification are classified as "salt wedge" estuaries. In salt wedge estuaries saline water intrudes from the ocean in a wedge-like layer along the bottom and remains distinct from overlying riverine water because strong vertical stratification at the density interface inhibits vertical mixing. This estuary type typically arises from a combination of high river discharge and weak tides (Schijf and Schonfeld 1953). Salt wedge estuaries can also occur with tidal forcing provided there is sufficient river input, and are termed "tidal salt wedge" estuaries (Geyer and Ralston 2011). Unlike their microtidal cousins, tidal salt wedge estuaries are marked by intratidal variability (Geyer and Farmer 1989; Geyer and Ralston 2011; Giddings et al. 2011; Partch and Smith 1978; Ralston et al. 2010a), and since these systems are typically "short" (i.e. the salinity intrusion length is on the same order as the tidal excursion), they are also highly spatially variable. Unlike well- and partially-mixed estuaries whose longitudinal salinity gradients span large distances and do not deviate significantly from the tidal mean, the longitudinal salinity gradient in a tidal salt wedge estuary is concentrated at the landward tip of the salt wedge, or toe, and is advected with the tide. Thus, unlike more well-mixed estuaries, intratidal variations in salinity structure in tidal salt wedge estuaries tend to be more important

dynamically than the tidal mean salinity structure. This has been shown both in theoretical analyses (Burchard and Baumert 1998; Jay and Smith 1990a) and observations (Chawla et al. 2008; de Nijs et al. 2011; Giddings et al. 2011; Jay 1987; Jay and Smith 1990a, 1990b).

Thus, tidal salt wedge estuaries present an observational challenge and most studies have focused on understanding the complex intratidal processes (de Nijs et al. 2011; Geyer and Smith 1987; Geyer and Farmer 1989; Partch and Smith 1978). Several studies have investigated fortnightly to monthly timescales (Giddings et al. 2011; Ralston et al. 2010a; Ralston et al. 2010b), but only Chawla et al. (2008) have captured the full seasonal variability in a strongly stratified estuary. Their study drew on a battery of measurements from over one year in the Columbia River Estuary, and determined that residual circulation in the Columbia depends on whether the system is strongly or partially stratified. Stratification there varies fortnightly and seasonally with the spring-neap cycle and the river hydrograph.

The Duwamish River Estuary is located just south of downtown Seattle, WA (Figure 2.1). It is a highly stratified estuary, made even more so as a result of channel modifications. The current highly engineered estuary state is a consequence of its proximity to Seattle and the rich history of the city's evolution in response to growing anthropogenic pressure. In the context of this study there are two facts that are relevant to the system's hydrodynamics. First, in the early 1900s the lower 10 km were channelized and straightened for improved navigation, thereby shortening the channel and increasing the bed slope by a factor of three or more relative to the natural slope. Second, throughout the early to mid 20th century untreated industrial waste was discharged into the waterway. Toxic hydrocarbons preferentially sorbed onto sediment particles, leaving the bed sediments laden with very slowly decaying contaminants such as PCBs, PAHs, and PDBEs among others (LDWG 2010). In 2001 the Environmental Protection Agency (EPA) named the lower 10 km of the estuary a Superfund Site. Many of the most highly contaminated locations have been remediated, but final site-wide remediation will continue for the next several years and will be monitored closely for decades. Investigating seasonal salt wedge dynamics is an important first step towards understanding seasonal and longer-term transport of contaminated bed sediment.

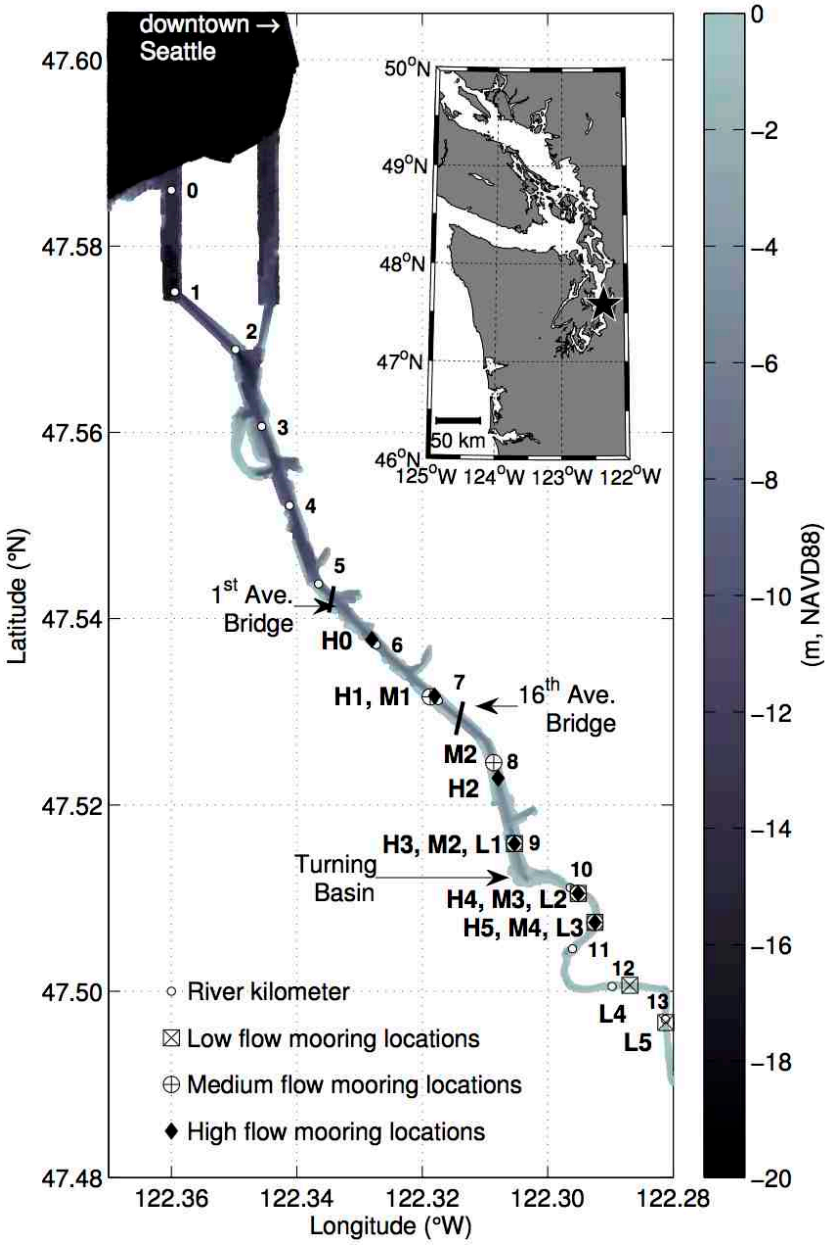

Figure 2.1. Local site map showing mooring locations.

Inset is regional site map of the Salish Sea and coasts of Washington and Vancouver Island. The black star is the Duwamish. Shading indicates bathymetry and mooring locations and mooring locations, River Kilometer, and features of interest are notes. Note that the shoreline corresponds to the edge of the shading since the Duwamish is so channelized.

Three studies in the late 1960s and early 1970s provided initial information about the salinity structure in the Duwamish. They noted that it is two-layered in nature throughout the year (Dawson and Tilley 1972), with the salt wedge intruding as far as 16 km up-estuary (Santos and Stoner 1972), and remaining below river kilometer (RK) 12.5 for flows over 28 m^3s^{-1} (roughly half a typical water year) (Stoner 1967). There are no observations of the salt wedge being completely flushed from the system, likely due to the deepened channel and flood control upstream.

The objectives of this study are: to characterize the salinity structure in the Duwamish across a typical annual range of river discharges, interpret the observed seasonal variability using a two-layer theoretical framework, and explore implications for subtidal transport. In this paper we present site background information in Section 2.2. We use two-layer hydraulic theory to develop an expectation for the seasonal response of the system in Section 2.3. In Section 2.4 we outline our in-situ observations that will be used to test the hypotheses proposed in Section 2.3. In Section 2.5 we present the observational results, focusing on the seasonal changes in salinity structure in the context of two-layer hydraulic theory. Finally, in Section 2.6 we discuss the potential effects of mixing and implications of our analysis, and Section 2.7 includes a summary of our conclusions.

2.2 STUDY SITE

This study focuses on the region of the Duwamish traversed by the toe of the salt wedge, from approximately river kilometer (RK) 5 to 14 (Figure 2.1). The geometry changes drastically at RK 10, an area known as the "Turning Basin", which marks the transition from a more natural system upstream to a highly engineered one below RK 10 (Figure 2.2). Seaward of the Turning Basin, the channel width is a relatively uniform 120 m and the center 40 m is actively maintained as a navigation channel by roughly biennial dredging. The channel cross-section is symmetric except at two slight bends at RK 5 and 8 and a nearly 90° turn near the Turning Basin. Pier protection at two bridges constricts the channel width by more than 50% at RK 5.5 and 7.5 (Figure 2.2). The lower 10 km has a relatively precipitous bed slope of 1.5×10^{-3}, while landward of the Turning Basin the bed slope is a gentler 2.4×10^{-4}. Up-estuary of the Turning Basin the channel narrows considerably to 45 m and exhibits more natural sinuosity. A rock pier protruding into the channel center causes a lateral constriction at RK 11.

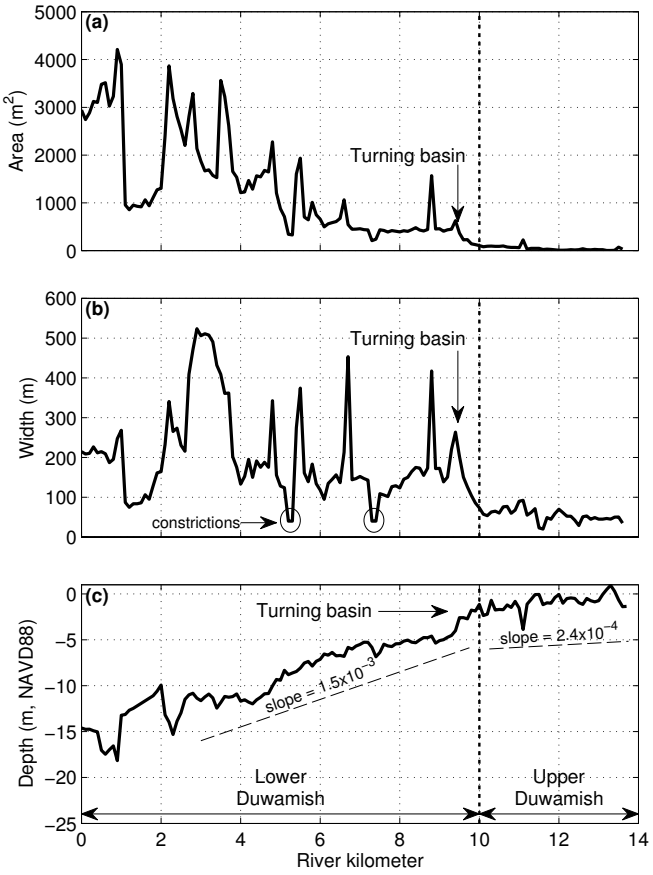

Figure 2.2. Channel geometry.

From top to bottom: a) channel cross sectional area, b) width, and c) thalweg depth. Constrictions at ~RK 5.5 and ~RK 7.5 are indicated in b) and the transition from a highly modified to more natural channel is indicated with the vertical dashed line at RK 10.

The nearest United States Geological Survey (USGS) gauging station (# 12113000) is located 50 km from the mouth in Auburn, WA, upstream of two small tributary creeks that contribute very little streamflow except during high precipitation events. In 1962 the Howard Hansen Dam was constructed 100 km from the mouth for flood control and has subsequently attenuated the peak river discharge events and decreased the annual range of river discharges delivered to the estuary. Post dam construction, the mean monthly minimum flow is 9 m^3s^{-1} in August and the mean monthly maximum is 68 m^3s^{-1} in January; the annual mean is 38 m^3s^{-1} (Figure 2.3). Flood stage is 255 m^3s^{-1} and is rarely exceeded due to flood control at the dam. Note that all river discharge statistics exclude measurements prior to the dam installation.

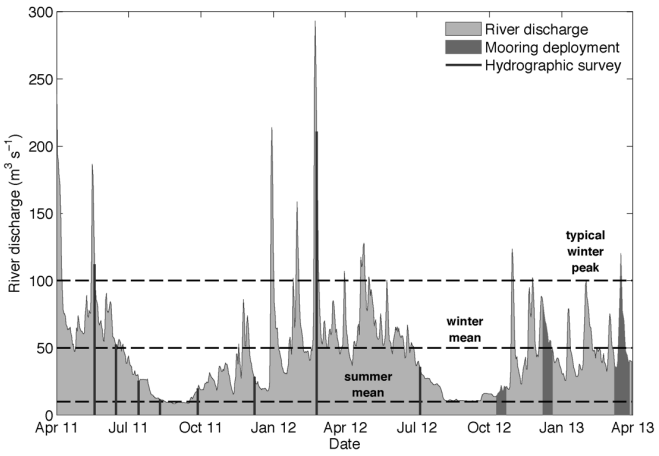

Figure 2.3. 2011-2013 discharge and deployment times.

Summary of 2011-2013 river discharge (gray shading). Dark gray lines indicate hydrographic surveys. Medium gray shading indicates low, medium, and high flow mooring array deployments, respectively. Black dashed lines indicate mean summer, mean winter, and a typical peak winter flow.

Tides in the Duwamish are mixed semi-diurnal and dominated at the mouth by the M2 and K1 constituents with amplitudes of 1.072 m and 0.834 m respectively. The mean tidal range is 2.3 m and the mean diurnal range is 3.5 m. Santos and Stoner (1972) noted that the tidal waveform does not change appreciably as it propagates up-estuary, and that it can propagate as far as RK 21 (Dawson and Tilley 1972). Under typical river discharge and tidal forcing, mean currents in the Duwamish are approximately 0.40 ms^{-1}, with a tidal velocity of 0.30 ms^{-1} and a river velocity of 0.10 ms^{-1}. The fastest currents were observed when the river discharge was 200 m^3s^{-1} and the tidal range was 2.5 m, resulting in a 0.27 m s^{-1} tidal current and 0.50 ms^{-1} river velocity, and, thus, a total depth-averaged current of nearly 0.80 ms^{-1} at maximum ebb. Depth-averaged currents lead the water surface by approximately 2 hr, which corresponds to a phase lead of 58°, consistent with a shallow frictional estuary (Friedrichs and Aubrey 1994).

Seasonal changes to the endpoint water masses in the Duwamish are minimal. The bay water mass intruding from Elliott Bay is set by conditions in the Salish Sea and has a nearly constant salinity of 28 psu with variations on the order of 0.5 psu and a seasonal temperature range from 8°C to 12°C. The fresh water input from the Green River varies between 4°C to 18°C. It is warmer than

the oceanic water from May-September, and colder than the bay water from October-March. The seasonal temperature variability increases the overall density gradient by an equivalent of 1 psu from May to September, and decreases the overall salinity difference by an equivalent of 1 psu from October-March, which is minimal relative to the persistent 28 psu range in salinity along the estuary. Therefore, seasonal variations in the endpoint water masses are negligible and the major seasonal forcing is driven by river discharge. Henceforth we will refer to seasonality and changes in river discharge interchangeably.

2.3 THEORETICAL BACKGROUND

Tidal salt wedge estuaries exhibit intratidal variability, spatial variability, and non-homogeneous along-channel density gradients. These characteristics make them poor candidates for the canonical estuarine theory developed by Hansen and Rattray (1966) and Chatwin (1976), which relies on a subtidal along-channel momentum balance and a constant horizontal density gradient. The nearly two-layered nature of the salt wedge lends itself more readily to one-dimensional, two-layer hydraulic theory, which we will now develop with the Duwamish in mind to provide insight as to how the salt wedge structure might be expected to change seasonally.

Following Schijf and Schonfeld (1953) and Geyer and Ralston (2011), we assume a two-layered system in which x is the along-channel direction, the upper layer has a density ρ_1, a layer-averaged velocity u_1, and a thickness h_1. Similarly, the lower layer has a thickness h_2, velocity u_2, and density ρ_2, where it is assumed that $\rho_2 > \rho_1$. The two layers do not interact except through interfacial drag, parameterized by an interfacial drag coefficient, C_i. The channel width, B, is constant and the volume fluxes in each layer are Q_1 and Q_2, where $Q_j = u_j h_j B$ for each layer. Since we are interested in seasonal changes in the layer thicknesses, it will be useful to consider the momentum balances in each layer in terms of their internal Froude numbers, $F_j^2 = Q_j^2/g'h_j^3B^2$. Here g' is the reduced gravity, which depends on the density difference between the upper and lower layers and can be expressed in terms of the salinity difference between the two layers $g' = g\beta\Delta s$ where $\beta = 8\times10^{-4}$ psu^{-1} when the densities are not strongly dependent on temperature (see Section 2.2). Then the steady momentum balance in the upper layer is:

$$g'F_1^2\frac{\partial h_i}{\partial x} + g\frac{\partial \eta}{\partial x} + \frac{C_i|u_1-u_2|(u_1-u_2)}{h_1} = 0 \qquad (2.1)$$

The first term is advective acceleration, where, like Geyer and Ralston (2011), we assume $\partial h_i/\partial x \approx -\partial h_1/\partial x$. The second term is the barotropic pressure gradient due to the slope of the water surface, η, and the third term is the interfacial drag. The steady momentum balance in the lower layer is:

$$-g'F_2^2\frac{\partial h_i}{\partial x} + g'F_2^2\frac{\partial h_b}{\partial x} + g\frac{\partial \eta}{\partial x} - \frac{C_i|u_1-u_2|(u_1-u_2)}{h_2} + g'\frac{\partial h_i}{\partial x} + g'F_2^2C_D = 0 \qquad (2.2)$$

Here the first two terms comprise the advective acceleration, which is due to the shape of the interface and the bottom slope. The third term is the barotropic pressure gradient; the fourth term is the interfacial drag; the fifth term is the baroclinic pressure gradient due to the sloping interface; and the sixth term is the bottom drag parameterized by a bottom drag coefficient, C_D. Note that both the water surface height, η, and height of the interface, h_i, are measured relative to a vertical datum, such that a flat bed slope is not necessary. This will be important for applying this theoretical framework to the Duwamish, which has a moderately steep bed slope. Bathymetry is incorporated into the term h_b, the height of the bed relative to a vertical datum, such that $h_i = h_2 + h_b$.

Common practice is to simplify Equations 2.1 and 2.2, by making assumptions based on the geometry and tidal phase of interest, and then subtract them to derive the baroclinic momentum balance. The channelized Duwamish has a roughly uniform width and a steep slope (see Section 2.2) so we will use a simplified channel geometry that has a constant width and a uniformly sloping bed. We will consider three cases: the arrested salt wedge, the up-estuary propagation of the salt wedge during the flood, and the retreat and destruction during the ebb.

2.3.1 *Arrested salt wedge*

As shown by Schijf and Schonfeld (1953), when the lower layer is stationary the salt wedge is said to be "arrested" and Equations 2.1 and 2.2 can be subtracted, resulting in an equation for the interface assuming constant width:

$$\frac{\partial h_i}{\partial x} = -C_i\frac{F_1^2}{1-F_1^2} + \frac{h_1+h_2}{h_1} \qquad (2.3)$$

Equation 2.3 can be integrated from the mouth, where the flow is assumed to be critical, landward to the toe of the salt wedge to determine the interface profile h_i and the salt wedge length, L as a function of F_1 and thus Q (Harleman 1961; Poggioli and Horner-Devine 2015). This results in a relationship between estuary length and river discharge: $L \sim Q^{-n}$, where n is between 2 and 2.5. In estuaries with moderate or steeply sloped channels, however, Poggioli and Horner-Devine (2015) have shown that L is much less sensitive to Q and n may be an order of magnitude smaller than the prediction for a non-sloping channel.

2.3.2 *Propagating salt wedge (flood)*

Following Geyer and Ralston (2011), we assume that the salt wedge shape does not change as it propagates up-estuary at a constant speed, and that in the moving reference frame of the salt wedge the interface height is not time-dependent. We do, however, assume some advective acceleration in the lower layer due to the bottom slope, thus we neglect the first term in Equation 2.2, but retain the second. We also assume that interfacial drag is negligible. In the upper layer (Equation 2.1) there is no acceleration under the assumption that the channel widens with height above the bed enough that advective acceleration is negligible. With these simplifications, subtracting Equations 2.1 and 2.2 yields an equation for the interface slope:

$$\frac{\partial h_i}{\partial x} = -F_2^2(S_0 + C_D) \tag{2.4}$$

where $S_o = \partial h_b / \partial x$, which we take to be constant for a uniformly sloping bed. Setting So = 0, Equation 2.4 reduces to the relationship derived by Geyer and Ralston (2011), which accurately described the interface shape during the flood in the relatively flat Fraser River Estuary.

2.3.3 *Retreating salt wedge (ebb)*

Unlike the flood, the only simplifying assumption that can be made for the ebb is that the interfacial drag terms in Equations 2.1 and 2.2 are negligible. Subtracting Equation 2.2 from 2.1 results in the following baroclinic momentum equation:

$$(1 - F_1^2 - F_2^2)\frac{\partial h_i}{\partial x} = -F_2^2\left(\frac{\partial h_b}{\partial x} \pm C_D\right) \tag{2.5}$$

The sign of C_D is consistent with that of the lower layer velocity (i.e., C_D is positive for positive u_2 and vice versa), such that the drag opposes the flow direction. Equation 2.5 is not easily solved

for the interface height. Equation 2.5 differs from Equation 2.4 in that it retains a dependence on F_1, and thus river discharge. This suggests that the ebb dynamics are sensitive to river discharge, but the flood dynamics (Equation 2.4) are not. This asymmetry is evident in our measurements and will be explored in Sections 2.5 and 2.6.

2.3.4 *Alterations due to contractions and mixing*

There are two factors not included directly in Equations 2.1 to 2.5 that are likely to be important in the Duwamish. First, the Duwamish has two constrictions (Figure 2.2, RK 5.3 and 7.4), thus the assumption of constant width may not be valid everywhere. Armi and Farmer (1986) developed a solution for barotropically forced two-layer flow through a contraction and found that the throat acts as a control point and the interface height landward of the contraction varies with barotropic forcing. Landward of the throat, flow is subcritical and the lower layer thins and intersects with the bottom with a shallow slope until the barotropic forcing is sufficient to push it into the throat. For strong forcing, the location of the front coincides with the control point, the front has a steep slope and the upper layer flow seaward of the control thins and is supercritical. Such strong forcing occurs preferentially during the ebb when the tide and riverflow both act in the seaward direction, and has been well-documented in the highly stratified Hudson River Estuary where the ebb salinity structure was locally modified by the hydraulic response at a constriction (Chant and Wilson 2000; Orton and Visbeck 2009; Peters 2003; Stenstrom 2004). The Duwamish has a more two-layered structure than the Hudson and the constrictions are slightly more severe, so we expect the hydraulic response at the bridges to locally alter the ebb salinity structure.

Second, the two-layer model approach may not capture the dynamics fully when conditions generate mixing and interfacial stress. For a subcritical flow the maximum velocity difference across the interface is limited to $\Delta u=(g'H)^{1/2}$ where H is the total water depth**.** Assuming the onset of favorable mixing conditions at a critical Richardson number, $Ri_{g,c}$ (Miles 1961), we can determine a stable pycnocline thickness (h_p) based on that amount of shear. The gradient Richardson number is given by $Ri_g = -(g/\rho_0)(\partial\rho/\partial z)(\partial u/\partial z)^{-2} \simeq -g' h_p / \Delta u^2$, where $h_p \sim \Delta z$ is the pycnocline thickness. During subcritical conditions these relationships predict a stable pycnocline thickness that then depends on $Ri_{g,c}$ and H: $h_p = Ri_{gc} H$ (Geyer and Smith 1987). For

supercritical flow, when the composite Froude number, $G^2 = F_1^2 + F_2^2$, exceeds 1, the shear is only limited by the strength of the barotropic forcing and thus h_p can grow rapidly. The subcritical case would be expected to occur preferentially during flood tides or potentially both phases of the tides if the river flow is sufficiently low. The supercritical case is expected to occur during ebb tides and strong discharge. As per Equation 2.2, a sufficient seaward surface tilt during the ebb will overwhelm the landward baroclinic pressure gradient and force the lower layer seaward. Once the lower layer is moving seaward, bottom drag acts to enhance shear with no limit as in the subcritical case (Geyer and Smith 1987). Mixing can continue until the salt wedge is destroyed or until the barotropic forcing decreases.

To summarize, two-layer theory does not give rise to an easily predictable ebb structure (Equation 2.5), and there are two other mechanisms that could potentially influence the ebb structure: a hydraulic response to lateral constrictions and shear-induced interfacial mixing. The former has been observed in a small number of studies (listed above), while interfacial mixing has been observed during the ebb in multiple salt wedge estuaries including the Fraser (Geyer and Farmer 1989; MacDonald and Horner-Devine 2008), Merrimack (Ralston et al. 2010b), Snohomish (Giddings et al. 2011), Connecticut (Geyer et al. 2017) and the Duwamish Rivers (Partch and Smith 1978).

2.3.5 *Seasonal behavior inferred from two-layer theory*

The foregoing discussion presents an analytical framework that we can use to formulate hypotheses as to how the salt wedge salinity structure varies seasonally. In the Duwamish, river discharge is the primary driver of seasonal variability (see Section 2.2). The mass flux due to river discharge is included in the mass flux of the upper layer (see Section 2.3). Therefore, seasonality is most clearly expressed through F_1, although river discharge can also influence the surface tilt term, $g\partial\eta/\partial x$. The structure of the advancing (flood tide) salt wedge is given by Equation 2.4 and is not dependent on either the upper layer Froude number or the barotropic pressure gradient, which suggests that the flood phase structure should be insensitive to river discharge. As described in Section 2.3.3, the ebb phase structure is dependent on F_1 and therefore should vary seasonally. Additionally, seasonal changes to the ebb structure could be the result of a hydraulic response to lateral constrictions or interfacial mixing as the salt wedge becomes supercritical (see Section

2.3.4). We expect an asymmetric ebb-flood response in the salt wedge structure to changes in river discharge. In Section 2.4 we present the observations that are used to evaluate this hypothesis.

2.4 OBSERVATIONS AND METHODS

Sampling occurred over a nearly two-year period from May 2011 to March 2013 and used two sampling modes. The first used high spatial resolution (~2–200m) hydrographic surveys during spring tide, greater ebb and flood conditions to characterize the entire salt wedge structure. The surveys spanned a large (twenty-fold) range of river discharge. The second used a coarsely spaced (~1km) mooring array near the toe of the salt wedge to investigate the full tidal range. The mooring array was deployed during mean summer, mean winter, and peak winter discharge.

2.4.1 *Hydrographic surveys*

Beginning in May 2011, 12-hr (greater ebb and flood) spring tide hydrographic surveys were completed on a roughly monthly basis. The conditions for each survey are summarized in Table 1 and Figure 2.3. Velocity profiles were measured with a boat-mounted 1200 kHz bottom-tracking ADCP (Teledyne RDI) operating at 1 Hz in Mode 1 with 25 cm bins. Salinity, temperature, and suspended sediment concentrations (SSC) were measured with a SeaBird 19+ V2 profiler. Data were viewed real-time on the boat in order to approximate vessel position relative to the toe of the salt wedge. With the exception of the July 2012 survey, casts were taken continuously ("tow-yo-ing") near the toe to ensure high spatial resolution in the most dynamic region. In the more uniform portion of the salt wedge, casts were spaced roughly 200 m apart. Casts during the July 2012 survey were spaced 400 m apart and those transects were not used in the following analysis. During select surveys a bottom-mounted 1200 kHz ADCP operating in Mode 12 with 25 cm bins, and top-bottom CT sensors were deployed at RK 7.5 for ~25 hrs (see Table 2.1). Note that biennial maintenance dredging by the United States Army Corps of Engineers (USACE) from RK 8-9.5 occurred in January 2012, altering the thalweg depth in that region for the 2012 surveys and subsequent mooring array deployments (see Section 2.4.2).

Table 2.1. Summary of hydrographic survey conditions

Date of hydrographic survey	Mean tidal range (m)	Mean river discharge (m^3s^{-1})
May 19, 2011	3.6	105
June 15, 2011	4.5	49
July 14, 2011	4.2	24
August 10, 2011	3.6	9
September 27, 2011	2.9	18
December 8, 2011*	3.8	25
February 24, 2012*	3.3	197
July 5, 2012*	4.5	35

**Indicates a concurrent 25-hr moored 1200 kHz ADCP with top-bottom CT sensors.*

2.4.2 *Mooring array deployments*

To further investigate intra- and inter-tidal effects, a mooring array was deployed for three two-week periods from October 2012 to March 2013, coinciding with typical mean summer, mean winter, and peak winter flows (see Figure 2.3). The mooring array consisted of five moorings with top and bottom salinity sensors, roughly equally spaced across the projected tidal excursion of the salt wedge toe. In addition to the salinity sensors, the central mooring was also equipped with an OBS-3+, and an upward looking 1200 kHz RDI ADCP. The utility of the mooring data for the work described in this paper was limited, however, due to challenges with placement of the central mooring relative to the predicted salt wedge location, dramatic modifications of the bathymetry due to dredging that preceded the medium discharge deployment and poor ADCP data return. During the second (medium discharge) and third (high discharge) deployments all moorings had bottom-mounted Onset pressure sensors and the center mooring had a bottom-mounted acoustic Doppler velocimeter (ADV, Nortek). The pressure sensors were used to estimate the barotropic pressure gradient, the ADV was used to estimate the bottom drag coefficient and the CTDs were used to determine tidal excursion distance.

2.4.3 *Methods*

2.4.3.1 Salt wedge length

We define the toe of the salt wedge as the landward-most occurrence of a top to bottom salinity difference that exceeds 5 psu. The toe was not encountered at the same tidal phase in each hydrographic transect, so the salt wedge length is estimated one-quarter of the way through the flood according to water surface elevation from a linear interpolation of two transects. The same method is used to determine salt wedge length from the moorings as well. For the mooring analysis, we split the tidal cycle to distinguish between the greater and lesser tides for a better comparison with the spatial surveys, which do not include the lesser tide.

2.4.3.2 Salt wedge stratification

Stratification in estuaries typically results from a competition between the stratifying influences of buoyancy inputs from the river or lateral sources and vertical mixing due to tides. This is often characterized using the estuarine Richardson number, Ri_e, (Fischer 1972), which suggests that higher river discharge will increase stratification due to the increase in buoyancy input. Here, we use the dimensionless parameter Ψ to quantify stratification within the salt wedge. The Ψ-parameter was developed in strongly stratified systems with a distinct three-layer structure consisting of a highly saline lower layer, a nearly fresh upper layer, and an intervening mixed layer. Ψ is defined as (MacDonald and Horner-Devine 2008):

$$\psi = \frac{1}{2}\frac{h}{z_{75}-z_{25}} \tag{2.6}$$

where z_{25} and z_{75} are the depths of the 25th and 75th percentile isohalines, respectively. The salinity range in the Duwamish is 0 to 28 psu making the 25th and 75th percentile isohalines 7 and 21, respectively. Ψ compares the thickness occupied by half the salinity range to half the water depth.

2.5 RESULTS

2.5.1 *Overview*

Selected surveys taken at maximum greater ebb and flood are shown in Figure 2.4, which demonstrate the changes in salt wedge structure over a range of river discharge. Both ebb and flood

transects show that the salt wedge is further seaward and the halocline thickness decreases with increasing river discharge. As hypothesized, the structure of the salt wedge on ebb tide shows a different response to river discharge than during flood. During the ebb, the pycnocline thickness decreases with increasing river discharge, indicating that stratification is increasing. In addition, the pycnocline moves closer to the bed with increasing river discharge; this corresponds with an increase in the upper layer thickness and a decrease in that of the lower layer. This is particularly clear when comparing the lowest and highest river discharge transects (Figure 2.4a, d). A prominent feature during the ebb is the local depression of the pycnocline near lateral constrictions at the 1st and 16th Avenue Bridges during moderate to large discharge (Figure 2.4b, c, d). This is evidence of the strong hydraulic response discussed in Section 2.3.4 and observed by Gardner and Smith (1978), and shows that it is strong enough to form a front for river discharges above 50 m^3s^{-1} (Figure 2.4c, d).

The flood transects change with increasing river discharge, but to a lesser extent than the ebb transects. As river discharge increases, the pycnocline thickness decreases slightly and the pycnocline height above the bed decreases relative to the toe of the salt wedge, however these changes are small relative to those observed at maximum ebb (Section 2.5.2). Apart from a slight expansion of the pycnocline near the 16th Ave. Bridge (Figure 2.4f, g) there is little response to lateral constrictions at low riverflows. Unfortunately, the flood transects lack the necessary coverage to conclusively determine the hydraulic response at the bridges on the flood.

The velocity fields show a similarly asymmetric ebb-flood response to river discharge. During the ebb, surface velocity increases with river discharge while velocities in the salt wedge remain weak. Velocity profiles (Figure 2.4) show that the shear increases and moves closer to the bed with increasing river discharge. The flood velocity profiles (Figure 2.4) show a subsurface velocity maximum in the pycnocline that is characteristic of strongly stratified systems (de Nijs et al. 2011; Geyer 1988; Geyer and Farmer 1989; Giddings et al. 2011; Ralston et al. 2010a). This feature arises because stratification inhibits penetration of bottom-generated turbulent stress into the pycnocline, allowing water above the boundary layer to accelerate under the influence of the baroclinic pressure gradient (Geyer 1988; Geyer and Farmer 1989). The seaward upper layer velocity increases with river discharge and that increases the shear at the top of the pycnocline.

However, velocity profiles show that the overall structure is not changing with riverflow as much as during the ebb phase (Figure 2.4). Comparing the lowest and highest river discharges, the vertical shear during the ebb increases in magnitude and proximity to the bed.

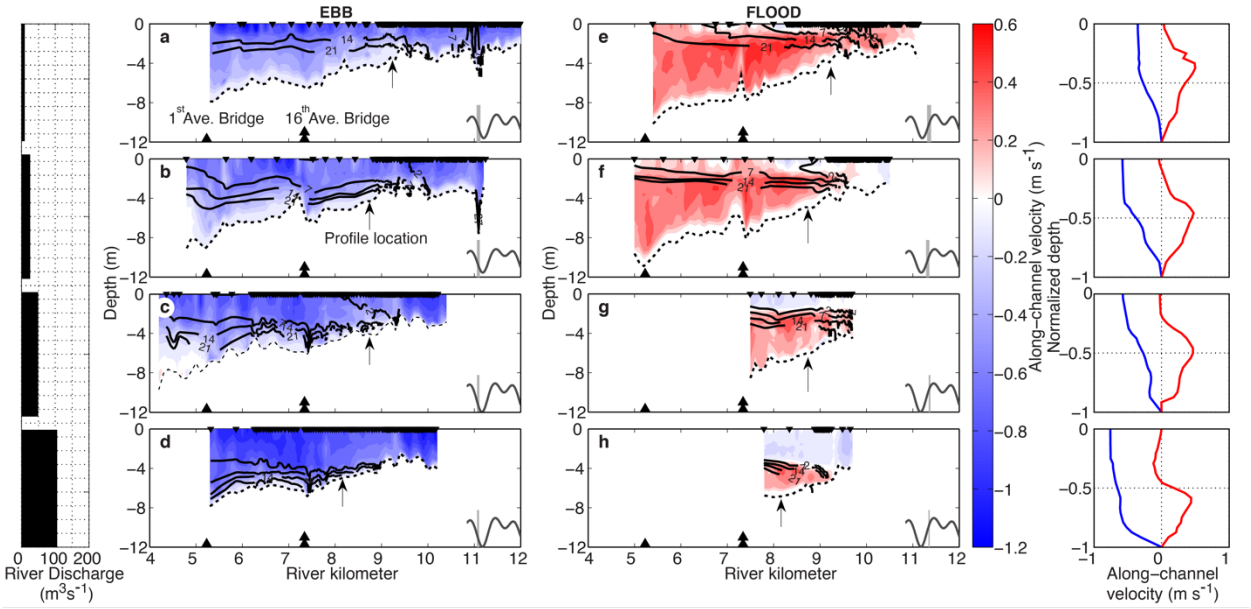

Figure 2.4. Ebb and flood transects.

Selected maximum ebb (a-d) and flood (e-h) transects are ordered from low to high river discharge as indicated on the far left bar plot. Color indicates along-stream velocity where negative (blue) is in the ebb direction. Thin black lines are isohalines, black triangles at depth = 0 indicate cast locations, and the black dotted line is the channel bed. The single and double large black triangles at depth = -12 m indicate the locations of the 1st and 16th Avenue Bridge constrictions, respectively. The ebb (blue) and flood (red) velocity profiles on the right panel correspond to the profile locations marked by the arrows and are shown in depth normalized coordinates (e.g., Giddings et al., 2014).

2.5.2 *Seasonal changes in salinity structure*

The two-layer theory presented in Section 2.3 suggests how the salt wedge structure will vary with seasonal changes in river discharge. In this section we describe changes in salt wedge length and thickness, surface slope, hydraulics and stratification across the range of observed river discharge

rates in order to test the predictions from theory and understand the seasonal changes in system dynamics.

2.5.2.1 Salt wedge length

Salt wedge lengths estimated from transects (Figure 2.5) show a power law fit: $Q^{-0.22\pm0.04}$. The lowest river discharge survey deviates from this trend and is excluded from the fit. On this day the salt wedge interacted strongly with a major constriction and scour hole at RK 11 (Figure 2.4a), which may have affected where our method located the toe. However, we cannot exclude the possibility of a significant change in behavior at very low discharge.

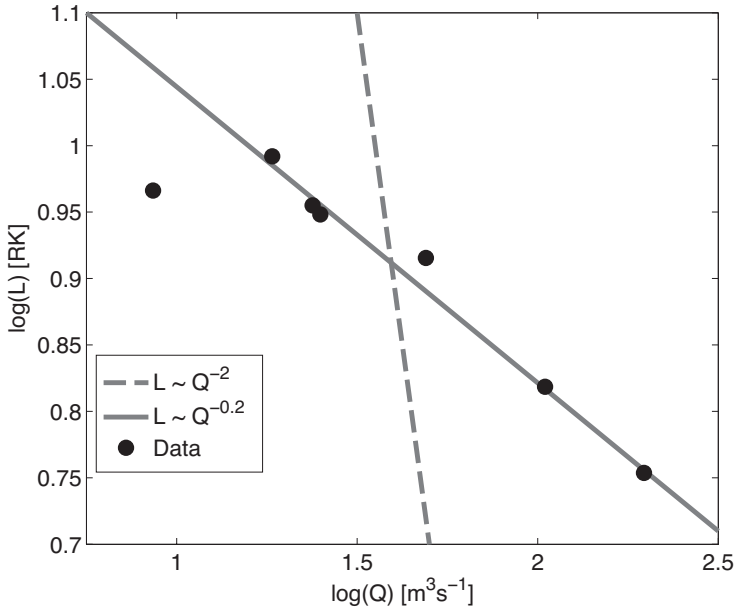

Figure 2.5. Salt wedge length versus discharge.

Salt wedge length (plotted as the logarithm of the length one-quarter through the flood) versus the logarithm of the river discharge. The dark gray line is a fit to all the transect data except the lowest river discharge estimate. The dark gray dashed line is the Schijf and Schönfeld theoretical relationship for a flat estuary.

As expected, the $L{\sim}Q^{-0.22\pm0.04}$ relationship indicates a much weaker dependence on river discharge than the canonical two-layer theory, which predicts $L{\sim}Q^{-2}$ (Section 2.3.1). This departure from theory can be attributed to the steep bed slope, which imposes a landward limit to L based on the bottom slope and reduces the sensitivity to Q (Poggioli and Horner-Devine 2015). The Duwamish

also differs from the theory in Section 2.3.1as the theory assumes that the only critical flow condition occurs at the mouth. As discussed in Section 2.5.2.3 flow can be critical at two lateral constrictions landward of the mouth and the salt wedge length should be determined by integrating Equation 2.2 from the most landward control point to the toe (Poggioli and Horner-Devine 2015).

2.5.2.2 Barotropic forcing

As discussed in Section 2.3.3 and 2.3.4, two-layer theory predicts a hydraulic response to barotropic forcing that will preferentially influence the ebbing salt wedge. Pressure time series from the high flow mooring array deployment are used to determine changes in barotropic pressure gradient with river discharge. The high flow deployment is used because it captured a sharp peak in river discharge that clearly illustrates the water surface response to river discharge. Figure 2.6a shows the phase-averaged surface profile during a tidal cycle. There is little difference between the lesser

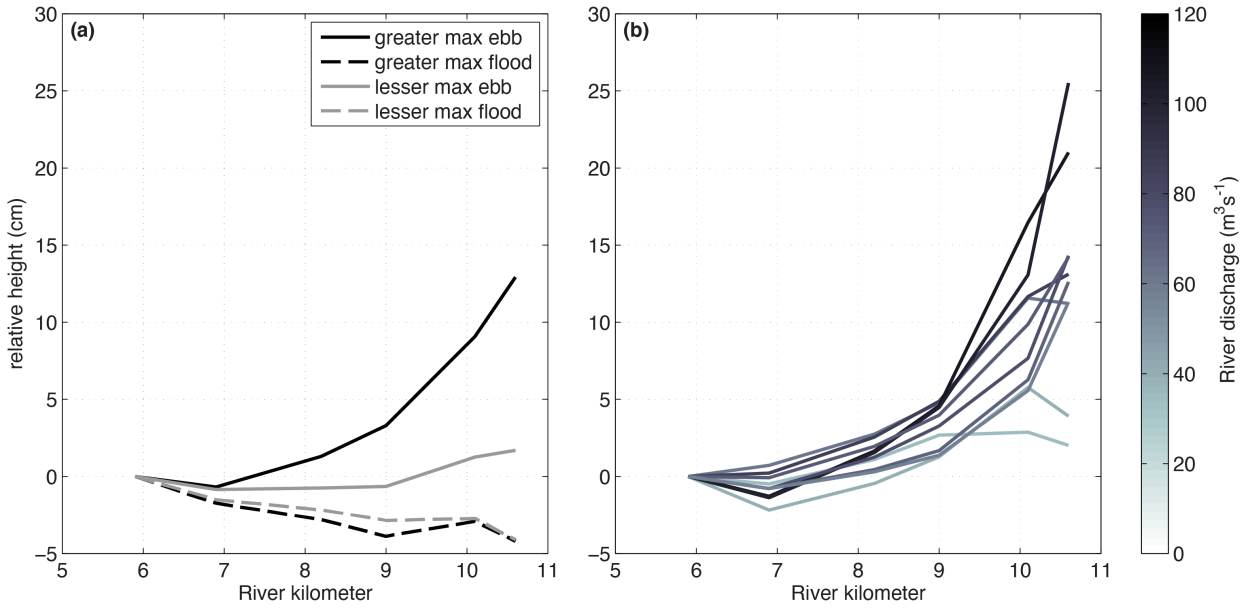

Figure 2.6. Barotropic pressure gradient.

Surface elevation profiles from the last mooring deployment, which included a peak in riverflow roughly halfway through the deployment. The left panel shows the surface tilt at key points in a 24-h tidal period, taken from a phase average of the entire deployment. The right panel shows the surface tilt at maximum greater ebb throughout the deployment. The color indicates the river discharge at a 1-day lag.

and greater flood, but the greater ebb clearly shows a stronger seaward barotropic pressure gradient compared to the other phases. Figure 2.6b shows the response of the water surface to a peak in river discharge, lagged by one day (the lag with the maximum correlation). This lag is likely due to a combination of the travel time from the USGS gauging station to the estuary, and the estuarine response to changes in river flow. The seaward tilt of the water surface increases with river discharge by nearly an order of magnitude. Thus, the barotropic pressure gradient during the ebb exceeds that during flood and is enhanced during high river discharge and strong tidal forcing.

2.5.2.3 Hydraulic state; subcritical and supercritical conditions

The strong barotropic forcing during ebb, which varies in response to river discharge, is indeed reflected in the hydraulic state. Figure 2.7c shows the composite two-layer Froude number, *G*, for each of the maximum ebb and flood surveys averaged over the salt wedge length. At maximum flood the flow is subcritical, with a slight decrease in *G* as riverflow increases. The hydraulic state at maximum ebb is close to critical for river discharges above 25 m^3s^{-1}. Under the highest sampled riverflow conditions there is only a small remnant of salt wedge landward of the 1st Avenue Bridge constriction, thus the composite Froude number estimate may be biased low because of how little salt wedge remains. This difference in hydraulic state appears to be reflected in the different salt-wedge structure observed between flood vs. ebb tidal phases over varying discharge as anticipated in Section 2.3 and described in more detail below.

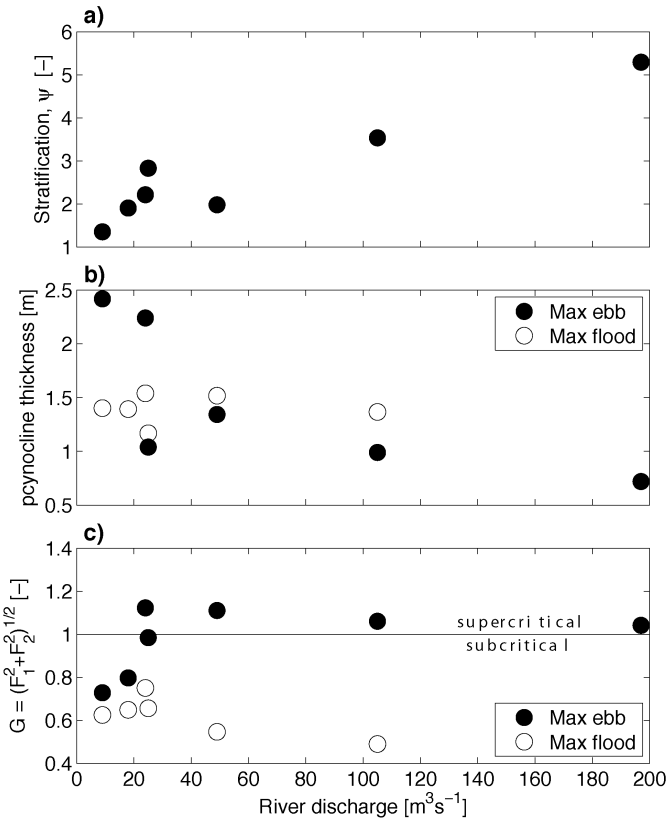

Figure 2.7. Salt wedge structure.

The top panel (a) shows a plot of the average stratification versus river discharge from each hydrographic survey, where stratification is quantified by the dimensionless stratification parameter, Ψ. The middle panel (b) shows the average pycnocline height in the salt wedge landward of RK 5.5 for maximum flood (open circle) and ebb (closed circle) transects over a range of river discharge. The lower panel (c) shows the average composite Froude number, G, as a function of river discharge for maximum flood and ebb transects.

2.5.2.4 Salt wedge stratification

As described in Section 2.4.3, salt wedge stratification is quantified in terms of Ψ. When Ψ reaches one, the system is partially mixed; the higher the value of Ψ, the more stratified and two-layered the system. An average Ψ was calculated for the maximum ebb longitudinal transects (Figure 2.7a). These data confirm that the salt wedge becomes more strongly stratified with higher discharge, consistent with Ri_e. The variation for points between 30 and 50 m^3s^{-1} is attributed to differences in the tidal velocity (not shown here). The changes in stratification are consistent with the observed decrease in the pycnocline thickness with increasing riverflow (Figure 2.7b), which is likely due

to increasing buoyancy input. However, there also appears to be a sudden shift in behavior at roughly 25 m^3s^{-1} that mirrors the transition from a subcritical to supercritical flow at maximum ebb (Figure 2.7c). The subcritical ebb pycnocline thickness is close to 2.5 m, while the pycnocline during supercritical flows is ~1 m thick. This behavior is discussed in more detail below.

Unlike during the ebb, the pycnocline thickness during the flood remains nearly constant across the observed range of riverflow. This suggests that the processes determining the stratification of the flooding salt wedge are insensitive to river discharge and do not depend on the stratification set by the preceding ebb. The stratification in the flooding salt wedge is a competition between the tendency of salt wedge propagation to increase stratification, the de-stratifying influence of the sub-surface velocity maximum advecting mixed salinity water over the lower layer, and mixing due to shear above and below the sub-surface velocity maximum. Because the flood is subcritical (Figure 2.7c), we can estimate the thickness of a stable pycnocline using $h_p = Ri_{g,c}H$ (Section 2.4.3). Assuming an average depth of 6 m over this region of the estuary, this equation yields a pycnocline thickness of 1.5 m, close to the average observed thickness of 1.4 m. This implies that the flood pycnocline thickness is maintained at a constant thickness by interfacial mixing, which is driven by shear and not influenced by river discharge, consistent with the theory presented in Section 3. At the lowest river discharge we find that the pycnocline is thicker at max ebb than at max flood. However, our method of defining the pycnocline as between the 7 and 21 psu isohalines may bias the average pycnocline thickness for the lowest river discharge on ebb because the 7 psu isohaline intersects the water surface very close to the toe (Figure 2.4a).

2.5.2.5 Interfacial height

The interface structure, defined by the low-pass filtered 21 psu isohaline, during the max flood phase (Figure 8a) is surprisingly insensitive to seasonal variations; it does not change appreciably across an order of magnitude change in river discharge. Unlike the flood phase, the interfacial height at maximum ebb shows enhanced seasonal variability (Figure 8b). As river discharge increases, the interface structure landward of RK 5.5 increasingly deviates from the flood structure; the interface is closer to and parallel with the bed. This suggests that the salt wedge is not merely being advected seaward, but that its structure is simultaneously being modified as river discharge increases. Below we describe these seasonal flood/ebb interfacial height differences in more detail

with comparison to the theory presented in Section 3 and given the hydraulic state of the flow described in Section 5.2.3.

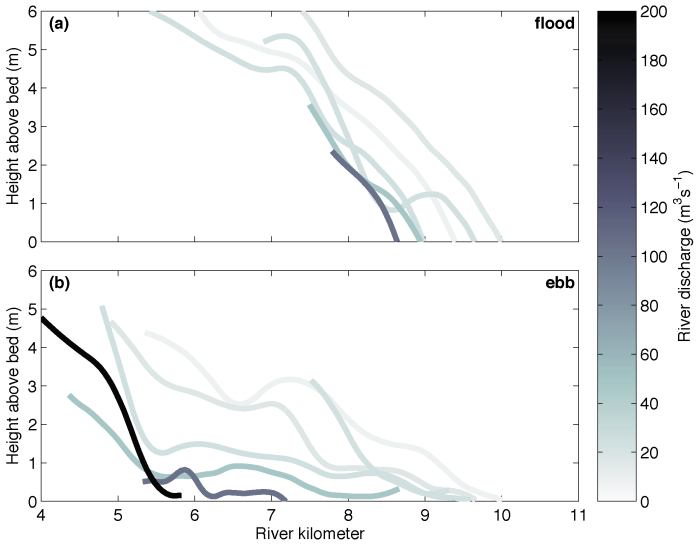

Figure 2.8. Interfacial height.

Halocline height (as defined by the 21 psu isohaline) above the bed versus river kilometer for each transect at roughly maximum greater flood (a, seven profiles included) and roughly maximum ebb (b, six profiles included). Shading indicates river discharge. Note that in both panels, the profiles of interfacial height have been smoothed with a low-pass filter to emphasize seasonal changes. Unsmoothed profiles are included in Figure 2.9 and Figure 2.10.

2.5.2.5.1 Flood phase interfacial height

Figure 9 shows the interface height during the flood phase from each survey plotted relative to the toe. Rattray and Mitsuda (1974) found that Equation 2.4 described the flooding salt wedge in the Duwamish during a single river discharge. We find that the interfacial heights across a tenfold range of river discharges collapse onto a single curve that compares favorably to Equation 2.4 using a drag coefficient of 3×10^{-3} and a salt wedge propagation speed of 0.40 ms^{-1}. The propagation speed was estimated from transects and the low flow mooring deployment when the salt wedge was landward of maintenance dredging, and the drag coefficient was estimated based on the best fit to the data. Measured drag coefficients, calculated from ADV measurements during the medium

and high flow mooring deployments, were smaller, on the order of 0.8 to 1×10^{-3}, but were likely influenced by local bathymetry. The good agreement with Equation 2.4, which is based on a frictional balance, is consistent with the observation that the phase lag between the depth averaged velocity and water surface elevation also suggests a frictional system (not shown). Furthermore, this agreement is notable considering the presence of effects such as the subsurface velocity maximum that are not described in two-layer theory. We also note that the interface is nearly parallel to the water surface downstream of the toe, since the interface slope, when plotted as depth above the bed, matches the bed slope (Figure 2.9).

2.5.2.5.2 Ebb phase interfacial height

Figure 2.10a-e shows the full salt wedge structure at maximum ebb for five river discharges. As seen in Figure 8b, when river discharge is low, the interface is well above the bed, and parallel to the water surface throughout the salt wedge (Figure 2.10a). This low flow structure is similar to

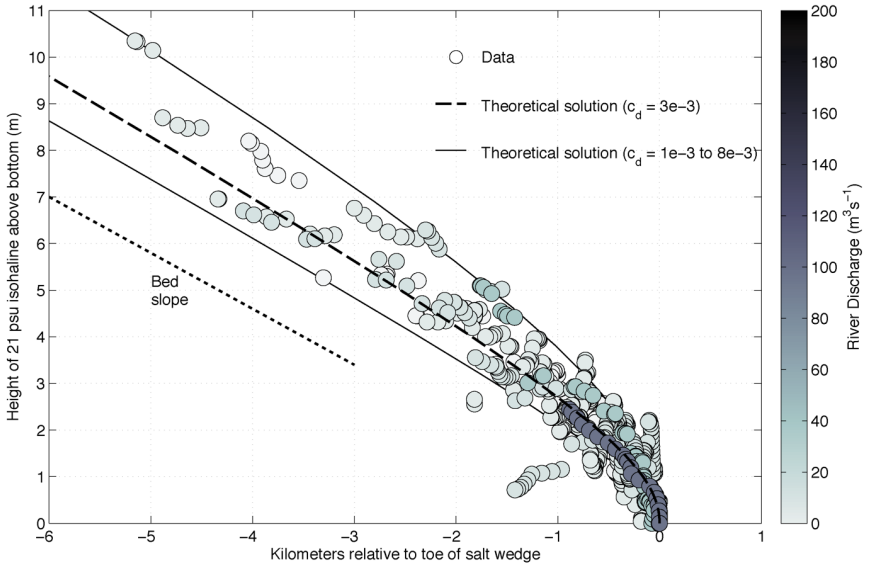

Figure 2.9. Flood interfacial height.

Flood interfacial height relative to toe. The height of the halocline above the bed at maximum flood (the same data from Figure 2.8, but not smoothed) plotted relative to the salt wedge toe. The black dashed line is the theoretical two-layer solution for a salt wedge propagating up-estuary at a constant velocity of 0.40 ms^{-1} along a bed-slope of 1.2×10^{-3}, with a bottom drag coefficient of 3×10^{-3}.

the flood structure. At medium river discharge the interface in the landward portion of the salt wedge becomes parallel with the bed (Figure 2.10b). As the river discharge increases, the interface up-estuary of RK 5.5 is suppressed towards the bed Figure 2.10c and d). Finally, at the highest observed river discharge (Figure 2.10e), the salt wedge has retreated to RK 5.5, where the interface is well off the bed and roughly parallel to the water surface. This location is just seaward of a lateral constriction and a substantial increase in depth. The toe of the salt wedge has never been observed below this location.

On ebb tide, when the upper layer is the active layer, two-layer theory suggests that the upper layer thickness is the dynamically important measure of the pycnocline location, rather than the pycnocline height. Figure 2.10f-j shows along-channel variations in upper layer thickness, pycnocline thickness, and in the composite Froude number for each transect in Figure 2.10a-e. The ebb salt wedge structure may be interpreted in terms of the critical depth, $h_c = (Q^2/B^2g')^{1/3}$, which is the active layer depth in a critical flow with discharge Q and width B. Two-layer hydraulic theory of flow over a sill with strong barotropic forcing predicts that the active upper layer thickness will adjust to h_c (Farmer and Armi 1986). Although there is no distinct sill in the Duwamish, there is a slope break at the Turning Basin (RK 9.5, Figure 2.2c) and we anticipate that the hydraulic response downstream of this point may be similar to that described by Farmer and Armi (1986).

The critical depth is compared with the salt wedge structure in Figure 2.10a-d. Here, g' is based on the local salinity difference across the interface of 14 psu. For low river discharges, the critical depth is shallow and the salt wedge toe is located at or landward of the slope break (Figure 2.10a, b, f, g). When the salt wedge is that far landward, flow through the constrictions is less distinctly two-layered than during higher flows, the hydraulic response is minimal, and the interfacial height shows no major modifications. As noted above, there is a change in behavior around 25 m^3s^{-1}. The critical depth is large enough to force the salt wedge seaward of the slope break and flow over the salt wedge is near-critical (Figure 2.10h, i, j). Interestingly, although the interface (defined above as the bottom of the pycnocline) approaches the bed, the top of the interface remains parallel to

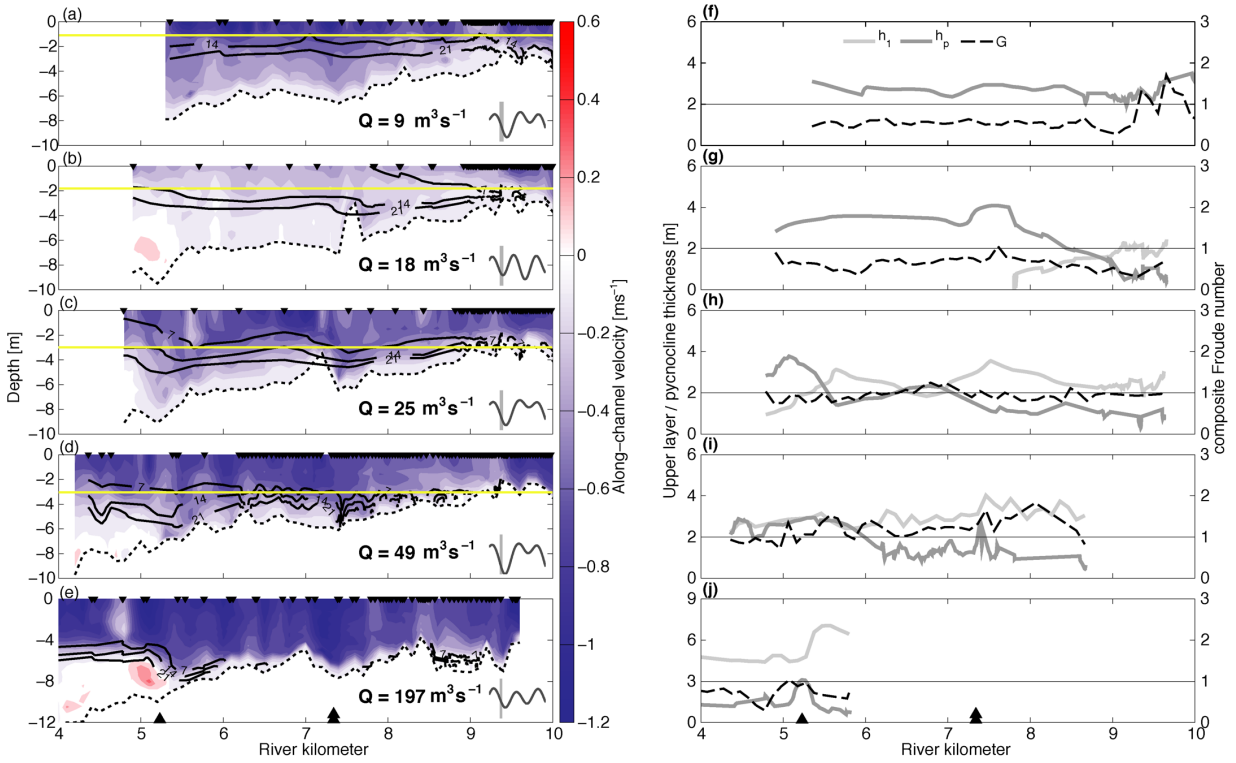

Figure 2.10. Ebb salinity structure.

Five examples of maximum ebb salinity structure from Figure 2.8b, but not smoothed. The left-hand panels (a-e) show the full ebb transects including along-stream velocity (color) and the 7, 14, and 21 psu isohalines. Yellow lines indicate the critical depth, h_c. The right-hand panels (f-j) show the upper layer thickness (light gray line), pycnocline thickness (dark gray line), and the composite Froude number, G (black dashed line) for the same five ebbs transects that are shown in (a-e). The single and double black triangles on the bottom panels indicate the 1st and 16th Ave. Bridge constrictions, respectively.

the water surface (Figure 2.10c, d). This is consistent with the quasi-steady solution for two-layered flow with barotropic forcing (Farmer and Armi 1986). The critical depth sets the upper layer thickness, and the interface remains flat and parallel to the water surface until forced by sudden changes in width or bathymetry. In Figure 2.10c and d this results in the formation of a front at the 16th Ave Bridge (RK 7.5). There is a sudden width expansion and increase in depth immediately seaward of the 1st Ave Bridge (RK 5.5), resulting in a larger increase in cross-sectional area than at the 16th Ave Bridge. When the critical depth locates the toe at or near the 1st Ave Bridge a front forms, which is similar to the lift-off front observed at river mouths (Figure

2.10e). The critical depth is much thicker than the observed upper layer thickness in this region, presumably because the width is increasing rapidly. The toe of the salt wedge has never been observed seaward of the 1st Avenue Bridge constriction, and it is likely that upstream regulation prevents riverflows that would push the critical depth further seaward. Thus, the Duwamish is actually not as "short" as most salt wedge estuaries where the salt wedge is completely flushed out of the estuary during strong ebbs. As a result, sediment and sorbed contaminants may be trapped in the lower estuary, even during very high flow conditions.

Lateral constrictions can be control points that force subcritical flow and a thinning lower layer landward, and supercritical flow and a thinning upper layer seaward (Armi and Farmer 1986). Realistically, rapid changes in upper layer thickness generate shear that likely triggers interfacial mixing (Geyer and Smith 1987), decrease the upper layer momentum, and result in subcritical flow. In Figure 2.10f-j the thickness of the pycnocline and upper layer are plotted for each of the corresponding transects in Figure 2.10a-e in order to differentiate hydraulic response from localized mixing. Thinning of the upper layer while the pycnocline thickness is increasing suggests interfacial mixing. Thinning of the upper layer and an unchanging or thinning pycnocline is indicative of a hydraulic response. Under slightly increased riverflow (Figure 2.10g) we observe an increase in pycnocline thickness near the constriction as the upper layer thickness goes to zero, which suggests that interfacial mixing has transitioned the flow to subcritical. The pycnocline thickens and does not get thinner for roughly 200 m, which suggests that the mixing is relatively localized. Seaward of the constriction flow is subcritical through the 1st Avenue Bridge and the interface is parallel with the water surface. In general, at higher riverflows, locations with sharp decreases in upper layer thickness show a corresponding increase in pycnocline thickness (Figure 2.10h, i, j approximately RK 5.5, 7.4, 5.3 respectively) suggesting an increasing influence of larger-scale interfacial mixing.

2.6 DISCUSSION

We have used a suite of observations spanning an order of magnitude range of river discharge to characterize the salt wedge salinity structure response to seasonal changes in river discharge (Figure 2.3). Our observations include 7 spring tide hydrographic surveys at maximum greater ebb

and flood, as well as three 10-20 day mooring array deployments. We use these observations to explore seasonal changes in stratification, salt wedge length, and intratidal variations in interfacial height. We find that increases in river discharge increase stratification (Figure 2.4 and Figure 2.7a) and thin the pycnocline during the ebb (Figure 2.7b). The salt wedge length decreases with increasing river discharge (Figure 2.5) and tidal amplitude (not shown).

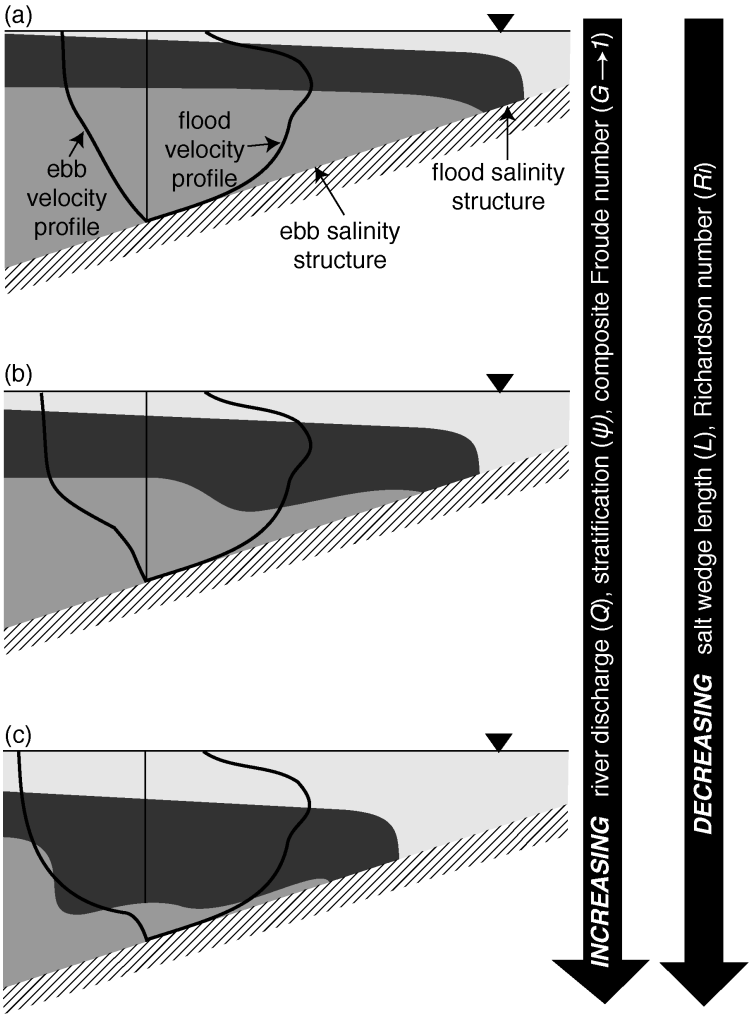

Figure 2.11. Conceptual schematic.

A conceptual schematic of the asymmetric ebb-flood response of the interface to low (a), medium (b), and high (c) river discharges. The arrows on the right indicate changes in relevant quantities with river discharge.

The height of the density interface responds to seasonal changes in river discharge in a tidally asymmetric manner as predicted by two-layer theory. Our observations show that the density interface at maximum flood is roughly parallel to the water surface and is well off the bed for most of the salt wedge length (Figure 2.8a). The shape is insensitive to changes in river discharge and is well described by two-layered theory (Figure 2.9). At maximum ebb, however, the interface height landward of RK 5.5 is pushed towards and parallel to the bed as increasing river discharge drives the ebb into a more supercritical state (Figure 2.7c and Figure 2.10a-e). These two behaviors combine to form a flood-ebb asymmetry in interfacial height that is modulated by changes in river discharge. The simple conceptual picture of the Duwamish salt wedge as described above is summarized schematically in Figure 2.11. However, this schematic and the preceding discussion have largely ignored two complicating factors: mixing processes and the intratidal evolution of the hydraulic state, which are discussed below. Finally, we hypothesize that the observed asymmetry will impact residual circulation and show some limited observations that support this hypothesis.

2.6.1 *Mixing*

Two-layer theory assumes very little exchange between the two layers, even when it predicts shear that should generate instabilities and vertical mixing. While our measurements were not designed to capture mixing, several observations suggest the importance of interfacial mixing (including the flooding salt-wedge pycnocline height – Section 2.5.2.4 and the ebbing salt-wedge response to lateral constrictions – Section 2.5.2.5). For medium to high river discharge we find sufficient shear for interfacial mixing and gradient Richardson numbers below the critical threshold during the ebb (Figure 2.12). Shear squared, $S^2 = \left(\partial u/\partial z\right)^2$, was calculated using the velocity difference between the top and bottom of the pycnocline (Figure 2.12b), and the bulk Richardson number (Ri_b, Figure 2.12c) was determined in a similar fashion. Although stratification increases with river discharge, it is overtaken by shear. For riverflows greater than 25 m^3s^{-1} conditions are increasingly favorable for mixing, which would tend to make the system less two-layered, likely modifying the hydraulic response. However, we observe a thinning ebb-phase pycnocline (Figure 2.10f-j and Figure 2.7b) with increasing riverflows and little evidence of mixed intermediate salinity fluid. There is some evidence (not shown) that suggests mixing may be highly episodic both spatially (discussed below)

and temporally (occurring earlier in the ebb with higher river discharge), which may explain the apparent absence of mixed fluid.

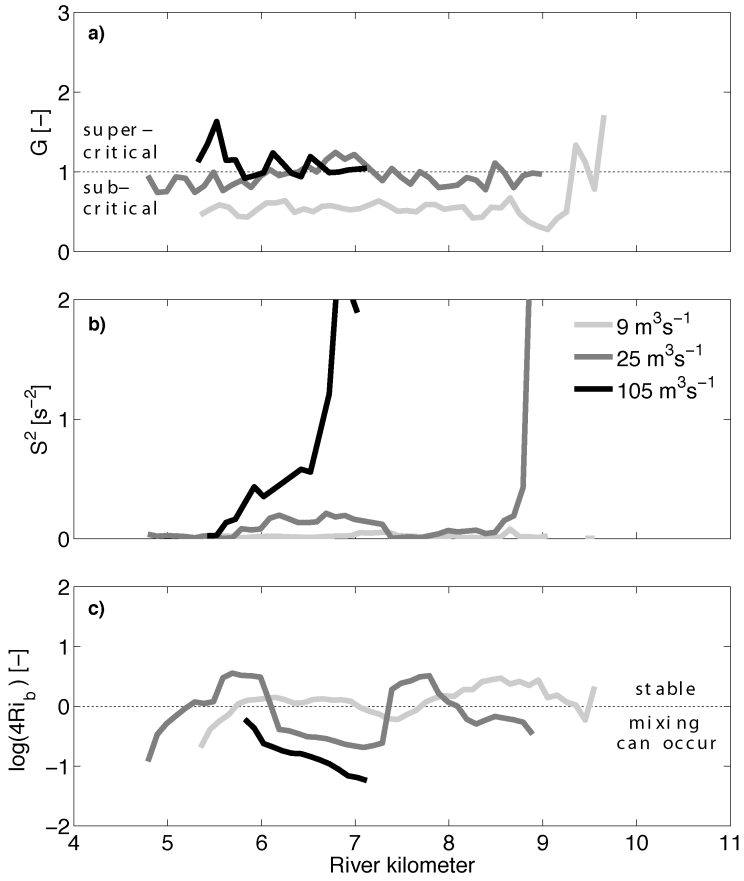

Figure 2.12. Localized mixing during ebb.

The composite Froude number G (a), S^2 (b), and $\log(4Ri_b)$ (c) are shown as a function of along-channel distance for low (light gray line), medium (dark gray line), and high riverflow (black line).

This description of salt wedge mixing is consistent with two studies in the Duwamish during the 1970s (Gardner and Smith 1978; Partch and Smith 1978) that observed short periods of intense mixing. Observations by Partch and Smith (1978) near RK 8 in low riverflow conditions (14 m^3s^{-1}) showed intense periods of vertical mixing during the greater ebb. These events were attributed to long internal waves breaking at the Turning Basin since Ri_g was above the critical value, suggesting interfacial mixing was not occurring. Later, Gardner and Smith (1978) observed

subcritical Richardson number values and evidence of enhanced mixing up- and down-estuary of the 16th Avenue Bridge likely due to enhanced shear from the hydraulic response. Their results suggest that localized interfacial mixing due to the constriction contributes to mixing. This was also observed in the Hudson River Estuary (Chant and Wilson 2000; Peters 2003). Our observations in the Duwamish suggest that this effect increases with river discharge and occurs over multiple locations along the salt wedge thus potentially greatly impacting the salt wedge structure. In summary, higher river discharges are associated with higher Froude numbers and lower Richardson numbers, suggesting that vertical mixing also increases with discharge, despite the fact that no direct evidence of mixing is observed in our measurements. We suggest, based on prior studies, that this is due to the spatial and temporal variability of mixing, which our measurements were not designed to capture.

2.6.2 *Seasonally modulated tidal asymmetry*

As described previously, the interface height in the advancing salt wedge (flood) is insensitive to river discharge. Conversely, the interface height during the ebb decreases with increasing river discharge. Thus, we observe an asymmetry in the interfacial height at maximum ebb and flood, the degree of which is modified seasonally by river discharge. Intratidal variability of interfacial height can generate subtidal circulation: if persistent throughout a tidal cycle, ebb-flood differences in interfacial height as observed can result in near-bottom landward transport. This is similar to the tidal asymmetry theory presented by Jay and Musiak (1996), and summarized in MacCready and Geyer (2010) whereby intratidal variations in vertical mixing create asymmetrical flood and ebb velocity profiles which drive a residual circulation into the estuary at depth, out at the surface. In the Duwamish, the intratidal asymmetry is driven by hydraulics, but the outcome is expected to be similar, i.e., the evolution of the ebb salinity structure will determine how much of an effect the asymmetry has on residual circulation. Unfortunately, the available moored ADCP timeseries are only 24-hr, thus, they are not long enough to determine meaningful residual velocity profiles (which should be calculated over longer intervals). Nevertheless, Figure 2.13 shows 24-hr averages for two different discharges when the ADCP was entirely within the salt wedge and when the depth average velocity is consistent with the river flow. These 24-hr average velocity profiles indicate increasing landward flow closer to the bed with higher discharge. While these observations are

anecdotal, the trend is consistent with the observed changes in pycnocline height and support the hypothesis that the asymmetry is likely to be important in modifying the residual circulation, which varies seasonally with river flow.

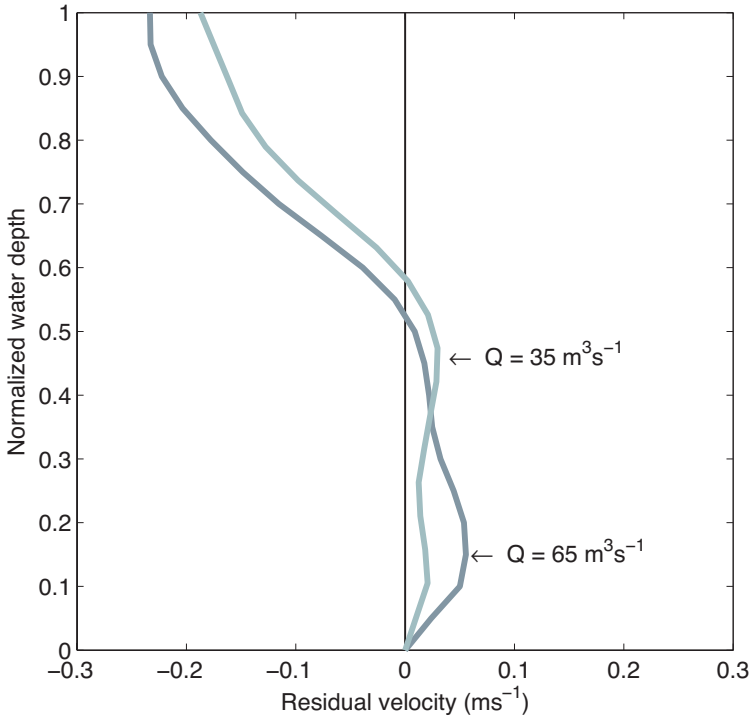

Figure 2.13. Residual velocity profiles.

24-h residual velocity profiles are shown for two river flows.

The ebb-flood asymmetry is driven by the hydraulic response during the ebb, which is in turn altered by changes in river discharge. Thus, for similar systems, both the deterministic tides and the semi-deterministic river hydrograph must be characterized in order to predict net annual residual transport. Additionally, the correlation between the spring-neap cycle and a river discharge peak is likely important in order to predict the net annual residual transport; high riverflow during a neap tide will induce a weaker hydraulic response than one occurring at a spring tide. This means that for the Duwamish and similar systems where net sediment transport is a concern due to legacy contamination, an accurate estimate of annual transport will require averaging that extends beyond the normal neap-spring fortnight and should include seasonal variations of the river hydrograph.

2.7 SUMMARY AND CONCLUSIONS

A combination of hydrographic surveys and moored measurements of salinity and velocity are used to characterize the seasonal variability of stratification in the Duwamish River Estuary, a tidal salt wedge estuary. These observations show that changes to the channel geometry, and in particular, a steep bed slope due to an artificially maintained navigation channel, influence the estuarine circulation and the salt wedge dynamics. The steep bed slope results in a salt wedge length that is less sensitive to changes in river discharge than in estuaries with a shallower bed slope. The ebb- and flood-phase salinity structures can be understood based on two-layer hydraulic theory. The flood phase structure is largely insensitive to changes in river discharge. The ebb-phase salinity structure, in contrast, is strongly influenced by discharge as a result of hydraulic response to strong barotropic forcing, a steeply sloping bed, and severe lateral constrictions. During the ebb, flow is near-critical over the salt wedge, and the upper layer thickness is set by the critical depth. Contractions near two bridges locally reduce the pycnocline height and can form fronts at high riverflows. At higher river discharges, we also find sufficient shear to create favorable conditions for mixing across the interface throughout the salt wedge. The overall effect is to maintain an upper layer depth equal to the critical depth, while the bottom of the pycnocline is shifted towards the bed with increasing river discharge. In combination with an unchanging flood structure, this results in a seasonally modulated ebb-flood asymmetry in the interfacial height. The ebb-flood asymmetry increases landward transport within the salt wedge and has implications for long-term residual scalar transport. Thus, seasonal changes in riverflow can drive variations in salt wedge structure (intrusion distance and stratification) and residual transport on seasonal or longer timescales.

Chapter 3. Upstream suspended sediment delivery to the Duwamish River Estuary

3.1 INTRODUCTION

The Duwamish River Estuary is fed by the Green River and empties into the Puget Sound at Elliott Bay near Seattle, WA, USA (Figure 3.1). The estuary's proximity to the city and Port of Seattle made it an attractive location for various industries—most notably Boeing—and through the mid-1900s industrial waste was discharged directly into the lower 10 km of the waterway. This legacy persists today in the presence of toxic hydrocarbons such as PCBs, PDBEs, and PAHs in the bed sediment (LDWG 2010). In 2001 the lower 10 km was added to the national list of Superfund Sites as the Lower Duwamish Waterway. Areas with the highest contaminant concentrations (Early Action Areas, roughly 29 ac) were cleaned up first via active remediation techniques such as dredging and capping. Over a decade later, in December 2014, a Record of Decision was issued recommending a remedial plan for the remaining 412 ac costing $342 million. While 177 ac will be actively remediated through some combination of dredging and capping, 57% (235 ac) relies on "monitored natural recovery", or the passive reliance on the burial of contaminated sediment by cleaner sediment originating from upstream. Thus, understanding upstream loading to the estuary is critical for determining the long-term viability of cleanup efforts.

Historically, direct measurements of total suspended sediment load are challenging to acquire, and while recently the technology required for continuous monitoring has become relatively inexpensive, installation, calibration, and maintenance can all be quite costly. Thus, use of a rating curve is still widespread. A rating curve uses sparse estimates of total suspended sediment load, L, and river discharge, Q, to develop a relationship that can be applied to a continuous time series of discharge or a flow frequency table. Typically the form of this relationship is $L = aQ^b$, where a and b are coefficients from a log-space regression (Campbell and Bauder 1940). Variations on this traditional form include taking a piecewise approach to accommodate slope breaks (Ryan and Porth 2007; Templeton and Jay 2013), developing separate rating curves for rising and falling limbs of the hydrograph (Glysson 1987), and developing separate rating curves for each season (Walling 1974). Although rating curves are widely used, there are drawbacks. While rating curves

generally capture mean loads well, scatter in the load estimates used for the regression can result in significant error when estimating instantaneous loads.

In this chapter we re-examine existing suspended sediment load data and rating curves to understand the magnitude and timing of suspended sediment coming into the estuary.

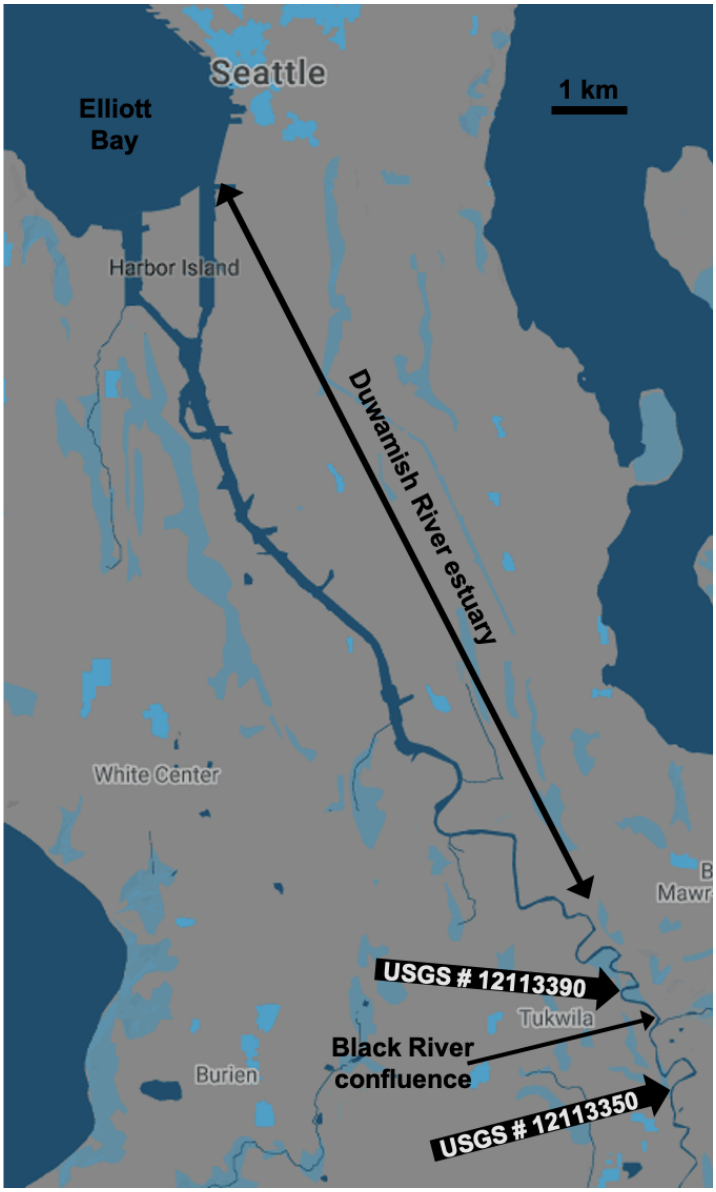

Figure 3.1. Site map.

Map of Duwamish River estuary, WA, USA and USGS stations #12113390 and #12113350 in Tukwila, WA. Relevant features, including the Black River confluence, are noted.

3.2 BACKGROUND

The Green River runs for approximately 150 km from the Cascade Mountains to Elliott Bay next to downtown Seattle, WA (Figure 3.1). It becomes the Duwamish River at the Black River confluence, 20 km from the mouth of the West Waterway. The Green River is regulated 100 km above the mouth at the Howard A. Hanson Dam, completed in 1961, to mitigate persistent downstream flooding. Since 1962, when the Howard A. Hanson Dam went into operation, peak flows have been attenuated while the annual mean discharge has stayed the same (Figure 3.2). Since the dam construction, the mean monthly maximum is 68 m^3s^{-1} and occurs in January, the annual mean is 39 m^3s^{-1}, and flood stage is 255 m^3s^{-1} and is rarely exceeded.

The United States Geological Survey (USGS) has maintained two major gauging locations along the Green-Duwamish River. Daily flow records from 1961-present are available at Auburn, WA (#12113000) 50 km from the mouth, and near Tukwila, WA above (#12113350) and below (#12113390) the confluence with the Black River. The two Tukwila stations are only 3 km apart and have intermittent flow records from 1961-present. There are two small tributary creeks between Auburn and Tukwila that contribute significant flow only in extreme precipitation events.

To date, two total suspended sediment load rating curves were developed to estimate upstream suspended sediment loading to the estuary. First using flows at Tukwila (#12113350) and load data from the 1960s at Tukwila (#12113350) (Harper-Owes 1981; Santos and Stoner 1972). Second, using flows at Auburn (#12113000) and 1990s load data at Tukwila (#12113390) (Embrey and Frans 2003). In this chapter we re-examine existing sediment load data, including new data from 2013-2020, to understand the magnitude and timing of suspended sediment coming into the estuary and attempt to find an improved rating curve method that can work across all existing datasets.

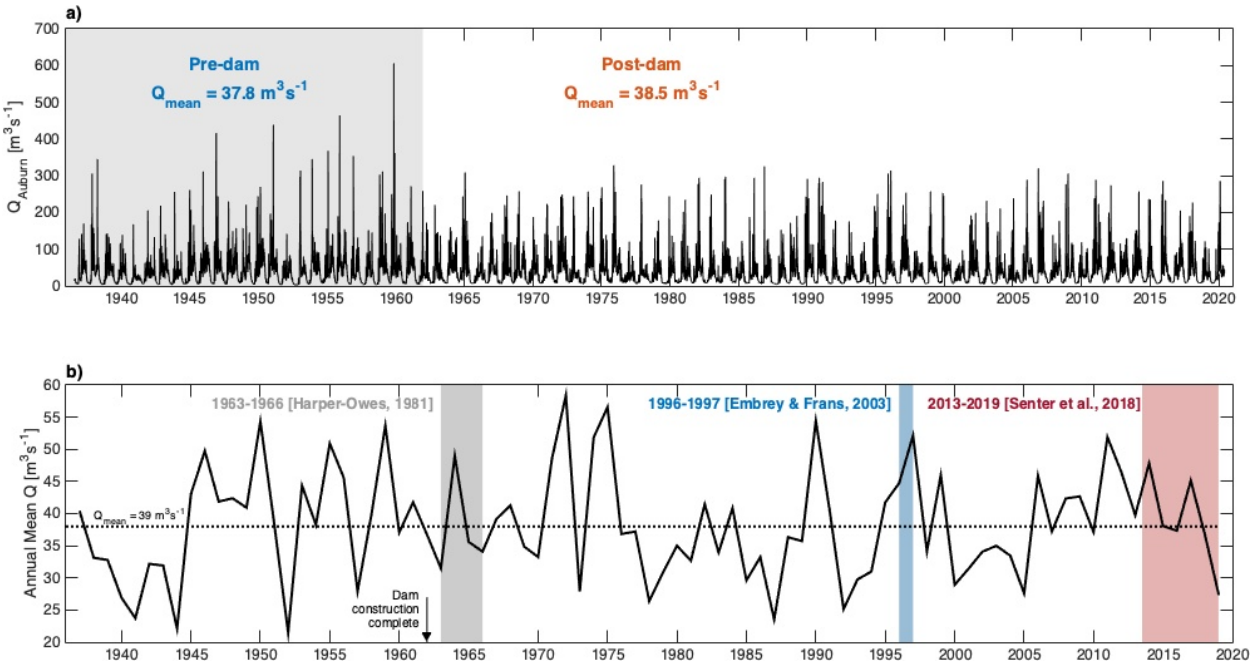

Figure 3.2. River discharge record at Auburn, WA.

River discharge (a) at Auburn, WA, with pre-dam period noted (gray shading). Annual flows for 1936-2019 (b) where black dotted lines indicate annual mean discharge and 1960s, 1990s, and 2010s data shown in gray, blue, and pink, respectively.

3.3 METHODS

3.3.1 *Data sources*

3.3.1.1 River discharge

Although flows at Tukwila are only 10% larger than at Auburn on average, the largest difference occurs at high flows when suspended sediment loads are likely to be largest. Since the Auburn station has a longer and more complete record of daily discharge, we use the available daily discharge measurements at Tukwila (both #12113350 and #12112290) to develop a linear relationship between daily discharge at the two locations. Note that developing independent regressions for the two Tukwila stations yielded coefficients that were statistically indistinguishable, despite the influence of the Black River. Thus we proceed to use one regression for flows at both stations as shown in Figure 3.3. This relationship does well, with an $R^2 = 0.97$. Additionally, the slope of 1.04 is similar to the ratio of the watershed areas, which is a good rule

of thumb for routing flows using a scaling approach. With the exception of the LDWG rating curve (see Section 3.3.2), we use daily discharge estimates at Tukwila that are derived from this regression for the remainder of the analysis.

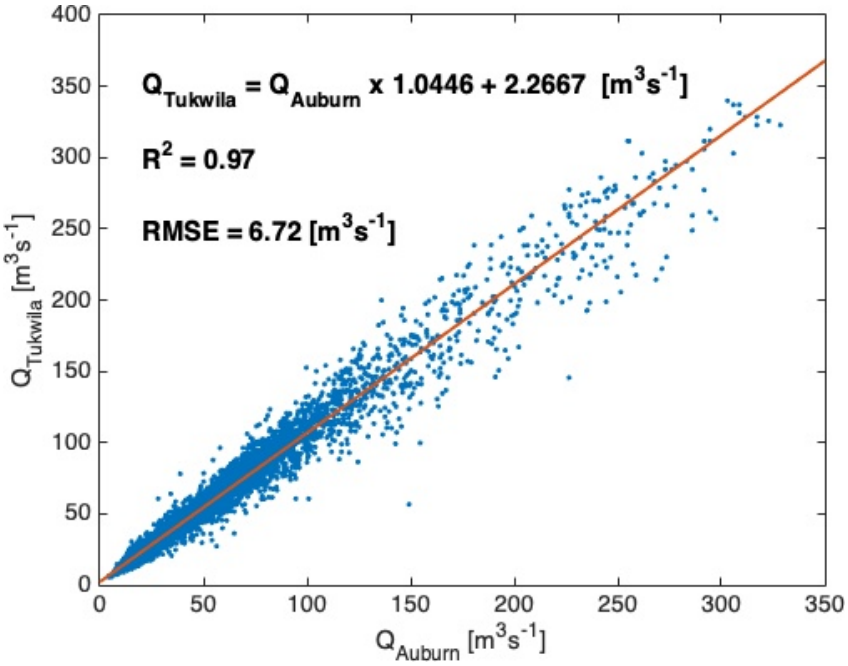

Figure 3.3. Auburn, WA to Tukwila, WA flow routing.

A regression model relating flows at Tukwila, WA to flows at Auburn, WA. Blue dots represent data and the linear regression is indicated by the orange line. Linear model, R^2, and root-mean-square error (RMSE) values noted.

3.3.1.2 Total suspended load

As described above, there have been three major USGS efforts to quantify total suspended sediment load delivery to the estuary. The first, daily mean single-vertical measurements at ~RK 18.7 (USGS #12113350) from 1963-1966, started just a year after construction was completed on Howard Hanson Dam (Santos and Stoner 1972). The second occurred approximately 3 km downstream (USGS#12113390) from 1996-1998 with approximately 13-20 instantaneous depth- and width- integrated samples per year (Embrey and Frans 2003). These data were presented and analyzed by Embrey and Frans (2003), however data collection continued through 2004. We use the full 1996-2004 dataset for our analysis. Because their estimates of *L* were generated from

instantaneous measurements of SSC and daily mean discharge their data is more scattered compared to the 1960s or 2010s data; some of the scatter in the data is likely due to tidal influence. Finally, from 2013-2017 a new effort used isokinetic depth- and flow-integrated methods to collect 33 discrete large-volume primary and replicate samples. The discrete samples were used in combination with 15-min. interval turbidity measurements to establish a relationship between turbidity and SSC and generate a time series of total suspended sediment load (Senter et al. 2018). The turbidity sensor has been maintained through 2020. There are brief periods where the turbidity sensor malfunctioned or was fouled, during which Senter et al. (2018) applied a relationship between SSC and daily discharge based on a regression of the discrete samples to fill the gaps. This regression is somewhat weak (R^2<0.6) due to scatter in the data and although drop-outs primarily occur during low flow and low loading conditions, here we have excluded those data. We apply a tidal filter to the remaining chunks of continuous data (each chunk >205 days) and generate daily averages.

The 1960s sampling was located just above the Black River confluence, however the Black contributes little sediment or flow, so for our purposes we consider all three datasets to be co-located. Despite being located within the tidal influence, the data did not show a dependence on tidal range, which suggests that local resuspension does not contribute significantly to the total suspended sediment load and that estimates at this location are representative of what is entering the estuary head at RK 14. All data are shown in Figure 3.4. When all three datasets are considered, two things are apparent: 1) the relationship between L and Q has evolved from the 1960s to the 2010s, and 2) each dataset indicates a different relationship between L and Q at low flow versus high flow.

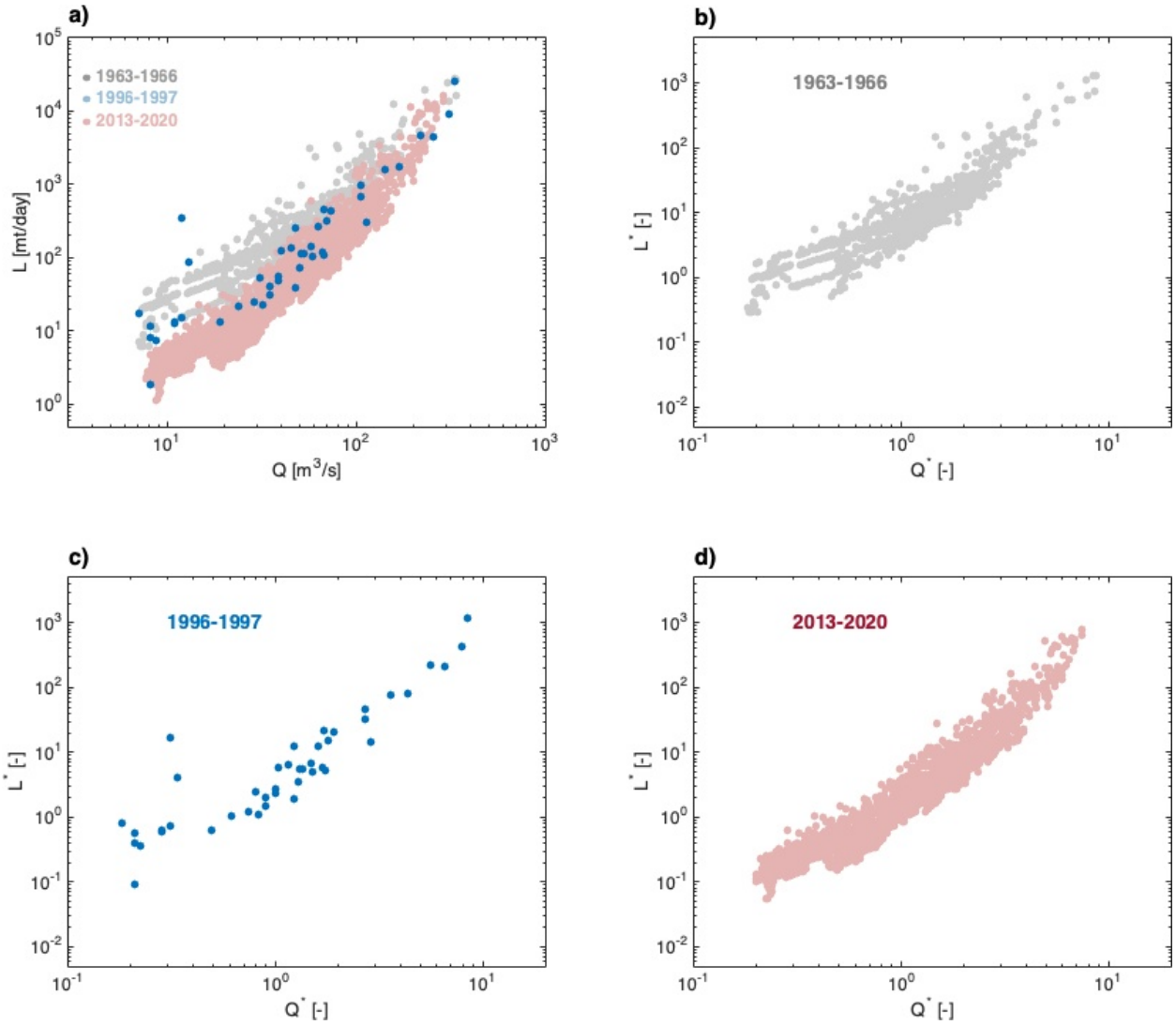

Figure 3.4. Existing total suspended sediment load data.

Panel (a) shows all three existing datasets from the 1960s (gray), 1990s (blue), and 2010s (pink). (b-c) Show individual plots of 1960s, 1990s, and 2010s data, respectively.

3.3.1.3 Fines and coarse suspended loads

Data for coarse and fine suspended loads are given in terms of the fines fraction (*FF*), or the fraction of the total suspended load composed of grain sizes less than 0.0625 mm. Existing FF data corresponds to the existing total suspended sediment load datasets detailed in Section 3.3.1.2. Older fines fraction data are considerably more scarce than total suspended load data. There are four and seven data points for the 1960s and 1990s, respectively. Modern fines fraction data is available from 2013-2017 at 15-min intervals.

3.3.2 *Previous approaches*

Three sediment rating curves have been developed for the total suspended sediment load at Tukwila, WA (see Figure 3.4). The first attempt was by Harper-Owes (1981) using the 1963-1966 dataset and using a relationship between total suspended sediment load (L) and mean daily discharge at Tukwila (Q) of the form $L = aQ^2$. Embrey and Frans (2003) used the linear attribution method to model L as $ln(L) = a + b\ ln(Q) + c\ [ln(Q)]^2$. The Lower Duwamish Waterway Group (LDWG) also developed a rating curve that was used to inform the Superfund Site remediation plan. The LDWG (2008)approach uses the Embrey and Frans (2003) curve for flows greater than the long-term mean and Harper-Owes (1981) below the long-term mean (LDWG 2008). The constant term in Embrey and Frans (2003) was increased from 12.6 to 13.4 to ensure load estimates are equal at the long-term mean. Additionally, the LDWG uses daily flows at Auburn, WA (~RK 48, USGS # 12113000) in their rating curve, despite the fact that it combines rating curves that were developed using flows at Tukwila, which are 5-15% larger. Senter et al. (2018) did not develop a rating curve, but their dataset contributes much-needed context for modern loads.

The shape of each dataset suggests that a piecewise approach might be helpful (Figure 3.4). A single linear relationship, such as the Harper-Owes (1981) rating curve will tend to underestimate high and low flow data. The Embrey and Frans (2003) approach addresses this, but the shape of the data do not suggest that a quadratic formulation is appropriate for all three datasets. The combined LDWG (2008) rating curve inherits the flaws of both approaches. Further, the trends in the datasets indicate a long-term decrease in loads, which suggests that no single rating curve is appropriate to estimate the entire 1962-2020 timeseries. We proceed to develop rating curves for each data set using a piecewise approach.

3.3.3 *Current approach*

3.3.3.1 Total suspended load

Piecewise rating curves are often used to develop rating curves (Ryan and Porth 2007; Templeton and Jay 2013). Instead of performing two regressions on two flow regimes, we use the following formulation such that only one regression per dataset is necessary (*D. Jay and S. Talke, personal communication*):

$$L^* = aQ^{*b}Max\left\{1, \left(\frac{Q^*}{Q_c}\right)^c\right\} \quad (3.1)$$

Where L^* is the non-dimensional total suspended sediment load, Q^* is the non-dimensional discharge, Q_c is the non-dimensional critical discharge, and a, b, and c are regression coefficients. Equation 3.1 becomes a multiple linear regression for $log(L^*)$ with $log(Q^*)$ and $log(max[1,Q^*/Q_c])$ as independent variables. The second term allows for a change in slope at Q_c. Sediment load and discharge are non-dimensionalized by 2013-2020 median sediment load (21.2 mt/day) and long-term mean discharge (38 m^3s^{-1}) to avoid constants with cumbersome units. Coefficients are determined using a robust regression that initially weights each point according to $w = [log(L^*)]^n$ where $0<n<6$ is determined iteratively to maximize R^2, minimize standard error, and produce symmetrical residuals. Q_c is chosen similarly and results were so similar (0.77-0.81) across the three datasets that Q_c = 0.80 or 80% of the long-term mean flow was used in each case. A change in slope can occur when sediment that is immobile or bed load at low flows is suspended during high flows. Since this process is dependent on discharge and the available grain sizes, it follows that Q_c is constant from 1963-2020 despite the fact that the dam likely reduces the overall supply of some grain sizes.

3.3.3.2 Fines and coarse suspended loads

Fine loads (L_{fine}) are calculated according to:

$$L_{fine} = FF \times L \quad (3.2)$$

Where FF is the fines fraction. Development of a fines rating curve proceeds in the same fashion as the total load rating curve, as described above, using L^*_{fine} in place of L^* in Equation 3.1. Similarly the fines load is non-dimensionalized by the median total load and discharge is non-dimensionalized by the long-term mean. Coarse loads are estimated from L-L_{fine} when the total and fine rating curves are applied to a time series of discharge.

3.4 RESULTS

3.4.1 *Total suspended load*

3.4.1.1 Previous approaches

Existing rating curves are shown in Figure 3.5. The Harper-Owes rating curve takes the standard form of $L = aQ^b$ and has an R^2 = 0.83. Compared to the 1960s data with which it was developed,

this rating curve tends to underestimate *L* at low flows and slightly underestimate it at high flows (Figure 3.5b). Compared to the entire 1966-2020 dataset, it is clear that it overestimates loads across the entire range of discharge.

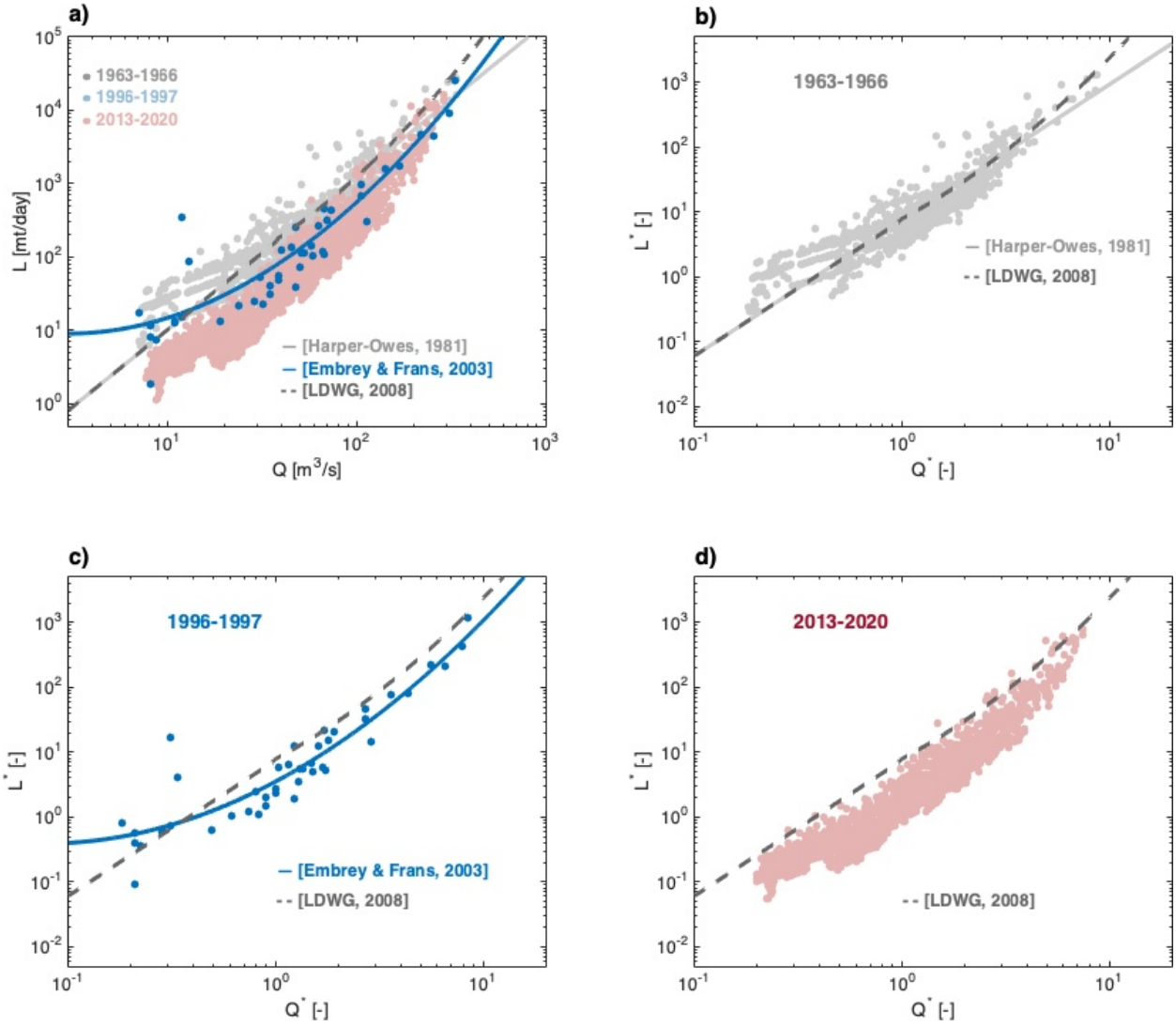

Figure 3.5. Existing total suspended sediment load rating curves.

Panel (a) shows 1960s, 1990s, and 2010s datasets in gray, blue, and pink circles, respectively. Gray solid, dark gray dashes, and solid blue lines represent the Harper-Owes, LWDG, and Embrey and Frans ratings curves, respectively. (b) shows 1960s data (gray circles) with Harper-Owes (gray solid line) and LDWG (dark gray dashed line) rating curves. (c) shows 1990s data (blue circles) with LDWG (dark gray dashed line) and Embrey and Frans (blue solid line) ratings curves. (d) shows 2010s data (pink circles) with LDWG rating curve (gray dashed line).

Embrey and Frans (2003) used the linear attributions method to develop a rating curve that is quadratic, i.e. $ln(L) \sim [ln(Q)]^2$. The authors did not report an R^2 value, but a visual inspection indicates that the quadratic approach generates a rating curve that fits the 1990s data well (Figure 3.5c). 1996 and 1997 were notable for high flows (see Figure 3.2) so these data could be biased and including the entire 1996-2004 dataset may be helpful. While the Embrey and Frans approach does well compared to the 1990s data, it does not accurately represent the other two datasets.
The LDWG rating curve is nearly identical to Harper-Owes, with a slight increase in the predicted load at high flows (Figure 3.5a,b). It tracks fairly well with 1960s data; while it probably overestimates low flow loads, it captures high load better than Harper-Owes (Figure 3.5b). However, the LDWG fit clearly overestimates 1990s for most of the discharge range (Figure 3.5c), significantly overestimates modern data (Figure 3.5d), and does not address the overall trend of decreasing loads (Figure 3.5a).

When all three datasets are considered and compared with existing rating curves, it is apparent that no individual rating curve is representative of the entire 1963-present period. Developing a rating curve for each time period would better represent long term trends, and taking a piecewise approach to individual rating curves would better represent loads throughout the range of discharges. Bearing in mind that accurately quantifying the amount of suspended sediment entering the estuary is critical for understanding the fate and transport of contaminated sediment within the estuary, we use these points as motivation to re-examine each dataset using a different approach.

3.4.1.2 Current approach

3.4.1.2.1 Total suspended load

For each of the three datasets a robust multiple linear regression was performed using Equation 3.1 and results are shown in Figure 3.6b,c,d. In each case the R^2 values are strong (>0.96) and the data are well represented throughout the range of flows. The coefficients derived from the 1998-2004 fit (Figure 3.6b) have the widest 95% confidence intervals because there are fewer data points than either the 1963-1966 or 2013-2020 datasets.

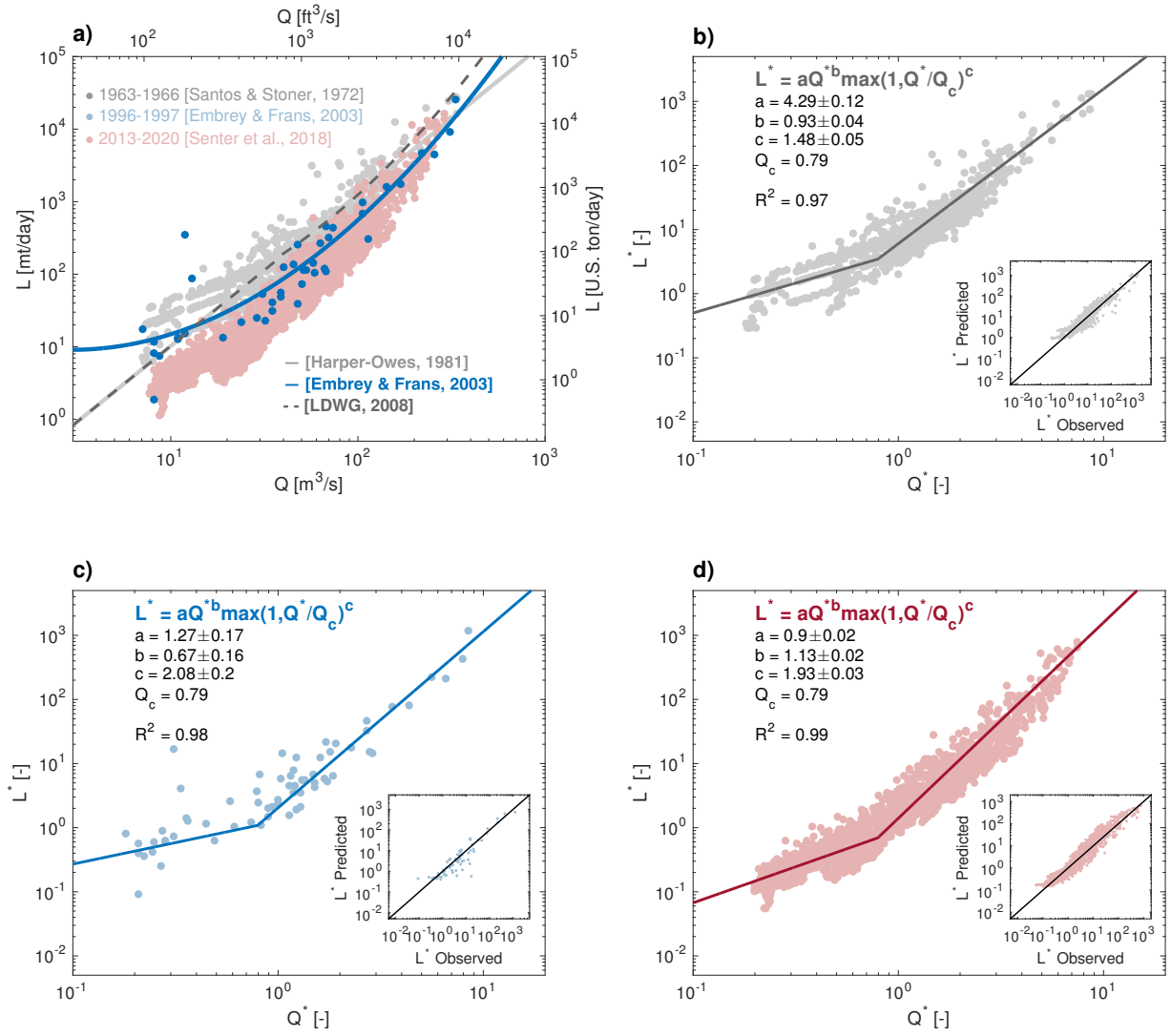

Figure 3.6. New suspended sediment load rating curves.

Panel (a) shows 1960s, 1990s, and 2010s datasets in gray, blue, and pink circles, respectively. Gray solid, dark gray dashes, and solid blue lines represent the Harper-Owes, LWDG, and Embrey and Frans ratings curves, respectively. (b) shows 1960s data (gray circles) and new rating curve (gray solid line) with fit parameters and performance at noted. (c) shows 1990s data (blue circles) and new rating curve (blue solid line) with fit parameters and performance as noted. (d) shows 2010s data (pink circles) and new rating curve (red solid line) with fit parameters and performance as noted.

The evolution of the coefficients also give some information about the changing relationship between L and Q from the 1960s to the 2010a. The constant term from Equation 3.1, a, has decreased from 3.8 to 0.75 indicating that the overall sediment load has decreased significantly. The coefficient b, which sets the slope until $Q = Q_c$, has increased slightly from 0.93 to 1.13. When flows exceed Q_c and part of the bed load is fully suspended, the slope, as given by $b+c$, has increased from 2.41 to ~3.06. Thus across the range of flows, L is more sensitive to Q. The 1990s regression fits this trend with two exceptions: first, c has already increased from 1.48 to ~2 and second, b is less than the other two fits. The likely reason for these discrepancies may be the larger error bounds due to this dataset having fewer points than the other datasets. However, since the upper portion of the rating curve is related to larger grained sediment suspended at high flows it also makes sense that c adjusted faster to "post-dam" conditions, as coarse sediment is likely to be trapped behind the dam.

The new fits also perform better when compared to data. Figure 3.7a shows daily average estimates of L from the new fit for the 2013-2020 data. The LDWG fit is shown for comparison since it is used to predict upstream "clean" sediment delivery. While the new fit fails to capture some of the higher frequency variations at low discharges, its fidelity to the overall trend is much improved, particularly at mid-range flows (10-100 m^3s^{-1}) where the LDWG fit tends to overestimate L by quite a bit. Figure 7b compares the 1960s timeseries of daily L with the LDWG and the new 1960s fit. Here, the current fit agrees well with the LDWG model for all but the lowest flows, where the LDWG tends to underestimate low flow loads. As low discharge loads tend to be quite minimal, it is likely that both models predict similar annual loads.

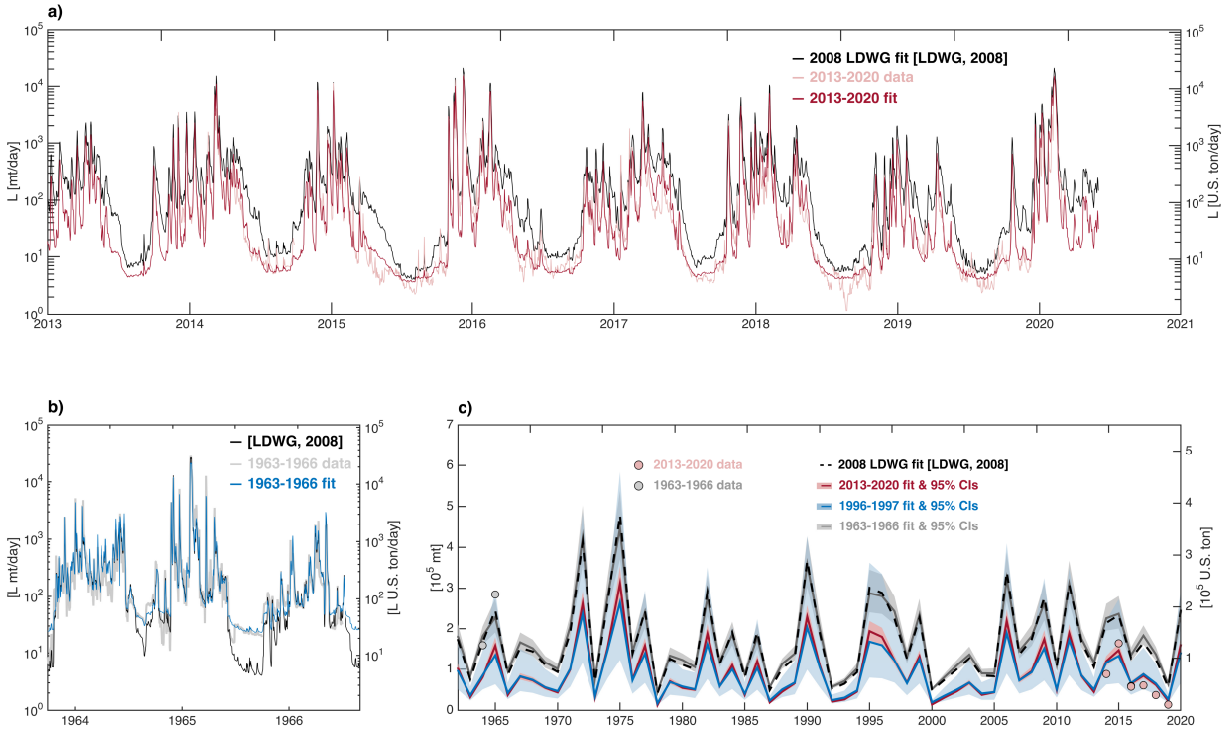

Figure 3.7. New daily and annual total suspended sediment load estimates.

Panel (a) shows new 2010s rating curve estimates (red) compared with 2010s data (pink) and LWDG rating curve estimates (black). (b) shows new 1960s rating curve estimates (blue) compared with 1960s data (gray) and LDWG rating curve (black). (c) compares annual load estimates from the LDWG rating curve (black dashed line), new 2010s rating curve (red solid line), new 1990s rating curve (blue solid line), and new 1960s rating curve (gray solid line). 95% confidence intervals for the new 2010s, 1990s, and 1960s ratings curve estimates are shown in pink, blue, and gray shading, respectively. Estimates of annual loads from 1960s and 2020s data are shown in gray and pink circles, respectively.

3.4.1.2.2 Fines and coarse loads

1960s and 1990s fraction fines data are not sufficient to develop meaningful rating curves (Figure 3.8a,b). It makes sense for 1960s to have a lower fines fraction as the system is still adjusting to the dam, which likely disproportionally affects the coarse suspended load. However it seems unlikely that the fines fraction in the 1990s would be higher than the 2010s. We proceed using the 2010s fines fraction data to develop a rating curve for the suspended fines load, and very roughly

estimate older loads assuming fines were 55% of the total load using the median of the 1960s fines fraction data.

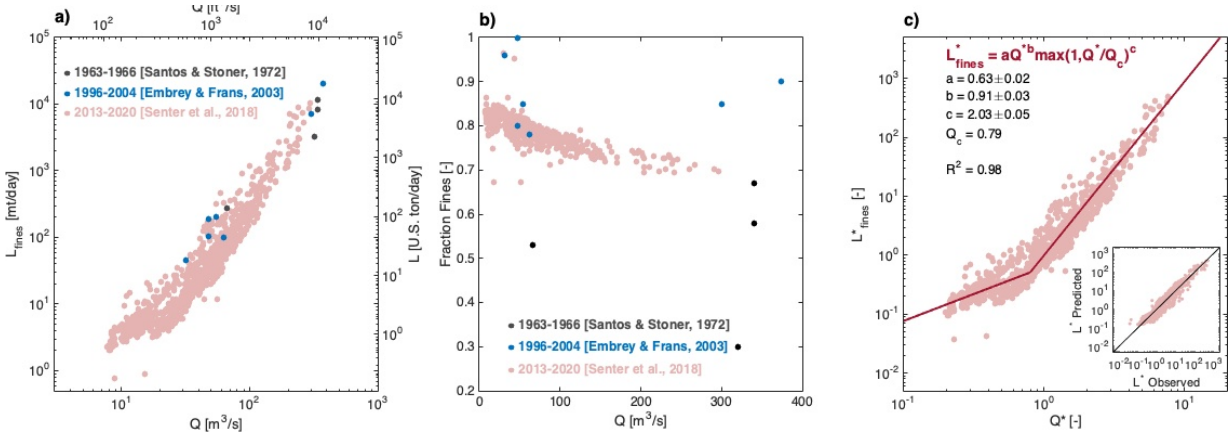

Figure 3.8. Existing fraction fines data and new fines suspended load rating curve. Panel (a) shows total suspended fines load as a function of river discharge for the 2010s (pink), 1990s (blue), and 1960s (gray). (b) shows fines fraction *FF* as a function of river discharge for the 2010s (pink), 1990s (blue), and 1960s (black). (c) shows the suspended fines load data (pink circles) compared with the new total suspended fines load rating curve (red solid line) with regression parameters and performance as noted.

A robust multiple linear regression was performed using the 2010s fines fraction and total load data. The fines load is not particularly variable and ranges from roughly 80% of the total load at low discharges to 70% at high discharges (Figure 3.8b). Regression results are shown in Figure 3.8c. The R^2 value for the fit is strong and 2013-2016 estimates compare well with the data (Figure 3.9a). Coarse loads are calculated by subtracting fines load estimates from total load estimates.

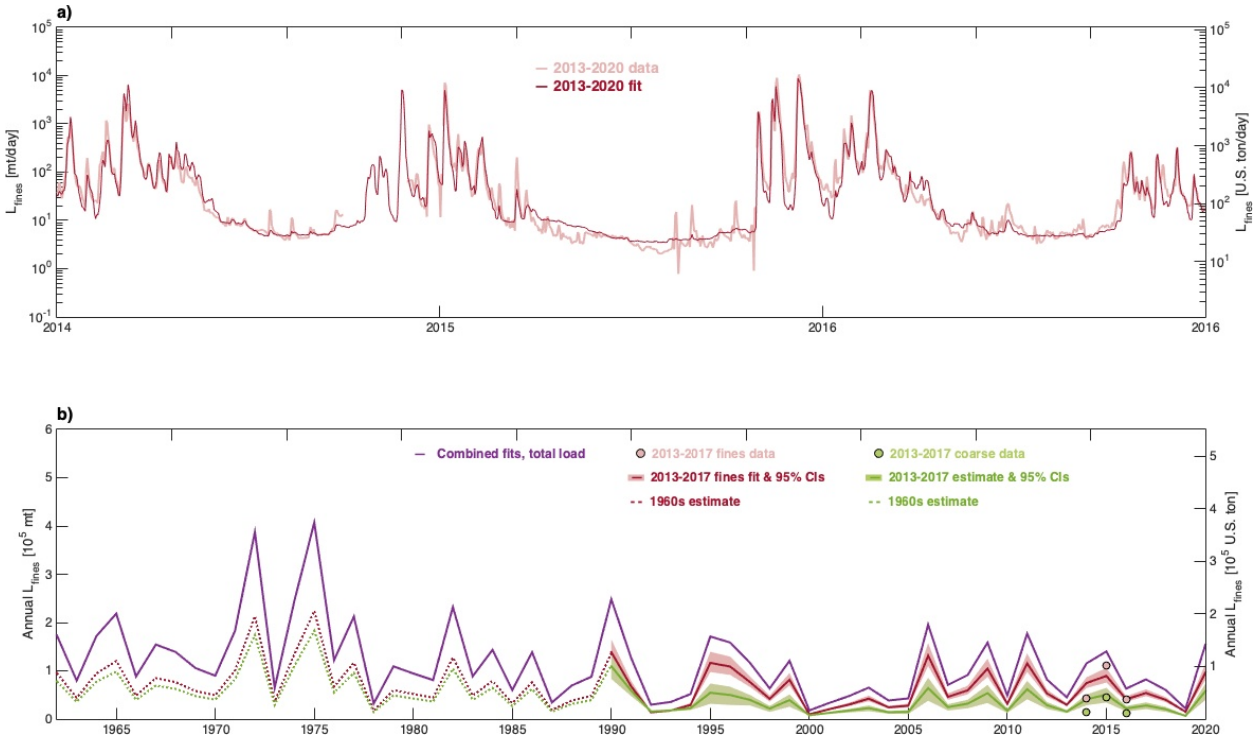

Figure 3.9. Daily and annual fines load estimates from new rating curve.

Panel (a) shows new 2010s rating curve estimates (red) compared with 2010s data (pink). (b) compares 2010s fines and coarse annual load data (pink and green circles) with new annual total suspended load estimates (purple solid line), new annual fines load estimates (red solid line), and new coarse load estimates (green solid line). 95% confidence intervals are shown in pink and green shading for the new fines and coarse rating curves, respectively. Pre-1990 projected fines and coarse annual loads are indicated by red and green dotted lines.

3.5 DISCUSSION

3.5.1 *Annual suspended load estimates*

Annual total suspended sediment loads were estimated using the three new fits (Figure 3.7c). The new 1960s rating curve produces estimates much higher than the other two new ratings curves, but is consistent with the two yearly load estimates from the 1960s data. The 1990s and 2010s ratings curves track very well with the yearly load estimates from the 2010s data. The LDWG fit produces the highest estimates of annual load and is consistent with 1960s data, while significantly

overestimating data estimates from the 2010s by a factor of 2. The trend in rating curve coefficients and annual load estimates from data suggest that the annual load has decreased since 1962, although without a longer time series the effect of climate change—either anthropogenic or natural variability—cannot be parsed. However, it is useful to generate a single time series of annual load that is informed by all three new models since no single model fits all of the available data.

To this end, we produce rating curves for intervening periods by interpolating model coefficients. The resulting "combined fit" matches the data (when available) and models for the three periods, while capturing the overall trend in decreasing load implied by the model coefficients (Figure 3.10). This approach is not definitive and there is no physical reason that rating curve coefficients should transition in a smooth linear fashion. These estimates merely represent a "best guess" that is as informed as possible by available data. The combined fit estimates suggest that the LDWG fit is much more appropriate for estimating 1960s and 1970s loads than more recent years, when it is increasingly an overestimate of annual load.

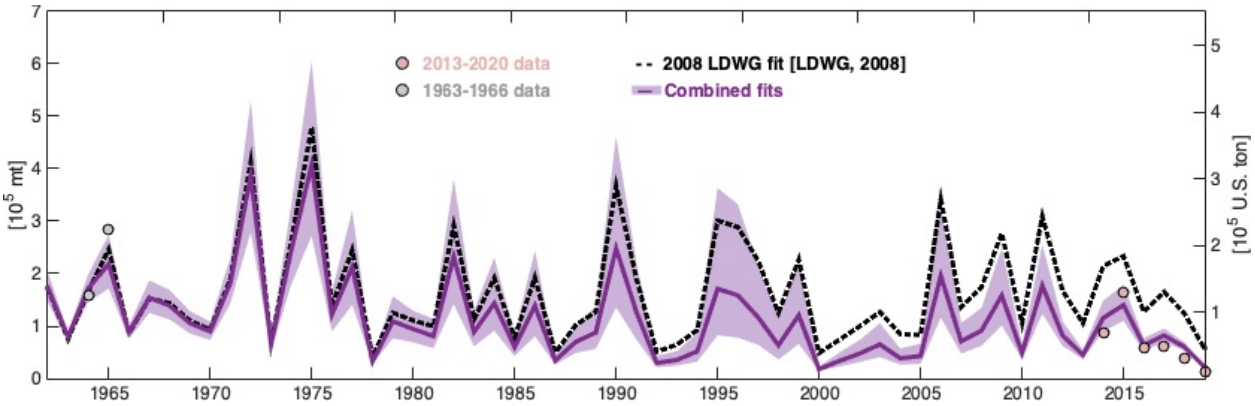

Figure 3.10. Annual total suspended sediment loads using combined new rating curves. Annual total suspended sediment load estimates using LDWG (black dashed line) and combines new rating curves (purple solid line) with 95% confidence intervals (purple shading). Annual load estimates from 1960s (gray circles) and 2010s (pink circles) are shown for comparison.

Published estimates of annual loads vary widely. Measurements of annual load for 1964-1966 were 52,000, 113,000, and 340,000 mt/year respectively, with 1964 being an average year in terms of discharge (Santos and Stoner 1972). Harper-Owes (1981) estimated annual loads to be 172,000-

205,000 mt/year for 1961-1981. Embrey and Frans (2003) estimated an annual load of 245,000 tons with a standard deviation of 54,000 for 1996-1997, which were both high flow years. Senter et al. (2018) estimate a mean annual load of 106,000 mt/year from 2013-2017. Taken together, and making allowances for interannual flow variability, these estimates are all roughly in agreement and one might assume that annual loads have been relatively unchanged at roughly 100,000 mt/year. However, the raw data show a clear trend in decreasing loads (Figure 3.4a) that is borne out in a time series of annual loads generated using all three rating curves (Figure 3.10). With this added context, it is clear that the agreement of previous estimates is simply the result of high interannual variability. If the Harper-Owes (1981) or LDWG (2008) rating curves were used to predict modern annual loads they would overestimate measurements by nearly a factor of two. 1962-1990 and 1991-2019 both have similar average values of PDO and ENSO indices, and we compare average loads from those two periods to estimate changes to annual load. We estimate annual loads to be 162,000±55,000 mt/year for 1962-1990 and 94,000±44,000 mt/year for 1991-2019. While both estimates indicate significant interannual variability, these results suggest that there is 42% less upstream sediment entering the estuary. This has major implications for the Superfund Site remediation plan, over 50% of which relies on monitored natural recovery.

Annual coarse and fine loads were calculated using the 2010s rating curve (Figure 3.9b), and both compare fairly well the estimates from data. On average, the annual total load is 70% fines and 30% coarse, which is consistent with fines fraction data and high discharges being responsible for the majority of annual sediment load. However, since the total load changed significantly over time, it is likely not meaningful to extend these estimates too far backwards. Despite the dearth of fines fraction data in the 1960s it is worth trying to estimate older fine and coarse annual loads using this data, if only very roughly. We use the median value of 1960s fines fraction, 0.55, across the entire range of discharges to estimate older fine and coarse loads. The two methods of estimation overlap in 1990 and we use that year as the dividing line between the two annual load estimates (Figure 3.9b).

3.5.2 *Timing of total suspended sediment loading*

Since the estuarine dynamics are driven by seasonal variations in discharge (McKeon et al. 2020), it is useful to examine the frequency and timing of suspended sediment loading. *Log(L)* shows a fairly strong correlation with the annual max discharge (Figure 3.11a), which suggests that loading is episodic and largely occurs during storm events. On average, 95% of the annual load is delivered in 181 days or roughly 50% of the year (Figure 3.11b). An examination of average monthly loads from 1962-2019 (based on "combined fit" estimates) shows that the relevant half of the year is from November to May (Figure 3.11c). November-February constitutes 73% of the mean annual load. However, it is worth noting that average spring and winter monthly loads show high interannual variability and can range from very little to nearly twice the mean annual load. This is reflected in the range of average annual loads, which range from 1.8×10^4 mt/year (2019) to 40.7×10^4 mt/year (1975). Loads during the summer (July-September) are uniformly quite low and show much less variability.

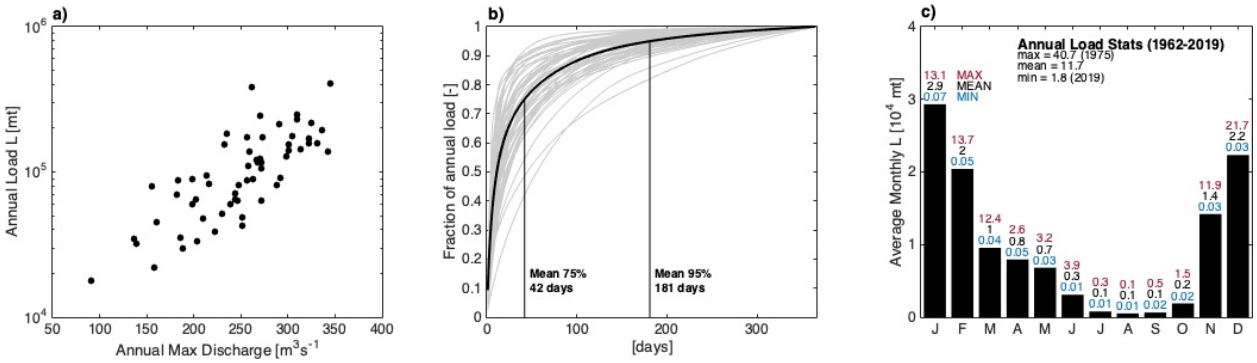

Figure 3.11. Timing of mean annual total suspended sediment load.
Panel (a) shows annual load as a function of annual maximum discharge. (b) shows 1962-2019 annual cumulative distribution functions (CDFs) in gray and mean annual CDF in black. The number of days to reach 75% and 95% of the mean annual load are noted. (c) shows mean monthly loads (black bars) for 1962-2019. Monthly mean, minimum, and maximum values are noted in black, blue, and red, respectively. Annual mean, minimum, and maximum values are provided for comparison.

3.6 CONCLUSIONS

A re-analysis of three existing datasets, ranging from 1966 to 2019, using an approach that allows for a change in slope in the suspended sediment load rating curve provides fits that are more representative of the data than previous attempts. We find a consistent slope break at 80% of the long-term mean flow and an increase in slope at larger flows, where most of the annual load occurs. A "combined fit" rating curve accurately estimates 1960s and 2010s annual loads, whereas no single model (generated here or previously) is appropriate for the entire period from 1961-present. Using the "combined fit", we find that most of the 11.7×10^4 mt long term mean annual load occurs from November-May during high discharge events. Modern annual load estimates may be closer to $9.4\pm4.4\times10^4$ mt/year. Estimates of fine and coarse loads derived from modern data indicate that 70% of the average annual total load is composed of fine sediment.

Chapter 4. Observations of suspended sediment in the Duwamish River Estuary

4.1 INTRODUCTION

Estuaries support a diverse array of industries and biological activity, and are often also in close proximity to urban populations (Ross 1995). The fate and transport of locally generated sediment and sediment from upstream is important for managing local ecosystems, exposure to contaminants, and coastal erosion. Estuarine sediment transport is controlled by the complex interactions of geometry, tides, riverflow, stratification, bottom sediment availability, and upstream sediment load (Geyer 1993). In many partially-stratified estuaries, this interplay often gives rise to one or more estuarine turbidity maxima (ETMs) that move with the salinity intrusion and can also be associated with geographic features (Burchard et al. 2018). In highly stratified estuaries with strong tidal currents, or tidal salt wedge estuaries, the interaction of tidal currents, strong vertical stratification, and suspended sediment is less well-studied.

In unstratified tidal flow, resuspension and erosion occur in a predictable cycle. Bed stress increases with velocity until a critical shear stress is exceeded (Shields 1936). Bed sediment is mobilized and entrained into the water column where it is held in suspension according to a balance between the vertical diffusion of bottom-generated turbulence and its own propensity to succumb to gravity and fall out of suspension. While in suspension, sediment is advected with the mean velocity and can travel some distance before it falls out of suspension and is deposited. As velocity decreases, so too does bottom-generated turbulence. Bed stress falls below the critical threshold and sediment is no longer brought into suspension. There is less turbulence diffused into the water column and the balance maintaining sediment in suspension tilts towards gravitational settling and deposition. This cycle is repeated according to the availability of bed sediment and may be modified by upstream loading.

Strong vertical stratification in the salt wedge interrupts this cycle in several important ways. Sharp vertical stratification, as is typical in the salt wedge, effectively divides the water column into two regions: the fresh upper layer, isolated from bed-generated turbulence and not in contact with the bed, and the saline lower layer. In the lower layer, stratification caps the vertical progression of

bottom-generated turbulence and thereby inhibits bed stress (Fugate and Chant 2005; Geyer 1993). The lower layer therefore has a decreased capacity to both suspend sediment and to maintain it in suspension. The saline and reduced-turbulence conditions are also favorable for flocculation. The upper layer, which generally carries sediment generated upstream, is isolated from bottom-generated turbulence, and is increasingly unable to maintain sediment in suspension (Kostaschuk 2002). The entrainment of salinity into the upper layer can also induce floc formation and increase gravitational settling into the lower layer.

The landward extent of vertical stratification, or the toe of the salt wedge, is the boundary between unstratified, high bedstress tidal flow and two-layered tidal flow. The location of the toe varies daily with the tides and seasonally with river discharge. In the Fraser, increased deposition was found during the advance of the salt wedge and enhanced resuspension was associated with the toe during retreat (Kostaschuk 2002; Kostaschuk and Luternauer 1989). Several studies have found that the tidal excursion of the salt wedge toe tends to be associated with trapping, in a tidally averaged sense (Geyer 1993; Jaeger and Nittrouer 1995). A study conducted in the Hudson found this to also be true of regions within the salt wedge that tend to form salinity fronts due to sharp changes in width and depth (Ralston et al. 2012). The ultimate fate of sediment trapped at the toe and within the salt wedge can also vary on longer timescales, as was also shown in the Hudson, where sediment tends to accumulate near the mouth during the freshet and is subsequently transported slowly landward with the salt wedge as riverflow drops (Woodruff et al. 2001).

The vertical structure of estuarine bed sediment can also play an important role in sediment transport. The bed is often covered by a very thin (2mm) “fluff layer” composed of loosely aggregated material that is easily remobilized and entrained into the water column (Maa et al. 1998; Mathew and Winterwerp 2017; Scully and Friedrichs 2007). Beneath the fluff layer, the bed may be either unconsolidated or settled (Mehta et al. 1989). Unconsolidated bed material has a higher porosity and can be resuspended when bed stress exceeds a critical value (Mehta et al. 1989). This material is also referred to as a “mobile pool” and is generally much thicker than the fluff layer (Geyer and Ralston 2018). Over time, hydrostatic pressure squeezes pore water from interstitial gaps and the material becomes consolidated and much harder to resuspend (Mathew and Winterwerp 2017; Mehta et al. 1989).

Consolidation is a complex process that is influenced by biological, chemical, and physical conditions (Winterwerp 2011). Very generally, and for a purely mud layer, consolidation time scales with the square of the layer thickness (Winterwerp 2011) and laboratory experiments have shown that the presence of sand increases consolidation rate (Torfs et al. 1996). Pure mud solutions in laboratory settings without external flow forcing can consolidate in 48 hr (Parker and Lee 1981) and Parchure and Mehta (1985) suggest that a muddy deposit a few centimeters thick might take a week to consolidate under moderate tidal forcing conditions. These timescales are on the order of the fortnightly neap-spring cycle and imply that consolidation must be considered in estuarine environments.

Some insight into consolidation timescales may be gained by considering modeling efforts. There are a variety of frameworks that may be employed (Winterwerp 2011), however observations of bed density showed an exponential approach to an equilibrium density (Hayter and Mehta 1986) and modeling consolidation empirically as a first-order relaxation has yielded good results (Sanford 2008). Using e-folding consolidation times of 1-3 days, the Sanford model (2008) showed that intratidal variations in bottom stress yield enough consolidation during and after slack to generate a small net deposit. This pattern is modified fortnightly by neap-spring variations in erosion, and is consistent with observations from the upper Chesapeake Bay (Sanford 2008) and Hudson River Estuary (Traykovski et al. 2004).

The Duwamish River Estuary is fed by the Green River and empties into the Puget Sound at Elliott Bay near Seattle, WA, USA (Figure 4.1). The estuary's proximity to the city and Port of Seattle made it an attractive location for various industries—most notably Boeing—and over time the waterway was engineered accordingly. In the early 1900s the lower 10 km were channelized and dredged for navigation; maintenance dredging is ongoing today. As a result there is a rapid increase in channel width at River Kilometer (RK) 10 and the slope of the lower 10 km is roughly three times steeper than prior to channelization (Figure 4.2). The legacy of discharging industrial waste directly into the waterway in the mid-1900s results today in the presence of toxic hydrocarbons such as PCBs, PDBEs, and PAHs in the bed sediment (LDWG 2010). In 2001 the lower 10 km was added to the national list of Superfund Sites. Locations with the highest concentrations of

contaminants have been remediated, but the large-scale cleanup is ongoing and will be monitored closely for several decades. Understanding sediment transport in this system is critical for determining contaminant fate and understanding the long-term viability of cleanup efforts.

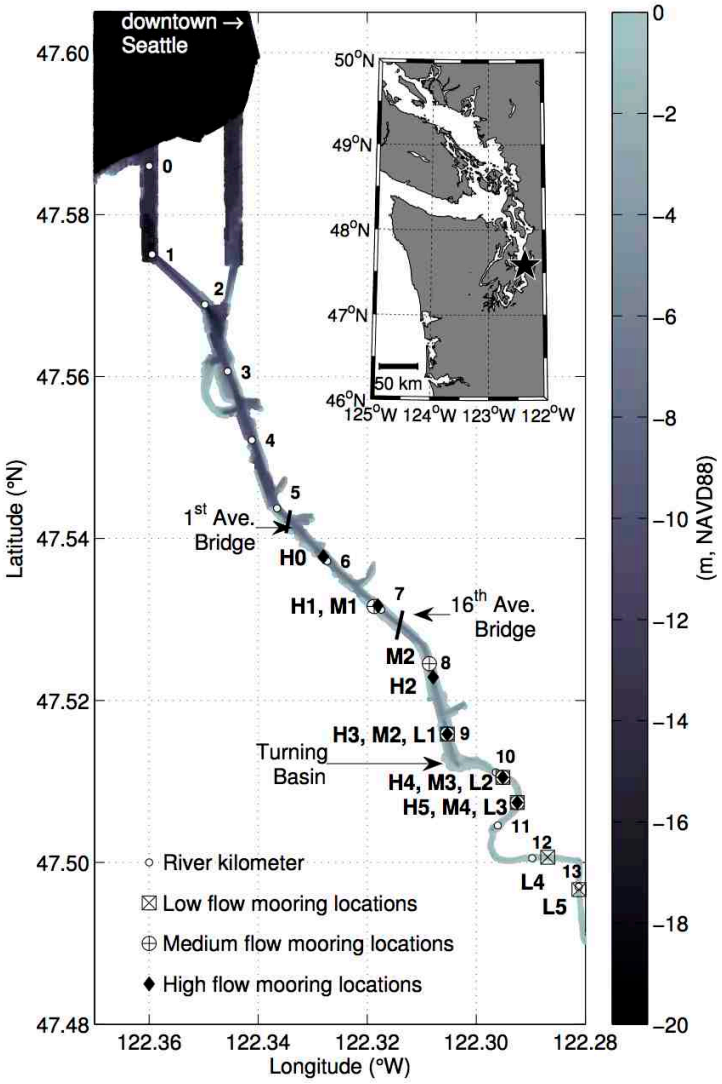

Figure 4.1. Local site map showing mooring locations.

Inset is regional site map of the Salish Sea and coasts of Washington and Vancouver Island. The black star is the Duwamish. Shading indicates bathymetry and mooring locations and mooring locations, River Kilometer, and features of interest are notes. Note that the shoreline corresponds to the edge of the shading since the Duwamish is so channelized.

Early studies on the Duwamish noted the persistence of a two-layered salinity structure throughout the year (Dawson and Tilley 1972) and estimates of salinity intrusion (Santos and Stoner 1972; Stoner 1967). Partch and Smith (1978) noted the occurrence of intense mixing periods during the ebb and attributed them to internal waves breaking at a slope break near the Turning Basin. Sediment loads were measured by the United States Geological Survey (USGS) from 1963 to 1966 and were determined to have an exponential relationship to mean daily discharge for loads exceeding 500 tons/day (Harper-Owes 1981). Using this analysis and flow frequencies dating back to 1961, the annual sediment load was estimated to be 172,000-205,000 mt/year, with 70-95% remaining in the estuary, primarily between RK 8 and the Turning Basin (Harper-Owes 1983).

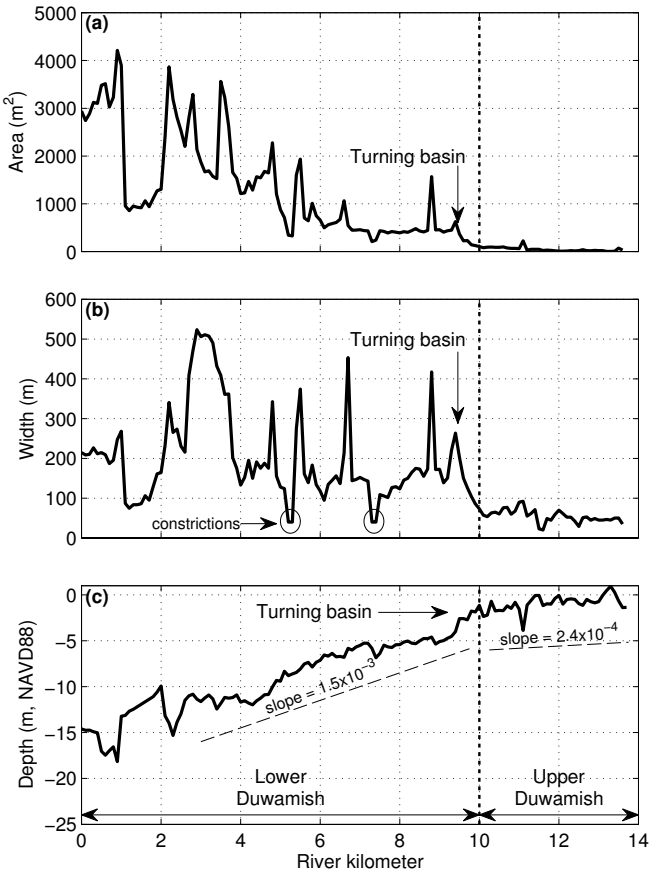

Figure 4.2. Channel geometry.

From top to bottom: a) channel cross sectional area, b) width, and c) thalweg depth. Constrictions at ~RK 5.5 and ~RK 7.5 are indicated in b) and the transition from a highly modified to more natural channel is indicated with the vertical dashed line at RK 10.

With its addition to the national Superfund List in 2001 due to toxic bed sediment came a number of studies characterizing bed sediment throughout the Duwamish. Bed sediments in the lower 10 km navigation channel are 80-90% clay and silt in the navigation channel with more variability on the benches (30-80% clay-silt) and little indication of a spatial pattern (LDWG 2009). Estimates of critical shear stress for locations in the navigational channel range from 0.16-0.24 Pa in the top 5 cm and 0.34-0.56 Pa for 5-10 cm (LDWG 2003). Age-dated cores indicate that the estuary is largely net depositional, although there is evidence of localized episodic erosion, with highly variable net sedimentation rates in the navigation channel ranging from 100 cm/yr in the Turning Basin to 1-10 cm/yr seaward of RK 8 (Harper-Owes 1983).

Early studies of the Duwamish focused on understanding salt wedge dynamics and Superfund Site work focused on characterizing bed sediment and contamination in the estuary. In this paper we present new measurements of SSC throughout the estuary from 2011-2013 in the form of transects and bottom-mounted moorings, which we use to investigate sediment sources in the estuary, transport pathways, the role of local resuspension, and relevant timescales.

4.2 BACKGROUND

The focus of this study is on the sediment transport processes within the salt wedge and the tidal excursion of the salt wedge, roughly from RK 5 to 14 (Figure 4.1). McKeon et al. (2020) found geometry to be a significant control on the salinity structure. RK 10 is a demarcation between the narrower, sinuous, more natural upstream geometry, and the highly engineered lower estuary (Figure 4.2). At RK 10, also known as the “Turning Basin”, the channel has a relatively uniform width of 120 m, the middle 40 m of which is dredged every two years to maintain a navigation channel. The channel cross-section is symmetric except at two slight bends at RK 5 and RK 8 (23° and 35°, respectively), and a nearly 90° turn at the Turning Basin. Two more significant lateral constrictions are located at RK 5.2 and 7.5 where bridge pilings are protected by wooden planks than span from the shore to the pilings.

Tides in the Duwamish are mixed semi-diurnal with M2 and K1 as the strongest constituents at 1.072 m and 0.834 m, respectively. The tidal range is 2.3 m and the mean diurnal range is 3.5 m. The tidal waveform is fairly unchanged as it propagates landward (Santos and Stoner 1972) and

the tidal influence extends to approximately RK 21 (Dawson and Tilley 1972). Under mean river discharge and tidal forcing, currents are roughly 0.40 ms^{-1} with a tidal velocity of 0.30 ms^{-1} and a river velocity of 0.10 ms^{-1}. Under high riverflow conditions (200 m^3s^{-1}) river velocities can reach 0.50 ms^{-1}. Depth-averaged currents lead the water surface by approximately 2 hr with a phase lead of 58° that is consistent with a shallow frictional estuary (Friedrichs and Aubrey 1994).

USGS gauging station # 12113000 is located 50 km from the mouth in Auburn, WA. There are two small tributary creeks below the gauging station that contribute significant flow only in extreme precipitation events. The Green River is regulated 100 km above the mouth at the Howard A. Hanson Dam, which was completed in 1961 to mitigate persistent downstream flooding. Since 1962, when the Howard A. Hanson Dam went into operation, peak flows have been attenuated and the mean discharge has decreased. Since the dam construction, the mean monthly maximum is 68 m^3s^{-1} and occurs in January. The mean monthly minimum is 9 m^3s^{-1} and occurs in August, and the annual mean is 38 m^3s^{-1} (Figure 4.3). Flood stage is 255 m^3s^{-1} and is rarely exceeded because of flow control at Howard Hanson Dam.

Santos and Stoner (1972) characterized the bed material in the lower 7.7 km as “estuarine ooze,” which may refer to a fluff layer that is often present in estuaries, and more recent observations indicate that little has changed. Particle grain size analysis shows that bed sediments in the lower 10 km are primarily fine-grained with an average mud-silt content of 60-80% in the navigation channel and 30-80% on the benches (LDWG 2009). Core data suggest that this area is net depositional over annual timescales and Sedflume data show an average critical stress of 0.16-0.25 Pa (LDWG 2009).

Chapter 2 found that seasonal changes to the salt wedge structure manifest during the greater ebb, when critical flow in the upper layer drives a strong response in the pycnocline at sudden changes in channel geometry, particularly for flows exceeding 50 m^3s^{-1}. By contrast, the shape of the flooding salt wedge is unaffected by changes in river discharge. Chapter 3 analyzed sediment loading to the estuary and found that upstream sediment loading occurs during only a few winter storms where flows exceed 150 m^3s^{-1}. Although river discharge may be high enough to

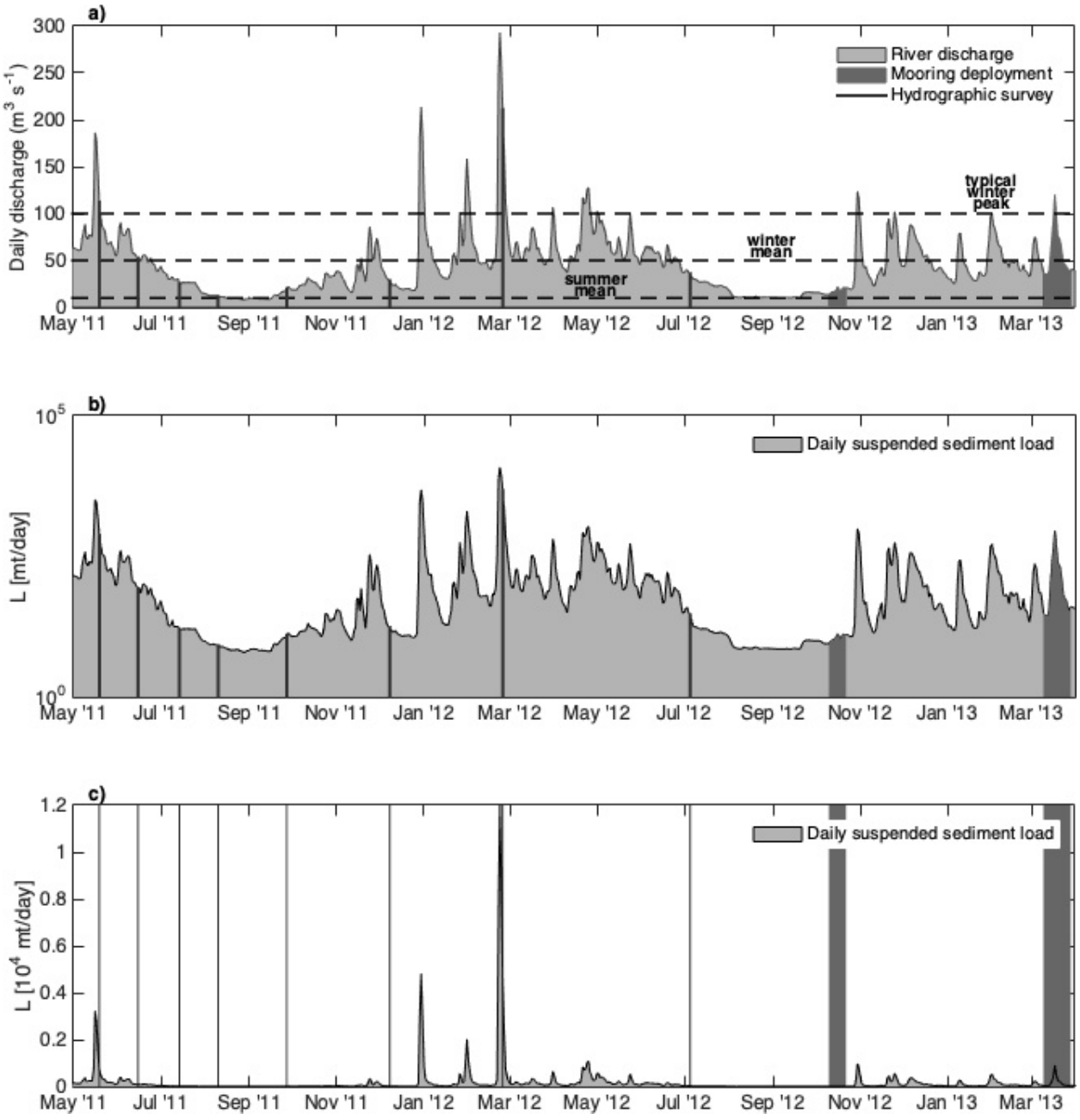

Figure 4.3. 2011-2013 daily discharge and total suspended sediment load.

From top to bottom: a) daily discharge at Auburn, WA, b) daily estimates of total suspended sediment loads (gray shading, see Chapter 3) shown on a logarithmic scale, and c) daily estimates of total suspended sediment loads (gray shading) shown on a linear scale. In each panel, field campaigns are indicated by dark gray vertical lines.

significantly affect the ebbing salt wedge, higher flows are needed for significant upstream loading. Very basically, estuarine suspended sediment concentration (SSC) tends to be a function of upstream loading, resuspension, and landward transport. In the Duwamish, upstream loading occurs at very high flows and may coincide with high bed stress and resuspension, particularly near the salt wedge toe. In addition, we expect that the salt wedge response near geometric features will influence SSC locally. Landward velocities in the flooding salt wedge are weaker than ebb velocities in the upper layer, but are independent of changes in discharge. Thus the salt wedge may be a weak, but persistent source of landward transport. Given that loading is relatively infrequent and confined to winter months, the time since loading may be a factor that influences supply in the estuary.

4.3 METHODS

4.3.1 *Sampling and instrumentation*

Beginning in May 2011 12-hr (greater ebb and flood) spring tide hydrographic surveys were completed on a roughly monthly basis. The conditions for each survey are summarized in Table 4.2 and Figure 4.3. Water velocity profiles were measured with a boat-mounted 1200 kHz bottom-tracking ADCP (Teledyne RDI) operating at 1 Hz in Mode 1 with 25 cm bins. Salinity, temperature, and SSC were measured with a SeaBird 19+ V2 profiler. Data were viewed real-time on the boat in order to approximate vessel position relative to the toe of the salt wedge. With the exception of the July 2012 survey, casts were taken continuously ("tow-yo-ing") near the toe to ensure high spatial resolution in the most dynamic region. In the more uniform portion of the salt wedge casts were spaced roughly 200 m apart. Casts during the July 2012 survey were spaced 400 m apart and those transects were not used in the following analysis of salt wedge salinity structure.

During select surveys a bottom-mounted 1200 kHz ADCP operating in Mode 12 with 25 cm bins, and top-bottom CT sensors were deployed at RK 7.5 for ~25 hrs. Note that biennial maintenance dredging by the United States Army Corps of Engineers (USACE) from RK 8-9.5 occurred in January 2012, significantly altering the thalweg depth in that region for the 2012 surveys and subsequent mooring array.

Table 4.2. Summary of hydrographic survey conditions

Date of hydrographic survey	Mean tidal range (m)	Mean river discharge (m^3s^{-1})
May 19, 2011	3.6	105
June 15, 2011	4.5	49
July 14, 2011	4.2	24
August 10, 2011	3.6	9
September 27, 2011	2.9	18
December 8, 2011*	3.8	25
February 24, 2012*	3.3	197
July 5, 2012*	4.5	35

**Indicates a concurrent 25-hr moored 1200 kHz ADCP with top-bottom CT sensors.*

While the tow-yo-ed transects provide excellent snapshots of spatial variability, they lack intratidal context that is necessary in a tidally dynamic system. In order to further investigate intra- and inter-tidal effects, an array of moorings was deployed for three two-week periods from October 2012 to March 2013. The mooring array consisted of five moorings with top and bottom salinity sensors, roughly equally spaced across the projected tidal excursion of the the salt wedge toe. The center mooring had a bottom-mounted SBE-16+, OBS-3+, and up-ward looking 1200 kHz ADCP (RDI) operating in Mode 12 with 25 cm bins. Note that bottom stresses were calculated using the lowest viable ADCP bin and a bottom drag coefficient of 3×10^{-3}. Below we examine the October 2012 and March 2013 deployments which were timed to capture typical mean summer and peak winter flows, respectively (Figure 4.3). During the high discharge deployment the ADCP failed after four days but was co-located with an acoustic Doppler velocimeter (ADV, Nortek) that was used to calculate bottom stress.

The OBS+ used for the transects and center bottom mooring was calibrated using 21 bottle samples collected from 2011-2012 using a 1-L Niskin sampler. Samples were collected under a wide range of tidal and river discharge conditions and there was no apparent seasonal pattern in the data. Since data were viewed real-time, bottle samples were strategically collected to encapsulate observed ranges of SSC. A linear regression was used to determine a relationship between OBS voltage and SSC, with a resulting $R^2 = 0.92$ (Figure 4.4).

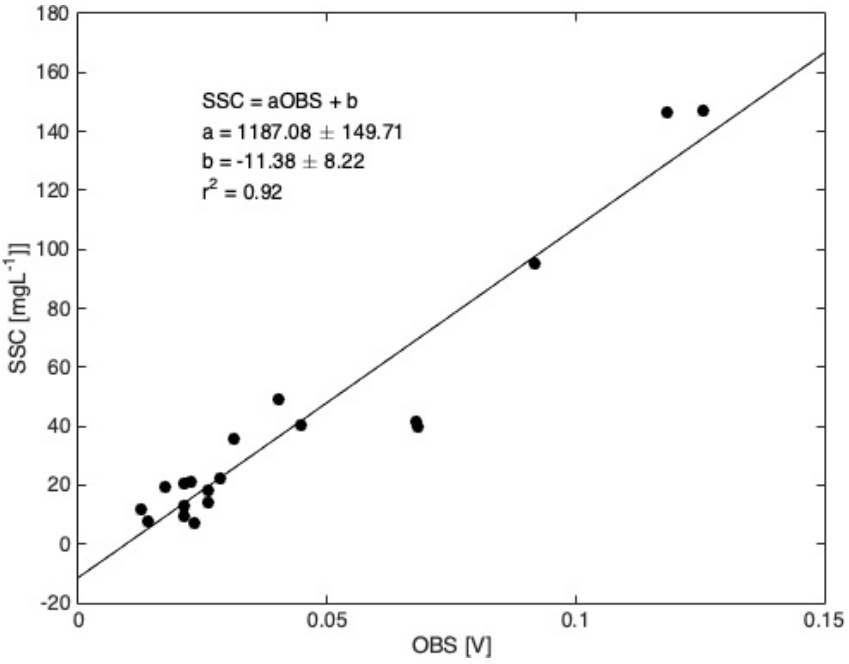

Figure 4.4. OBS calibration.

SSC derived from bottle samples plotted against co-located OBS values (black circles) and a calibration based on a linear regression (black line). Details of the linear regression are shown.

Figure 4.3 shows daily total suspended sediment load estimates for 2011-2013 (see Chapter 3). 2011 and 2012 experienced near average annual loads, while 2013 annual load was below average. For a modern annual total suspended sediment load of 9.5×10^4 mt, 0.5×10^4 mt and 0.2×10^4 mt (metric tons) contribute 5.3% and 2.1%, respectively. On this basis we define a major loading event as one with a peak exceeding 0.5×10^4 mt/day and a minor one to be between 0.2-0.5×10^4 mt/day. Events below the 0.2×10^4 mt/day threshold are not a significant portion of the annual load. The last major loading event before the October 2012 mooring deployment took place in March 2012 and the last minor event took place in May 2012. Thus the October 2012 deployment was well after any upstream loading. The 2013 annual load was below average; the winter of 2012/2013 saw only two storms that exceeded average peak winter flows and there were no major loading events. The high flow deployment took place during one of the peak flow events, and although it likely contributed significantly to the below average annual load for that year, the magnitude of the sediment load (10^3 mt/day) was an order of magnitude smaller than a major event (10^4 mt/day).

4.3.2 *Bottom stress*

Bottom stress, τ_b, is given by:

$$\tau_b = -\rho\langle u'w'\rangle \quad (4.1)$$

Where *u'* and *w'* are turbulent velocity fluctuations that can be estimated from bottom-mounted ADV measurements and angular brackets indicate a 10-min average. The density of water, ρ, can be determined from a co-located CTD. Without an ADV a quadratic drag law formulation is used in lieu of Equation 4.1:

$$\tau_b = \rho C_D u_b^2 \quad (4.2)$$

For transects and mooring deployments without an ADV, the bottom velocity, u_b, is estimated from the nearest ADCP bin to the bottom, typically 0.8 mab (meters above bottom). The bottom drag coefficient, C_D, is typically 3×10^{-3} for estuarine environments. Water density is determined from the nearest cast depth or a co-located CTD sensor.

4.3.3 *Suspended sediment flux*

In the case of lateral homogeneity, along-channel suspended sediment flux, *F*, at an along-channel location *x* is given by:

$$F = \int_0^h ucbdz \quad (4.3)$$

Where *u* is along-channel velocity, *c* is suspended sediment concentration, *b* is the channel width, and integration occurs from the bed to *h,* the height above the bed. When calculating near-bottom flux from bottom-mounted moorings *h* is the height of the velocity measurement, 0.8 mab, and both velocity and SSC are assumed to be uniform over that distance.

4.3.4 *Upper layer removal rate*

The removal rate of suspended sediment from the upper layer between two locations x_1 and x_2 can be estimated by taking a control volume approach:

$$F_1(x_1) - F_1(x_2) = -\int_{x_1}^{x_2} w_s cbdz \quad (4.4)$$

Where $F_1(x)$ is the upper layer sediment flux at along-channel location *x*, w_s is the settling velocity, *c* is the suspended sediment concentration, and *b* is the channel width. The difference between

upper layer sediment fluxes is upper layer removal rate, which is given by gravitational settling. Upper layer flux is calculated using Equation 4.3, with integration bounds spanning the upper layer thickness, which is defined by the distance between the 14 psu isohaline and the water surface. The major simplifying assumption used here is that there is very little vertical exchange between the upper and lower layer, either via mixing or turbulent diffusion. Mixing would be indicated by a change in salinity from x_1 to x_2 and would be likely to affect the mass of suspended sediment in the control volume by dilution since stratification in the pycnocline inhibits turbulence and the ability to maintain sediment in suspension (Kostaschuk and Luternauer 1989). No change in salinity means that there is little mixing happening and would be evidenced by horizontal isohalines. Further evidence that mixing is unimportant can be estimated from the upper layer flow rate at the upstream and downstream boundaries. We further assume that vertical turbulent diffusion of near-bottom SSC is inhibited by stratification and can also be neglected for this calculation.

4.4 OBSERVATIONS

4.4.1 *Hydrographic surveys*

Fifteen transects (T1-T15) from discharges ranging from 9-197 m^3s^{-1} are shown in Figure 4.5. This range of flows includes an annual maximum loading event (T1-T3), a smaller loading event (T4-T6), and a period of low flows and negligible loading (T7-T15). The locations of elevated SSC in these transects point to several different processes that contribute to sediment fluxes in the system, which differ between survey conditions.

Examination of the intratidal variability of SSC within the tidal excursion of the salt wedge provides a qualitative description of the processes that may trap, resuspend and export sediment during a tidal cycle. During maximum ebb there is often elevated SSC near the salt wedge toe; this is most clearly illustrated in Figure 4.5: T4. Later in the tide, ebbing velocities wane in the upper layer and the salt wedge is pushed to its seaward limit for the tidal cycle (Figure 4.5: T3, T5, T8, T11, T14). The area recently occupied by the salt wedge shows high SSC despite lower velocities and presumably lower bed stress. This may be the result of easily resuspended material that was shielded by the presence of the salt wedge earlier in the ebb. On flood, there can be a significant

amount of sediment carried in the salt wedge despite the absence of upstream loading (Figure 4.5: T9, T12). Transects suggest a pattern of resuspension, re-entrainment, and landward transport of SSC near the salt wedge toe. Material is resuspended during max ebb; a fraction of the material is exported seaward and some settles into the salt wedge. Salt wedge retreat during later ebb exposes easily re-entrained material that is suspended into the water column. The flooding salt wedge carries retained material landward.

Seasonally, SSC in the estuary varies widely in response to upstream loading. During a major loading event SSC in the estuary is dominated by SSC in the upper layer (Figure 4.5: T1-T3). The salt wedge appears to have very little sediment from early ebb to early flood, although a transect capturing the full flooding salt wedge is not available. After a smaller loading event (Figure 4.5: T4-T6) SSC in the upper layer is comparable with SSC in the salt wedge during maximum ebb (Figure 4.5: T4). Late ebb (Figure 4.5: T5) again shows high SSC in an area recently occupied by the salt wedge and not experiencing high velocities. Again, only a small portion of the flooding salt wedge was captured (Figure 4.5: T6), but the lack of SSC right at the toe and slightly higher near-bottom concentrations just seaward suggest that higher SSC is being advected from seaward portions of the salt wedge. Subsequent transects occur one month (Figure 4.5: T7-T9), 83 days (Figure 4.5: T10-T12), and 203 days (Figure 4.5: T13-T15) after the smaller loading event. The upper layer no longer carries a significant amount of suspended sediment; the highest SSCs occur in the salt wedge, just above the toe, or in low velocity areas recently occupied by the salt wedge. Overall, transects indicate that upper layer SSC is linked to upstream loading and that salt wedge SSC is not. Periods when SSC in the salt wedge exceeds that of the upper layer suggest that the source of sediment is not from upstream—at least recently. However, nearly 7 months after the smaller loading event, there is very little suspended sediment anywhere in the estuary (Figure 4.5: T13-T15); whatever retention mechanisms are at work maintaining a portion of incoming sediment within the upper estuary after a loading event, there are clearly diminishing returns.

The ebbing salt wedge structure varies seasonally with discharge, and in particular, width constrictions at the bridges can induce a sharp landward tilt in the pycnocline when upper layer velocities are sufficient for critical flow (McKeon et al. 2020). These areas appear to be associated with locally high SSC in the salt wedge regardless of whether or not the pycnocline intersects with

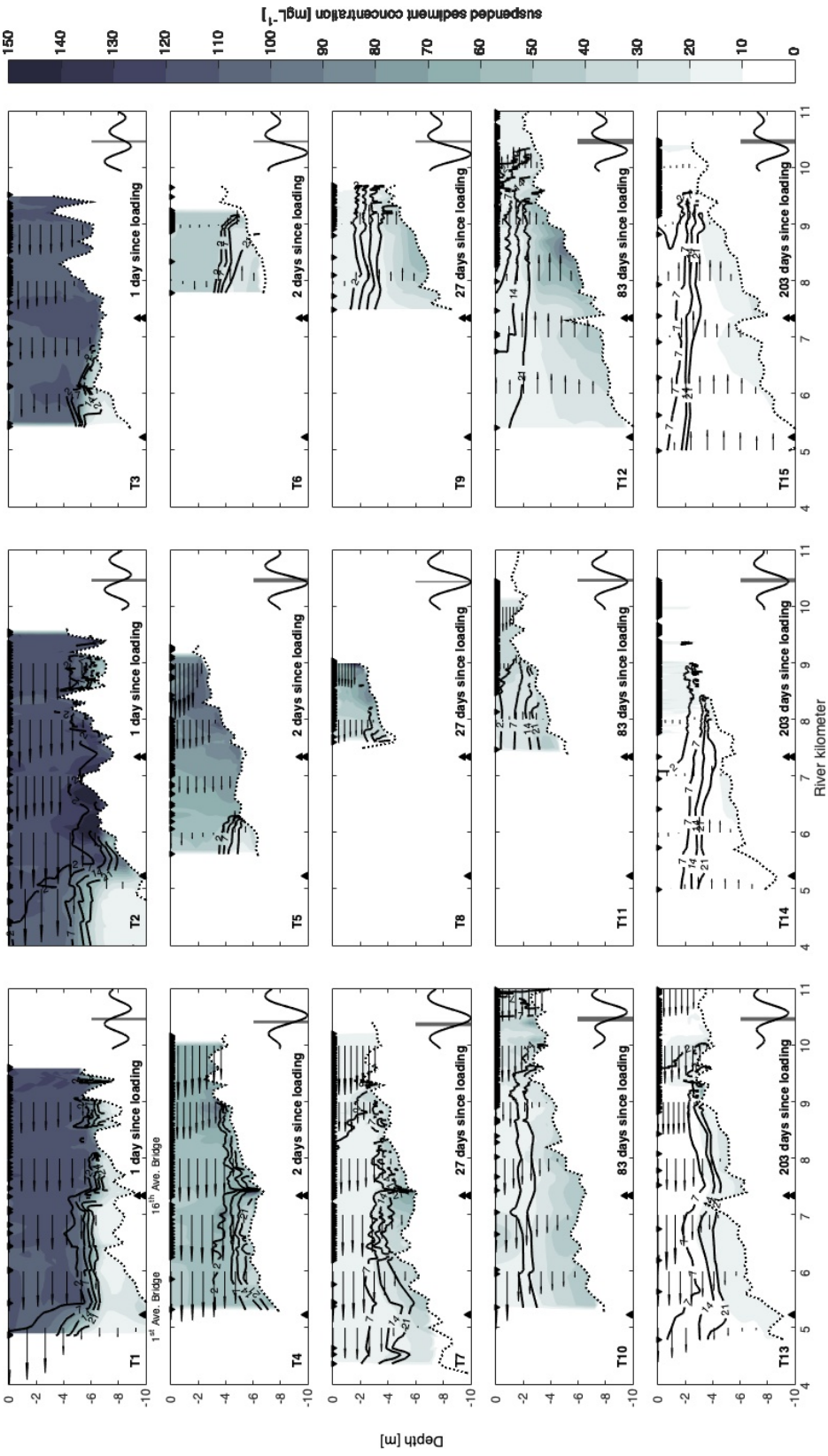

Figure 4.5. Along-channel transects of SSC.

(T1-T3) February 2012 transects, Q = 197 m^3s^{-1}. (T4-T6) May 2011 transects, Q=105 m^3s^{-1}. (T7-T9) June 2011 transects, Q=48 m^3s^{-1}. (T10-T12) August 2011 transects, Q=9 m^3s^{-1}. (T13-T15) December 2011 transects, Q=25 m^3s^{-1}. For all panels (a-o) 2,7,14, 21 psu isohalines (thick black lines), along-channel velocity (thin black arrows) , cast locations (small black triangles at depth = 0), bottom depth (dotted black line), and tidal stage (gray line) is approximately from peak ebb to late ebb to peak flood, from left to right. Single and double black triangles at depth = -10 m are the 1st and 16th Ave Bridge constrictions.

the bottom to form a salinity front (Figure 4.5: T1, T2, T4, T7). In the case of T2, the constriction forces the pycnocline to tilt landward enough for the baroclinic pressure gradient to overcome the ebbing tide and generate landward flow in the salt wedge (Figure 4.5: T2). The near-bottom flow convergence may help to maintain the local SSC maxima and to retain incoming sediment in the estuary.

Overall, high-resolution transects show a high degree of SSC variability in the estuary, but several patterns emerge. Suspended sediment in the upper layer is determined by the magnitude of upstream loading and the amount of time that has passed since the most recent loading event. The highest SSC is observed throughout the ebbing upper layer during loading events. There is a recurring local SSC maximum during late ebb associated with areas recently occupied by the salt wedge and relatively low velocities. The maximum does not persist throughout the tide and the magnitude decreases with time from loading event. The salt wedge shows higher SSC after loading events, although eventually there appears to be no available source of sediment. Taken together, this suggests that some fraction of incoming sediment is kept in the estuary, and that the retained sediment is available to be reworked over several months. Some mechanism—for example, either the seaward transport of near-toe material or consolidation—gradually depletes the supply of retained sediment.

4.4.2 *Moorings*

4.4.2.1 Low flow

Data from the center mooring during the low flow October 2012 deployment (L3, Figure 4.1) are shown in Figure 4.6. Although 2012 was an average year in terms of annual load, the deployment period is months removed from the last loading event (Figure 4.3c). Discharges are near the mean low-flow throughout, although there was a small storm event (Figure 4.6a). For the range of flows during the deployment the salt wedge toe was mostly upstream of the Turning Basin where the channel is narrower and shallower (Figure 4.2), and the bottom is sandier (LDWG 2009). The mooring was located at ~RK 10.6. Tidal elevation shows that tides transitioned from neap to spring during the deployment (Figure 4.6b). Bottom salinity varies between fresh and 28 psu (Figure 4.6d), which indicates that the mooring was located in the tidal excursion of the toe. During the last three days of the deployment, the increase in discharge coincides with the transition to spring

and the salt wedge was pushed further seaward. This is evident in the bottom salinity which shows longer periods of zero salinity during greater ebb.

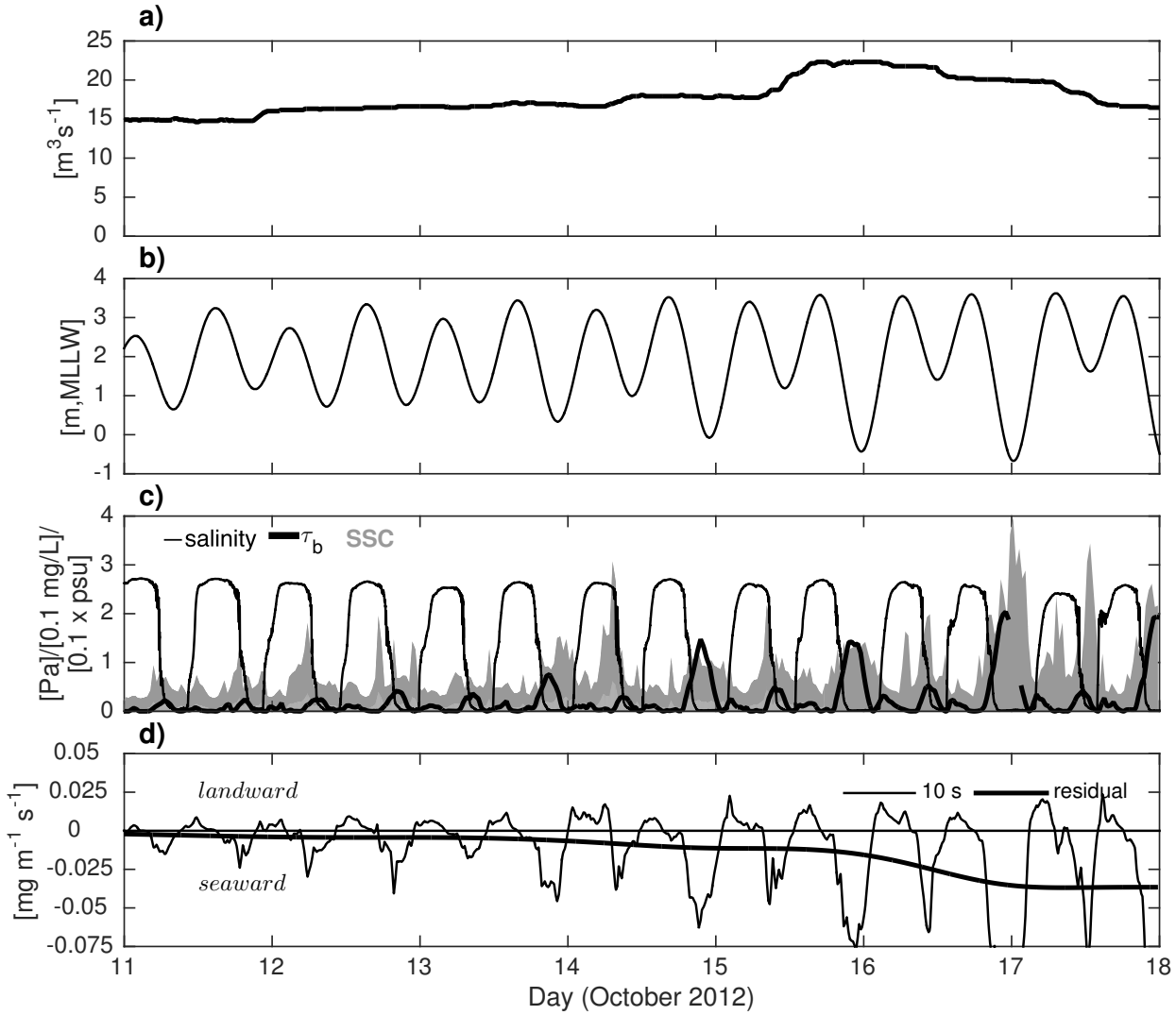

Figure 4.6. Low flow mooring data.

Low flow mooring deployment daily discharge at Auburn, WA (a), and tidal variation (b). Panel c) bottom salinity (thin black line), SSC (gray shading), and bottom stress (thick black line). Salinity and SSC are scaled by a factor of 0.1 for ease of visualization. d) shows the instantaneous (thin black line) and residual (thick black line) near-bottom along-channel sediment flux per unit.

The landward edge of the toe has been associated with enhanced resuspension in the Fraser (Kostaschuk 2002; Kostaschuk and Luternauer 1989) and the potential for this to occur in the contaminated reaches of the Duwamish is of interest. Bottom stress is greatest during the ebb, and increases during the greater ebb with increasing discharge and the transition to spring tide Figure 4.6c). As the salt wedge is pushed seaward the bed is exposed to unstratified flow and higher bed stress for more of the ebb. The LDWG (2003) estimated that the critical stress for resuspension is 0.16-0.25 Pa and we see peaks in SSC that correspond with bottom stresses that match or exceed those values (Figure 4.6c). In combination with the fact that there is very little upstream loading (Figure 4.3c), this suggests that local resuspension is occurring. However, there are also peaks in SSC that coincide with the passage of the toe rather than bottom stress, for example the greater ebb on October 14 (Figure 4.6c). This may be the re-mobilization of fluff or sediment resuspended upstream, trapped in the toe, and advected past the sensor.

Near-bottom along-channel sediment fluxes are shown at 10 s intervals and tidally filtered in Figure 4.6d. Early in the deployment net transport is slightly seaward due to sediment pulses associated with the passage of the toe. Stronger seaward transport occurs during spring tides as greater ebb bed stress increases and coincides with SSC peaks. This suggests that resuspension in the toe can be a driver of seaward transport during spring tides, and that the advection of SSC associated with the toe can result in a small amount of seaward transport.

4.4.2.2 High flow

High-flow mooring data (H2) are shown in Figure 6. H2 was located at ~RK 8 (Figure 4.1) for nearly two weeks in March 2013. The deployment captures the transition from the long-term mean (40 m^3s^{-1}) to a 125 m^3s^{-1} storm event (Figure 4.7a). While this is considered a large discharge event, estimated upstream loading is quite moderate (Figure 4.3c). In fact, the annual load for 2013 was below average and there were no storms big enough to produce a major loading event. Tides vary from neap (or minimal diurnal equality) at the beginning of the deployment period to spring (or increased diurnal inequality) toward the middle and end. Bottom salinity (Figure 4.3b,d) stays high except during the greater ebb during the storm (Figure 4.7b). Salinity decreases markedly during the storm but never becomes entirely fresh. The presence of the toe—indicated by decreasing, but not entirely fresh, salinity—inhibits bottom stress so that the highest stresses are

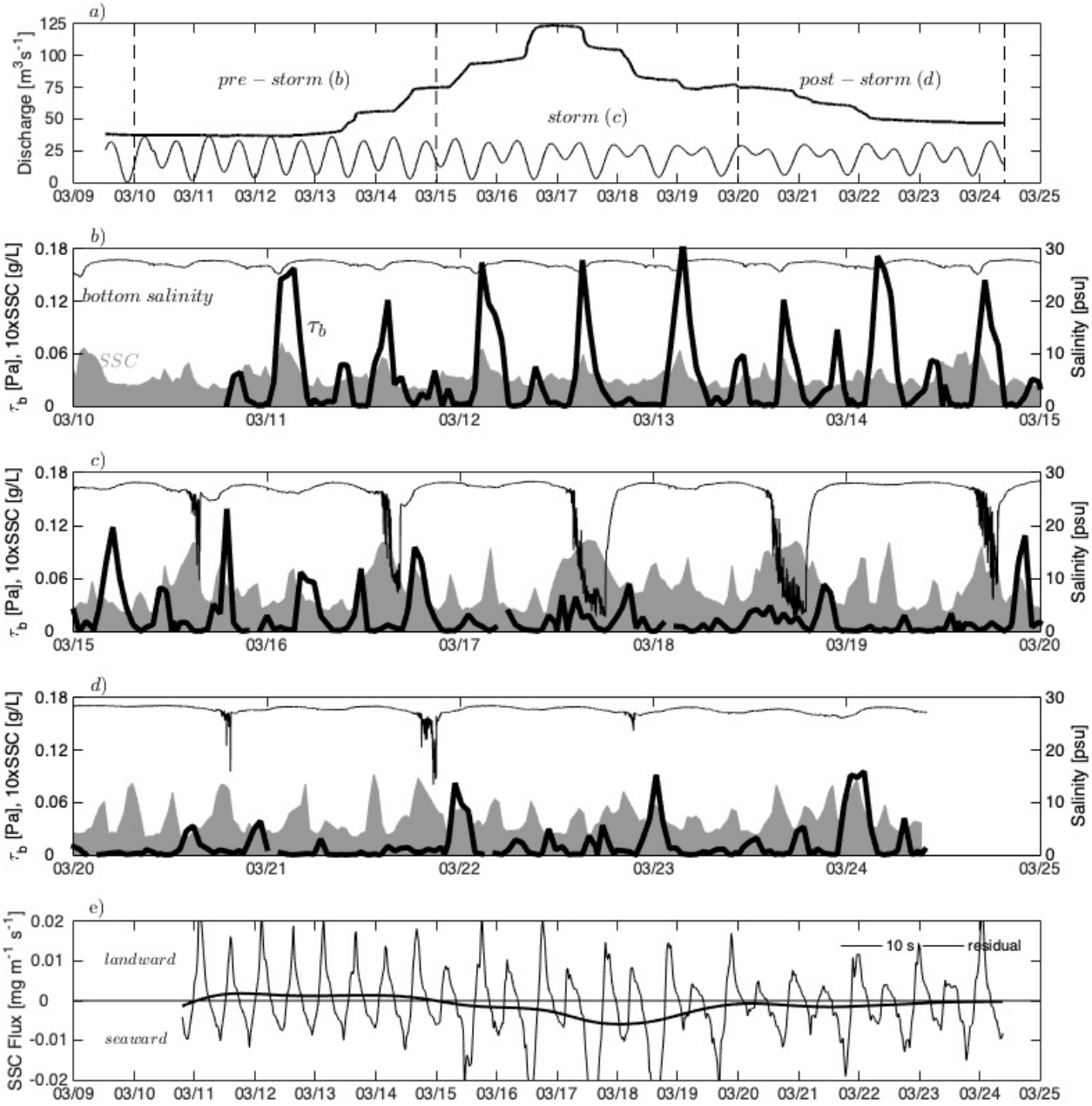

Figure 4.7. High flow mooring data.

Panel a) shows high flow mooring deployment daily discharge at Auburn, WA (thick black line) and tidal variation (thin black line). Relevant periods (storm, pre-storm, post storm) are label accordingly and correspond to (b-d). (b-d) bottom salinity (thin black line), SSC (gray shading), and bottom stress (thick black line). SSC is scaled by a factor of 0.1 for ease of visualization. e) shows the instantaneous (thin black line) and residual (thick black line) near-bottom along-channel sediment flux per unit.

still during the flood. Thus the mooring is in the salt wedge, except during the storm, when it is in the toe on greater ebb. For greater clarity, we break the deployment up into three periods: pre-storm, storm, and post-storm.

4.4.2.2.1 Pre-storm

During the pre-storm period (Figure 4.7a) the mooring is in the salt wedge. Bottom stress peaks during the flood but is nearly an order of magnitude smaller than bottom stress peaks in the tidal excursion of the toe. In the salt wedge SSC is quite small, but there are small increases that coincide with bottom stress peaks, which suggests local resuspension.

4.4.2.2.2 Storm

During the storm, the mooring is increasingly in the toe of the salt wedge during greater ebbs. High bottom stress is associated with the flood—and increasingly the greater flood—until the mooring is in the toe during greater ebb from 3/16-3/19. The presence of the toe inhibits bottom stress on both greater ebb and greater flood. Unlike the pre-storm period, however, the highest SSC is associated with decreasing salinity and does not appear to be driven by resuspension. An analogous transect may be T2 (Figure 4.5) which shows small, but persistent near-bottom salinity and elevated SSC from RK 5.2-8.5.

4.4.2.2.3 Post-storm

In the post-storm period (Figure 4.7d) the mooring returns to being in the body of the salt wedge and peaks in bottom stress occur during the greater flood once more. While increases in SSC do coincide with increases in bottom stress, there are many SSC peaks of equal magnitude that do not coincide with bottom stress. One explanation may be that the salt wedge received an injection of easily resuspended material during the storm. The source of this material may be from the toe on 3/17-3/18 or sediment that fell out of suspension in the upper layer, but once in the salt wedge it appears to be advected with the tides regardless of bottom stress.

4.4.2.2.4 Residual near-bottom transport

Figure 4.7e shows near-bottom along-channel sediment flux per unit width. Near-bottom transport in the body of the salt wedge is slightly landward during the pre-storm neap period. It appears to be driven by resuspension, but may be limited by sediment availability. During the storm, we see strong seaward transport despite low bed stress. It appears to be driven by high SSC associated

with the toe on greater ebb. The post-storm period shows slightly seaward transport trending towards net zero as the mooring is increasingly in the salt wedge and out of the toe and SSC associated with the toe.

Taken together, the mooring data suggest three potential transport pathways: 1) resuspension and seaward transport in the tidal excursion of the toe, 2) seaward advection of SSC associated with the toe, and 3) resuspension-driven landward transport in the salt wedge. During the flood bed stress appears sufficient for resuspension, thus the salt wedge may be capable of landward transport, depending on sediment availability. In the toe, spring tides and SSC associated with the toe drive net seaward transport. We observe net seaward transport in the tidal excursion of the toe that appears to be driven by local resuspension during greater ebb. Some of the near-bottom material exported from the tidal excursion of the toe or advected with the toe during spring tides can be carried down-estuary in the upper layer, leaching the upper estuary sediment supply. Net landward transport in the salt wedge can counter this to a degree, but is limited by lower bed stress.

In the following sections, we attempt to sketch in further details regarding: sources of sediment in the estuary, transport pathways, the role of resuspension, and timescales for sediment retention.

4.5 DISCUSSION

4.5.1 *Sourcing sediment in the estuary*

Using updated estimates of daily suspended sediment load (Chapter 2) and daily discharge, we can calculate a daily mean SSC and compare it to average SSC in the salt wedge and in fresh water, or the upper layer (Figure 4.8). The salt wedge is defined as any water seaward of the toe and having salinity exceeding 14 psu. The upper layer is defined by salinities less than 14 psu. For May 2011 and February 2012, the salt wedge and upper layer were defined by the 2 psu isohaline. SSC in the upper layer, particularly during max ebb, tracks with the trend in upstream loading. February 2012 was a major loading event that likely saw a higher fraction of coarser material in suspension. Coarse material is likely to fall out of suspension as the channel widens seaward of the Turning Basin and may explain the discrepancy between upstream loading and upper layer mean SSC. The

upper layer SSC generally matches upstream loading for the three highest loads, suggesting that the source of upper layer material is upstream.

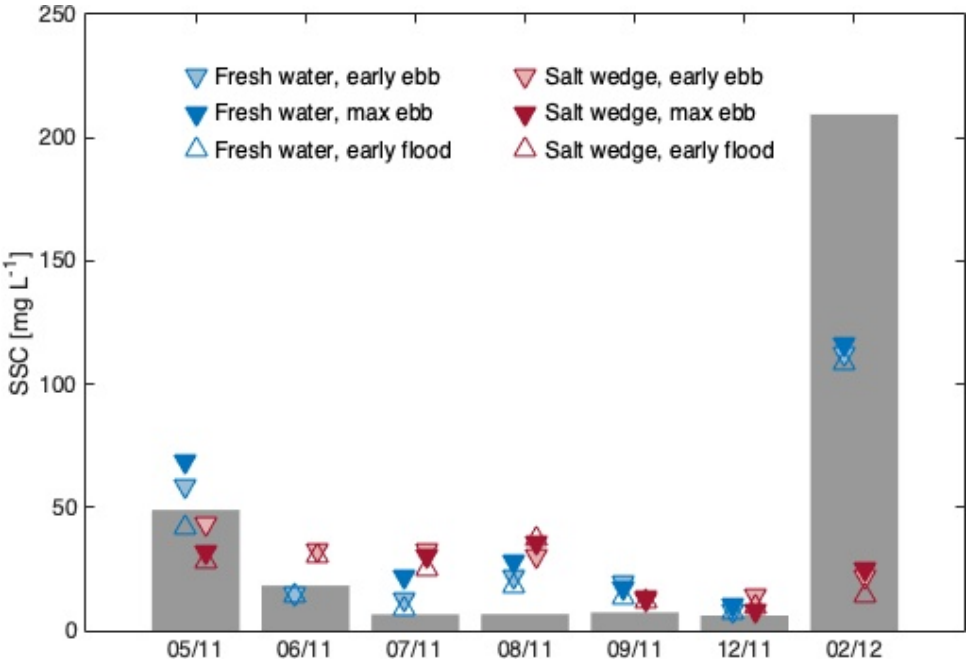

Figure 4.8. SSC in the estuary compared to upstream loading.

Average upstream SSC (gray bars) for each transect date. Average freshwater and salt wedge SSC are shown in blue and red, respectively.

SSC in the salt wedge is well short of upstream SSC for February 2012. It is plausible that seaward advection largely bypasses the salt wedge, but the available transects are insufficient to say definitively. Salt wedge SSC is comparable to upstream loading in May 2011 and stays relatively constant despite a subsequent decrease in upstream loading. This suggests that the material in the salt wedge through August 2011 does not derive from upstream loading. Since only minor loading events have occurred in the intervening time, this material has been retained in the system since May 2011. By September and December 2011 the salt wedge shows SSC comparable with upstream load estimates suggesting that the retained material has been depleted.

4.5.2 *Transport pathways*

To investigate potential transport pathways, we examine max ebb profiles of along-channel velocity, suspended sediment concentration, and suspended sediment flux per unit width at RK 8,

a location occupied by each transect (Figure 4.9). Seaward velocities are strongest when high discharge combines with the ebb tide (Figure 4.9f,g). In the presence of the salt wedge the velocity profile exhibits vertical shear, which reduces the seaward transport capacity in the lower water column (Figure 4.9h,i,j). The flood velocity profiles show landward velocity in the salt wedge and very little velocity at the surface (Figure 4.9d,g,j,m). A subsurface velocity maximum, commonly found in flooding salt wedges, is apparent 4 mab (Figure 4.9g,j,m) and 3 mab (Figure 4.9d). During the highest discharge velocity is still seaward at the beginning of the flood (Figure 4.9a), but we would expect to see landward velocity later in the flood.

SSC decreases steadily with time after the most recent loading event (Figure 4.9k-o). SSC is uniformly distributed across the water column during loading events (Figure 4.9b,e) and is found increasingly in the lower half of the water column (Figure 4.9h,k) until there is very little suspended sediment present at all (Figure 4.9n).

Sediment flux requires both transport capacity, i.e. velocity, and the presence of suspended sediment. Thus seaward transport is largest at high flows where transport capacity coincides with the presence of suspended sediment throughout the water column (Figure 4.9c,f). We find the strongest seaward transport during a high flow, major loading event (Figure 4.9c). Transport capacity in the salt wedge, though smaller in magnitude, is always present and increases as SSC in the salt wedge increases (Figure 4.9c,g,f). With sufficient suspended sediment in the salt wedge landward transport outweighs seaward transport (Figure 4.9l). Finally several months after the last major loading event, there is so little sediment suspended in the water column (Figure 4.9n) that sediment flux is insignificant (Figure 4.9o) despite strong ebb and flood velocities (Figure 4.9m).

The above analysis suggests that the presence and location of suspended sediment in the water column are important factors for determining the direction and magnitude of suspended sediment transport. In particular, the presence of suspended sediment in the salt wedge is necessary for landward transport. Sediment removal from the upper layer to the salt wedge due to gravitational settling can be an important pathway by which sediment is transferred to the salt wedge. Upper layer removal rate is dependent on the presence of sediment in the upper layer, horizontal advection, and the fall velocities of sediment in suspension. Larger fall velocity, due to grain size

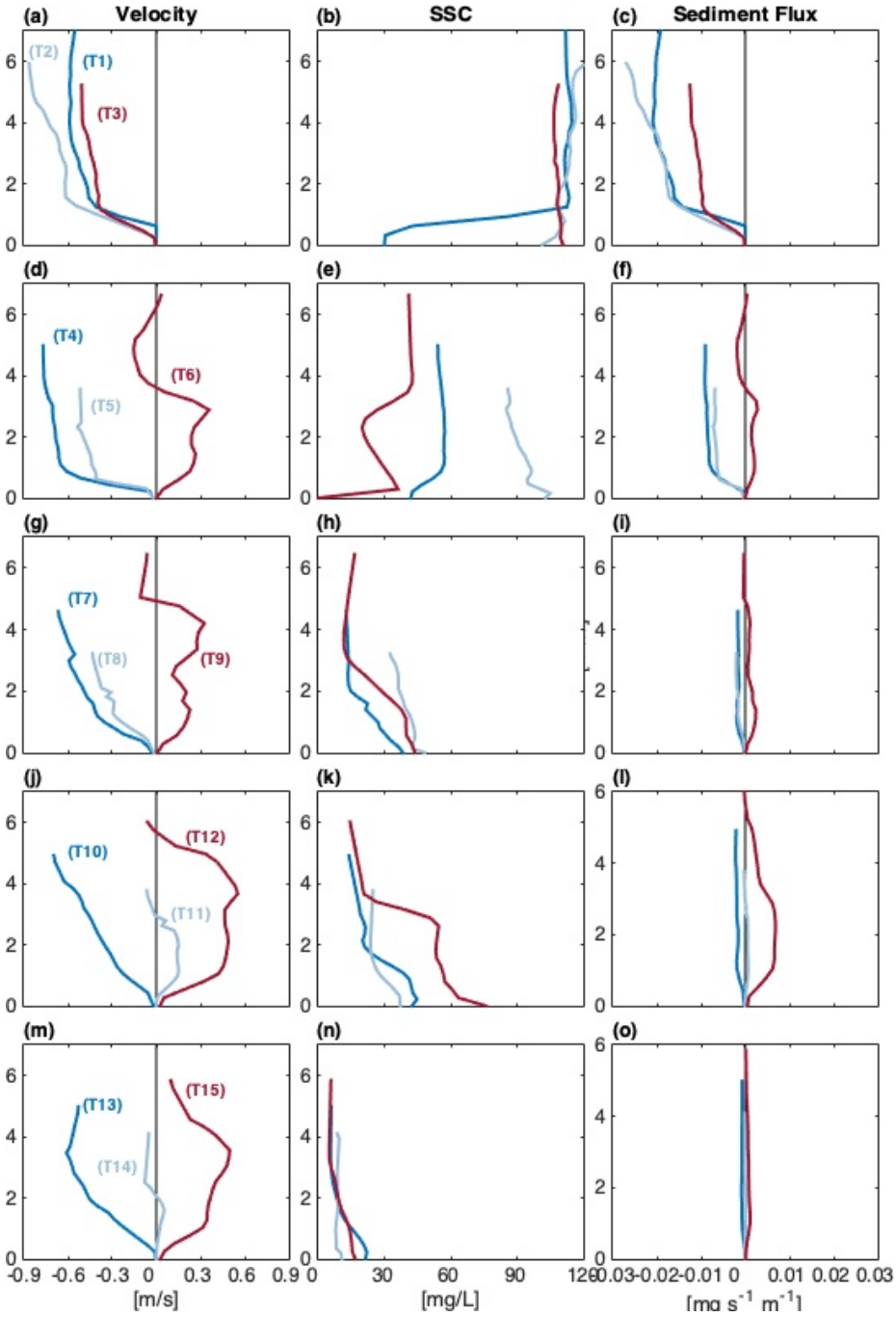

Figure 4.9. Profiles of along-channel velocity, SSC, and SSC flux.

Profiles of along-channel velocity (first column), SSC (second column), and SSC flux per unit width (third column). Negative and positive fluxes and velocities are directed seaward and landward, respectively. Rows correspond to transects in Figure 4.5, as indicated. As in Figure 4.5, time since loading increases downward. All profiles are located at RK 8.

or flocculation, will tend to transfer sediment into the salt wedge faster. Strong horizontal advection causes suspended sediment to travel further downstream before falling into the salt wedge. In a given section, the amount of sediment transferred from the upper layer to the salt wedge depends on the amount of sediment in the upper layer, and on the balance between horizontal advection and fall velocity.

We choose a straight, uniform section of the estuary (RK 7.6-8.6) to estimate the rate of sediment removal from the upper layer using maximum ebb transect data. Across the range of flows observed there is little (1-3%) change in upper layer salinity or along-channel velocity in this region, which is consistent with the assumption made in Section 4.3.4 that there is very little mixing between the upper and lower layer. The upper layer removal rate is higher during loading events and quickly decreases in magnitude in the absence of significant upstream loading (Figure 4.10a). However the fraction of incoming sediment that is removed to the salt wedge is lowest (~50%) during a strong loading event, and increases to roughly 70% during minimal loading (Figure 4.10b). It should be noted that retention during the highest discharge is likely influenced by recent dredging; the upper layer removal rate may be smaller in un-dredged conditions. High upper layer removal rates and salt wedge retention rates are consistent with past studies that have shown that the Duwamish retains 70-90% of incoming material (Harper-Owes 1983). Additionally this area overlaps with an area of very high sedimentation rates that decrease rapidly seaward (Harper-Owes 1983).

During upstream sediment loading events horizontal advection appears to outweigh larger fall velocities; this may be due to the influence of the Turning Basin, where larger grain sizes may settle out even at high flows. However, there is so much sediment in the upper layer that despite increased horizontal advection, the salt wedge receives a substantial influx of sediment from the upper layer. During times of low flow and low loading, the amount of sediment delivered to the salt wedge from the upper layer decreases substantially, although that sediment represents a higher fraction of incoming sediment. Removal of sediment from the upper layer is an important mechanism for retaining upstream sediment in the estuary during loading, and for keeping that sediment in the estuary throughout the low flow period.

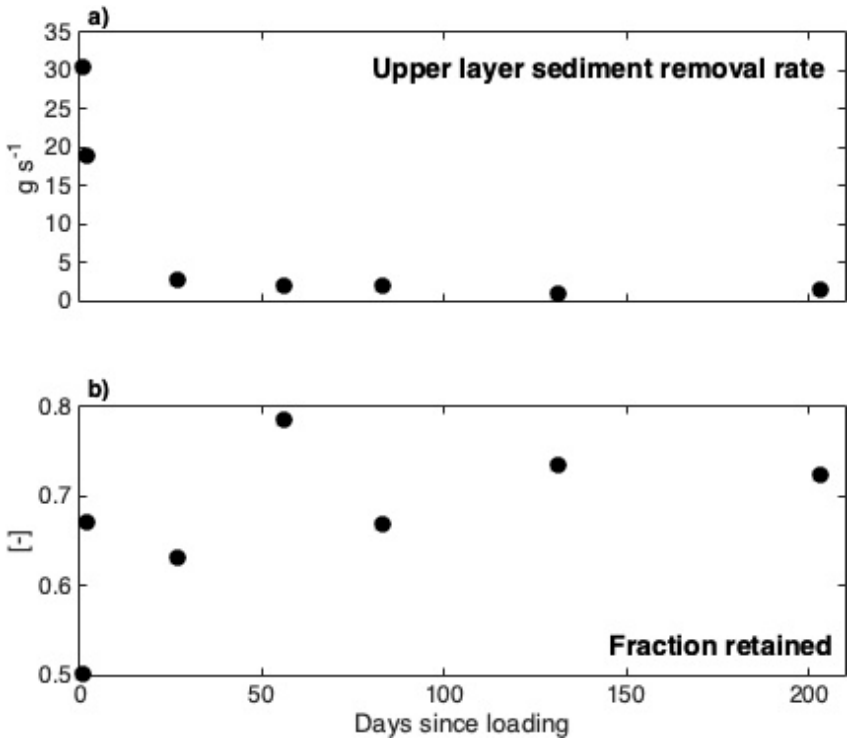

Figure 4.10. Maximum ebb upper layer removal rate and retention from RK 7.6-8.6. Estimates of upper layer removal rate (a) and fraction of incoming material removed (b) from RK 7.6-8.6 during maximum ebb.

4.5.3 *Role of resuspension*

We examine SSC and bed stress from mooring data to identify conditions under which local resuspension occurs in the tidal excursion of the toe and in the salt wedge (Figure 4.11); SSC increasing with bed stress is generally an indication that resuspension is occurring. High or increasing SSC in the absence of bed stress can indicate advection from upstream resuspension or the local re-entrainment of fluff. The clearest evidence of resuspension occurs in unstratified ebb conditions when the salt wedge has passed seaward (Figure 4.11a). High ebb SSCs also occur at bed stresses below the critical threshold, regardless of bottom salinity. As noted above (Figure 4.11c), these peaks are associated with the seaward passage of the toe.

Values of bed stress and SSC are much smaller in the salt wedge and their relationship is tidally reversed in the salt wedge (Figure 4.11b). Lack of SSC may be related to 2013 being a sediment-poor year, however the largest bed stresses in the salt wedge during the flood only just exceed the

minimum critical bed stress for resuspension. Bed stress maxima occur during the pre-storm period, but despite coinciding with SSC peaks (Figure 4.7b) there is not a clear trend between bed stress and SSC. During the storm and post-storm periods there is some evidence for a weak relationship (R^2 = 0.62) between SSC and bed stress. As bed stresses are insufficient for resuspension during this period, this material must be re-entrained fluff that was delivered to the estuary during the storm. The difference between pre- and storm/post-storm periods may be related to the age of the material. Fresh fluff may be more easily re-entrained than older sediment that has been reworked for several weeks (and up to months). Similar to the tidal excursion of the toe, there are low-stress SSC peaks during ebb that coincide with the passage of the toe (Figure 4.7c).

Mooring data indicate that resuspension is important in the tidal excursion of the salt wedge toe on ebb. Bed stresses in the salt wedge are generally at or less than the minimum critical threshold for resuspension, however there is evidence that the flooding salt wedge is capable of re-entraining fluff, and in particular recent fluff. We use the transects to add seasonal context to the role of resuspension. Average mean bed stress and near-bottom SSC from the within and outside of the salt wedge are calculated for each transect. Thus bed stress in the salt wedge is sufficient for re-entrainment of fluff and nearly sufficient for resuspension.

Particularly for freshwater, upstream of the salt wedge, SSC can be a function of discharge in two ways: through increased bed stress and upstream loading. In order to disentangle the two effects we examine bed stress as a function of discharge and SSC as a function of bed stress. Bed stress in freshwater regions of the estuary increases with discharge, as we might expect (Figure 4.12a). Bed stress estimates from the highest discharge may be biased low—bottom salinity was particularly persistent, leaving few areas of unstratified flow at maximum ebb (see Figure 4.5, T2). Based on the low flow mooring deployment (15-20 m^3s^{-1}) we expect bed stresses above the Turning Basin would exceed 2 Pa during max greater ebb for a discharge of 200 m^3s^{-1}. If suspended sediment upstream of the salt wedge and in the upper layer was driven by resuspension we would expect SSC to increase with bottom stress. Instead, SSC is consistently low until a sudden increase

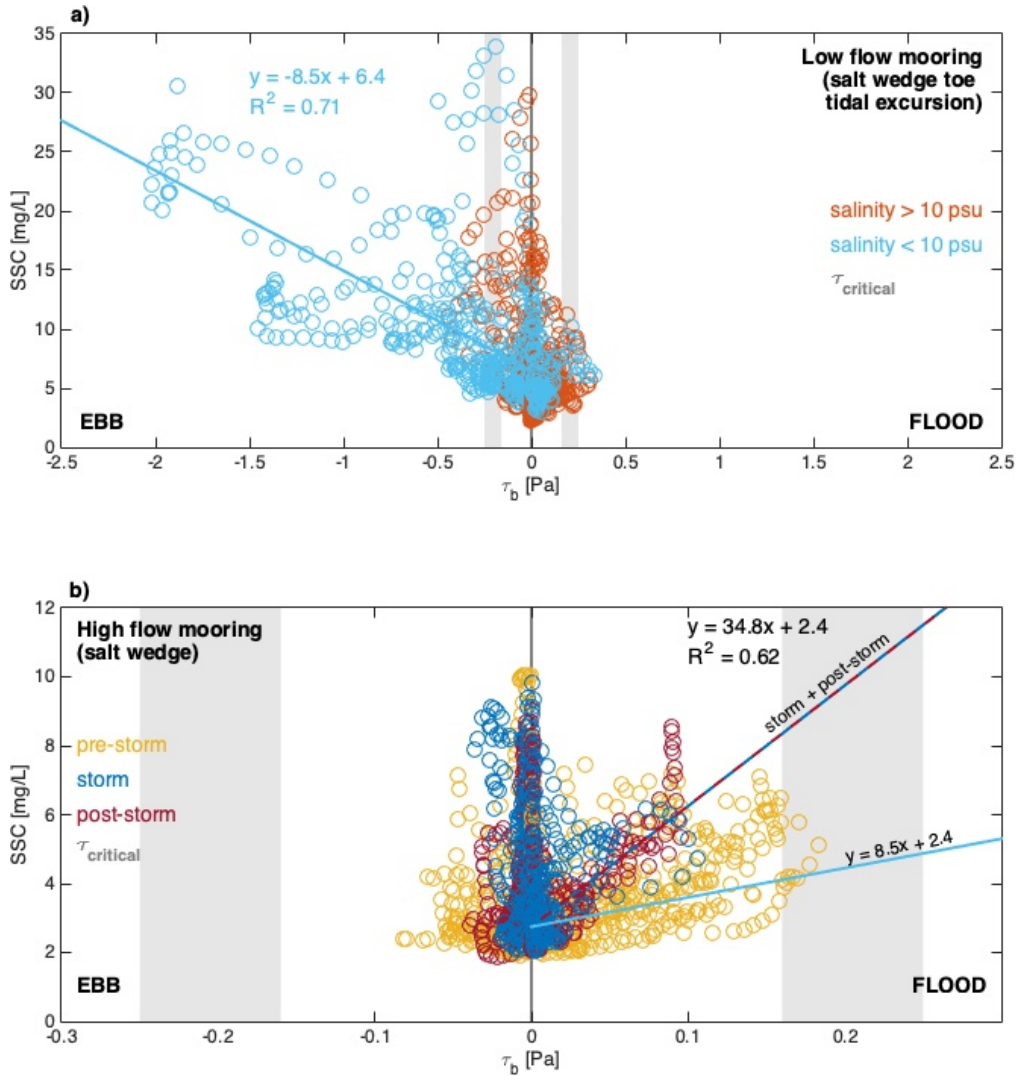

Figure 4.11. SSC and bottom stress for high- and low-flow mooring deployments. Panel a) shows SSC versus bottom stress, τ_b, for the low flow mooring deployment when the mooring was in the tidal excursion of the toe. Bottom salinity above (orange) and below (blue) are shown. A linear fit to data less than 10 psu and -0.5 Pa is provided (blue line). SSC versus bottom stress for the high flow mooring deployment is shown in panel (b), when the mooring was in the salt wedge. Colors indicate pre-storm (yellow), storm (blue), and post-storm (red) periods, see Figure 4.7. A linear fit to storm and post-storm data exceeding 0.025 Pa is shown (red-blue line) and a line with the same slope as the fit in (a) is plotted for comparison. In both panels gray shading shows the range of critical stress values, and positive and negative bottom stresses are directed landward and seaward, respectively.

for bed stress greater than 0.8 Pa (Figure 4.12b). These two data points correspond to loading events. Despite increases in average bed stress, SSC only increases in the presence of significant upstream loading. While the mooring data show resuspension locally in the tidal excursion of the toe, it is not dominant enough to drive average freshwater SSC over larger spatial scales.

In the salt wedge on flood, bed stress does not depend on discharge (Figure 4.12d), which is consistent with previous findings showing that the flooding salt wedge structure does not vary with discharge (McKeon et al. 2020). Bed stress generated in the salt wedge is much smaller compared to upstream and hovers at or just below the minimum critical bed stress. Mean SSC appears to increase with bed stress in the salt wedge, however the two instances of lower bed stress coincide with transects occurring months after a loading event, which suggests that a lack of sediment availability may explain those low values (Figure 4.12e). It is notable that SSC at low bed stress in the salt wedge (~40 mg/L) exceeds freshwater SSC with bed stress above the critical threshold in the absence of loading (~10 mg/L). Although limited by low bed stress and sediment availability, it appears that re-entrainment is an important mechanism in the salt wedge for a period of time after upstream loading.

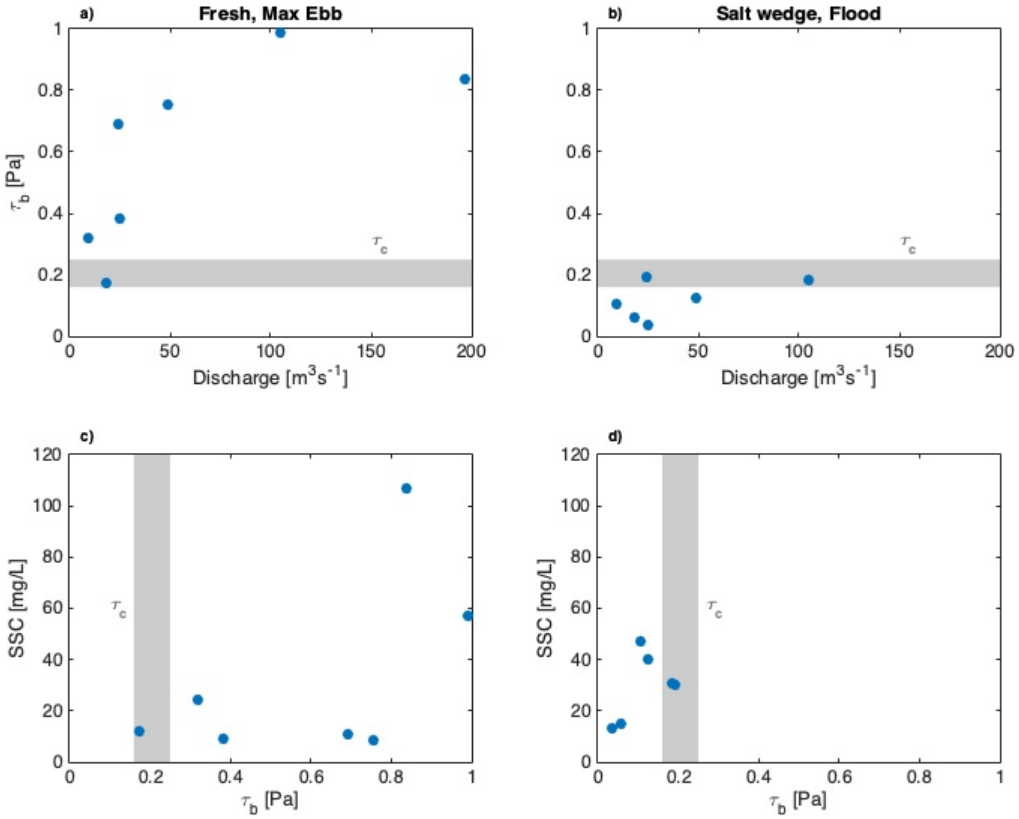

Figure 4.12. SSC and bottom stress for transects.

Panel a) average freshwater ebb stress as a function of discharge, b) average near-bottom SSC versus average bed stress for freshwater, c) average salt water bed stress as a function of discharge, d) average near-bottom SSC versus average salt water bed stress. Ranges of critical stress are shown in gray for all plots.

4.5.4 *Timescales*

Chapter 3 showed that most of the annual sediment load is delivered to the estuary during a few peak loading events (Figure 3.11 and Figure 4.3). Much of the incoming sediment is transferred to the salt wedge via gravitational settling. In the days and months following the peak loading event sediment is re-entrained and transported landward in the salt wedge. Resuspension within the tidal excursion of the toe at max ebb and re-entrainment of fluff exposed by salt wedge retreat during late ebb transfers material from the salt wedge to the upper layer. Some of this sediment is exported from the estuary and some settles into the salt wedge again. Toward the end of the summer, data show low suspended sediment concentrations everywhere in the estuary, suggesting that the available sediment has been exhausted. This conceptual picture of the fate of sediment in the

estuary suggests that it can be understood in terms of the timescales of delivery and retention. These timescales have important implications for the health of the estuary since they define the active time that clean upstream sediment stays and is re-worked and possibly re-contaminated in the estuary.

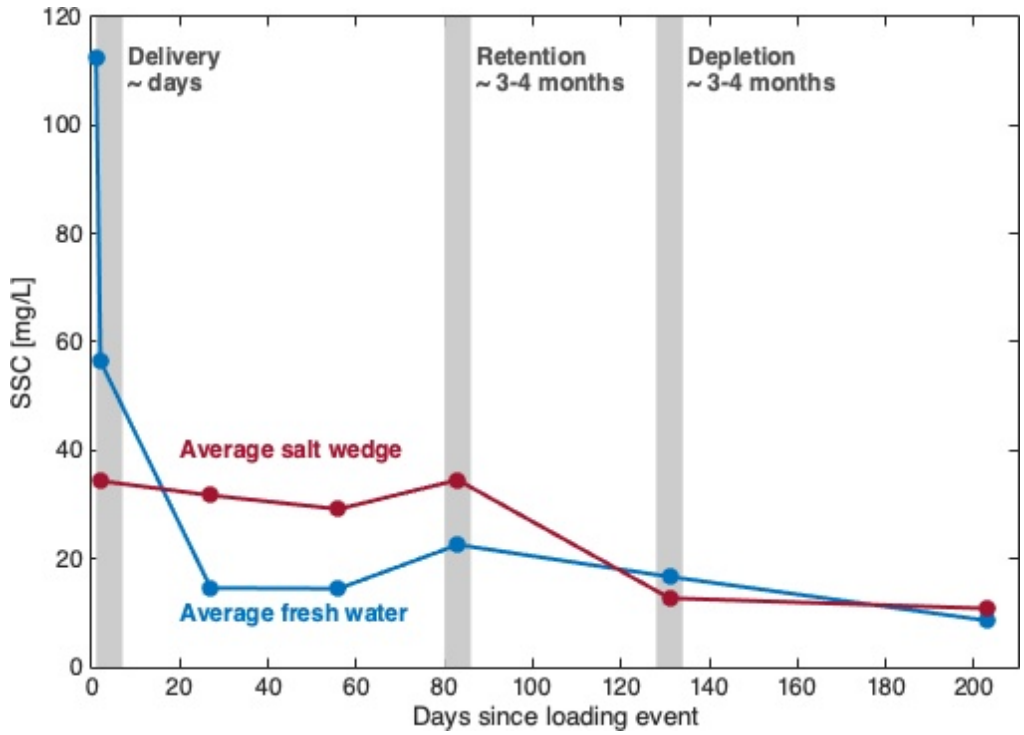

Figure 4.13. Timescales for SSC delivery, retention, and depletion.
Average fresh water (blue) and salt wedge (red) SSC versus time since loading event. Gray shading indicates delivery, retention, and depletion timescales as noted.

In order to estimate the timescales associated with sediment fate in the estuary, we compare average freshwater and salt wedge SSC as a function of time after the most recent loading event (Figure 4.13). There are three periods and associated timescales that are evident in these results: delivery of sediment, retention of sediment, and depletion of sediment. First, the delivery timescale is associated with the injection of sediment into the estuary via upstream loading. This timescale is likely on the order of days, or the duration of a major loading event. The next round of sampling was three weeks after a loading event, but given our estimations of upper layer removal rates, it seems unlikely that sediment remains in the upper layer for that long. During this time SSC in the upper layer is set by the magnitude of upstream loading and exceeds SSC in the salt wedge. After

the input of sediment during delivery, sediment is retained and reworked in the salt wedge in the absence of upstream loading. The timescale associated with the retention of sediment in the estuary in 2011 is ~3-4 months. 2011 was an average year in terms of annual load and this timescale may vary with the magnitude of winter loading. During that time SSC in the salt wedge is greater than SSC in the upper layer. Finally, after ~3-4 months the retained material is depleted and SSC is low in and out of the salt wedge.

There are several plausible explanations for the apparent depletion of retained material. First, resuspension and re-entrainment on ebb may export a small fraction seaward each tidal cycle, particularly during spring tides (Fain et al. 2001). Second, consolidation within the low bed stress environment of the salt wedge may slowly leach the supply of easily re-entrained material. Likely both seaward export and consolidation play roles. Other studies have found that unconsolidated sediment, in the form of a mobile pool, is available to be reworked and redistributed over seasonal timescales (Geyer and Ralston 2018; Grabemann et al. 1997; Migniot 1971; Schoellhamer 2011; Wellershaus 1981; Woodruff et al. 2001). This suggests that typical consolidation timescales can be on the scale of months and years. The Duwamish appears to behave somewhat differently, and while the present measurements cannot fully elucidate how retained sediment is depleted after 3-4 months, we can make some inferences. First, the Duwamish is a small system, thus the supply of mobile sediment may be much smaller than in systems where it is reworked on seasonal and even interannual timescales. Second, bed stresses in the salt wedge are sufficient to re-entrain fluff while resuspension is only accessible to the tidal excursion of the toe on ebb. In other systems the mobile pool can be resuspended both seaward and landward, slowing down consolidation. Third, the Duwamish is also a much steeper system; seaward of the Turning Basin (RK 9.5) the channel is much deeper than it would be naturally. Thus bed sediments are subject to a relatively deep water column and the associated hydrostatic pressure may decrease relevant consolidation timescales. Finally, the salt wedge is always present seaward of RK 5.2, so in some sense this represents the seaward boundary of the estuary. The artificially deepened channel leads to smaller velocities, thereby inhibiting landward transport in the salt wedge such that sediment exported seaward of RK 5.2 may be lost from the portion of the estuary that is actively reworking sediment.

4.5.5 *Summary and synthesis*

High values of suspended sediment concentration in the Duwamish are driven by a few large storm events. During a storm event sediment is primarily carried in the upper layer. A substantial fraction of the incoming sediment is retained in the upper estuary and is reworked in the salt wedge for 3-4 months afterward. After this period, the retained material is depleted either through seaward transport or consolidation into the bed.

Transport pathways associated with the salt wedge support the conceptual model of retention and depletion of sediment. During loading, gravitational settling removes sediment from the upper layer and transfers it to the salt wedge. The flooding salt wedge generates small, but consistent landward transport that helps retain sediment in the estuary. Seaward transport is observed in the tidal excursion of the toe associated with resuspension during spring tides, and in the advection of SSC associated with low bottom stress conditions in the toe. These seaward pathways, possibly in tandem with the gradual consolidation of retained material into the bed, slowly leach the supply of retained sediment available for transport in the upper estuary.

The reworking of retained sediment over the course of months allows for the possibility that legacy contamination is slowly mixed with newer clean sediment from upstream. Our estimates of seaward transport suggest that mixed material may be exported seaward, but consolidation timescales do not preclude the possibility that the mixed material stays within the estuary. Local resuspension during the ebb does not drive large-scale transport, but does allow for the possibility of contaminant transport confined to the tidal excursion of the toe during spring tides. Further work must be done to determine the degree to which estuarine and riverine sediments mix during reworking and to place more precise limits on seaward export.

4.6 CONCLUSIONS

Upstream sediment is delivered to the estuary in only a handful of storm events that last on the order of days. Gravitational setting transfers upstream sediment to the salt wedge during loading events. As the salt wedge retreats during ebb, retained material is resuspended and re-entrained into the upper layer. The upper layer exports some material seaward, but some re-settles into the

salt wedge. The flooding salt wedge re-entrains and transports fluffy material landward. Thus retained material is reworked for 3-4 months after delivery until it is depleted through seaward export and consolidation.

Chapter 5. Summary and recommendations

5.1 SUMMARY

This dissertation elucidates seasonal hydrodynamics and suspended sediment transport in the Duwamish River estuary, WA, USA. Observations of hydrodynamics and suspended sediment are used to investigate salt wedge dynamics and suspended sediment transport in the estuary. Existing suspended sediment load data are re-analyzed to better understand upstream delivery to the estuary. Results are discussed in the broader context of existing body of work on strongly stratified estuaries and in the specific context of on-going contaminant remediation in the Duwamish.

In Chapter 2 a combination of hydrographic surveys and moored measurements of salinity and velocity are used to characterize the seasonal variability of stratification in the Duwamish River Estuary, a tidal salt wedge estuary. These observations show that changes to the channel geometry, and in particular, a steep bed slope due to an artificially maintained navigation channel, influence the estuarine circulation and the salt wedge dynamics. The steep bed slope results in a salt wedge length that is less sensitive to changes in river discharge than in estuaries with a shallower bed slope. The ebb- and flood-phase salinity structures can be understood based on two-layer hydraulic theory. The flood phase structure is largely insensitive to changes in river discharge. The ebb-phase salinity structure, in contrast, is strongly influenced by discharge as a result of hydraulic response to strong barotropic forcing, a steeply sloping bed, and severe lateral constrictions. During the ebb, flow is near-critical over the salt wedge, and the upper layer thickness is set by the critical depth. Contractions near two bridges locally reduce the pycnocline height and can form fronts at high riverflows. At higher river discharges, we also find sufficient shear to create favorable conditions for mixing across the interface throughout the salt wedge. The overall effect is to maintain an upper layer depth equal to the critical depth, while the bottom of the pycnocline is shifted towards the bed with increasing river discharge. In combination with an unchanging flood structure, this results in a seasonally modulated ebb-flood asymmetry in the interfacial height. The ebb-flood asymmetry increases landward transport within the salt wedge and has implications for long-term residual scalar transport. Thus, seasonal changes in riverflow can drive

variations in salt wedge structure (intrusion distance and stratification) and residual transport on seasonal or longer timescales.

In Chapter 3, a re-analysis of three existing datasets, ranging from 1966 to 2019, using an approach that allows for a change in slope in the suspended sediment load rating curve, provides fits that are more representative of the data than previous attempts. We find a consistent slope break at 80% of the long-term mean flow and an increase in slope at larger flows, where most of the annual load occurs. A "combined fit" rating curve accurately estimates 1960s and 2010s annual loads, whereas no single model (generated here or previously) is appropriate for the entire period from 1961-present. Using the "combined fit", we find that most of the 11.7×10^4 mt long term mean annual load occurs from November-May during high discharge events. Modern annual load estimates may be closer to $9.4\pm4.4\times10^4$ mt/year. Estimates of fine and coarse loads derived from modern data indicate that 70% of the average annual total load is composed of fine sediment.

Chapter 4 explores suspended sediment transport in the Duwamish. Upstream sediment is delivered to the estuary in only a handful of storm events that last on the order of days. Gravitational setting transfers upstream sediment to the salt wedge during loading events. As the salt wedge retreats during ebb, retained material is resuspended and re-entrained into the upper layer. The upper layer exports some material seaward, but some re-settles into the salt wedge. The flooding salt wedge re-entrains and transports fluffy material landward. Thus retained material is reworked for 3-4 months after delivery until it is depleted through seaward export and consolidation.

5.2 RECOMMENDATIONS AND FUTURE WORK

While there is still much to learn and many avenues for future work, taken together, the work presented here is a considerable advancement of the understanding of hydrodynamics and sediment transport processes in the Duwamish, and makes a contribution to overall knowledge of strongly stratified estuaries. Because the Duwamish is a Superfund Site that is currently undergoing a $342 million remediation plan (LDWG 2014), we make the following recommendations based on the work presented in this dissertation:

1) According to the 2014 Record of Decision (LDWG 2014) roughly 60% of the remaining contaminated area is designated as "monitored natural recovery" (MNR). MNR depends on "clean" upstream sediment permanently burying contaminated sediment. Estimates of recent annual loading presented in Chapter 3 suggest that the LDWG overestimates upstream sediment loading by roughly a factor of two. Therefore we suggest that MNR areas are closely monitored. It is likely that MNR areas will recover more slowly than anticipated.
2) Results from Chapter 4 suggest that upstream sediment delivered to the estuary is re-worked for 3-4 months through re-entrainment in the salt wedge and resuspension at the salt wedge toe. This introduces the possibility that "clean" upstream sediment acquires some amount of contamination while being re-worked, and that some of that sediment is exported seaward on ebb. To this end we suggest two avenues of future work:
    a. Tracking sediment retained in the estuary after an injection of upstream material, and in particular, the biogeochemical evolution and changes in contaminant concentration of the fluff layer within the salt wedge during the low discharge retention period. As porewater exchange may be a mechanism of contaminant transfer through the bed (Parker and Lee 1981), we suggest contemporaneous measurements of porewater transport.
    b. Material resuspended at the salt wedge toe on greater ebb may be exported seaward or settle back into the salt wedge. Seaward export of resuspended material is a potential pathway for contaminant transport. The measurements presented here are not sufficient to quantify the fraction of resuspended material that is exported. We recommend a study in which this is more precisely quantified.
3) We were not able to address the role of the width constrictions at the 1st and 16th Avenue bridges in along-channel suspended sediment transport with the available measurements. We hypothesize that width constrictions may interrupt landward transport during flood and seaward transport during ebb. Width constrictions are common in urbanized estuaries and understanding their role in estuarine sediment transport is relatively unexplored. For the Duwamish, a better understanding of their impact may shed some light on spatial patterns of contamination and help inform long-term monitoring post-remediation.

BIBLIOGRAPHY

Armi, L., and D. M. Farmer, 1986: Maximal 2-layer exchange through a contraction with barotropic net flow. *J. Fluid Mech.*, **164,** 27-51.

Burchard, H., and H. Baumert, 1998: The formation of estuarine turbidity maxima due to density effects in the salt wedge. A hydrodynamic process study. *Journal of Physical Oceanography*, **28,** 309-321.

Burchard, H., H. M. Schuttelaars, and D. K. Ralston, 2018: Sediment Trapping in Estuaries. *Annual Review of Marine Science*, **10,** 371-395.

Campbell, F. B., and H. A. Bauder, 1940: A rating-curve method for determining silt-discharge of streams. *Transactions.*, **21,** 603-607.

Chant, R. J., and R. E. Wilson, 2000: Internal hydraulics and mixing in a highly stratified estuary. *Journal of Geophysical Research-Oceans*, **105,** 14215-14222.

Chatwin, P. C., 1976: Some remarks on mainenance of salinity distribution in estuaries. *Estuarine and Coastal Marine Science*, **4,** 555-566.

Chawla, A., D. A. Jay, A. M. Baptista, M. Wilkin, and C. Seaton, 2008: Seasonal variability and estuary-shelf interactions in circulation dynamics of a river-dominated estuary. *Estuaries and Coasts*, **31,** 269-288.

Dawson, W. A., and L. Tilley, 1972: Measurement of salt-wedge excursion distance in the Duwamish River estuary, Seattle, Washington, by means of the dissolved-oxygen gradient. *Measurement of salt-wedge excursion distance in the Duwamish River estuary, Seattle, Washington, by means of the dissolved-oxygen gradient.*

de Nijs, M. A. J., J. D. Pietrzak, and J. C. Winterwerp, 2011: Advection of the Salt Wedge and Evolution of the Internal Flow Structure in the Rotterdam Waterway. *Journal of Physical Oceanography*, **41,** 3-27.

Embrey, S. S., and L. M. Frans, 2003: Surface-water quality of the Skokomish, Nooksack, and Green-Duwamish rivers and Thornton Creek, Puget Sound basin, Washington, 1995-98. Tacoma, Wash. : U.S. Dept. of the Interior, U.S. Geological Survey ; Denver, CO : Information Services distributor.

Fain, A. M. V., D. A. Jay, D. J. Wilson, P. M. Orton, and A. M. Baptista, 2001: Seasonal and Tidal Monthly Patterns of Particulate Matter Dynamics in the Columbia River Estuary. *Estuaries.*, **24,** 770-786.

Farmer, D. M., and L. Armi, 1986: Maximal 2-layer exhange over a sill and through the combination of a sill and contraction with barotropic flow. *J. Fluid Mech.*, **164,** 53-+.

Fischer, H. B., 1972: Mass-transport of mechanisms in partially stratified estuaries. *J. Fluid Mech.*, **53,** 671-&.

Friedrichs, C. T., and D. G. Aubrey, 1994: Tidal propagation in strongly convergent channels. *Journal of Geophysical Research-Oceans*, **99,** 3321-3336.

Fugate, D. C., and R. J. Chant, 2005: Near-bottom shear stresses in a small, highly stratified estuary. *Journal of geophysical research.*, **110**.

Gardner, J. S., and J. D. Smith, 1978: Turbulent mixing in a salt wedge estuary. *HYDRODYNAMICS ESTUAR***,** 79-106.

Geyer, W. R., 1988: The advance of a salt wedge front: Observations and dynamical model. *Physical Processes in Estuaries***,** 181-195.

Geyer, W. R., 1993: The Importance of Suppression of Turbulence by Stratification on the Estuarine Turbidity Maximum. *Estuaries.*, **16,** 113-125.

Geyer, W. R., and J. Smith, 1987: Shear instability in a highly stratified estuary. *Journal of Physical Oceanography JPYOBT*.

Geyer, W. R., and D. M. Farmer, 1989: Tide-induced variation of the dynamics of a salt wedge estuary. *Journal of Physical Oceanography*, **19,** 1060-1072.

Geyer, W. R., and D. K. Ralston, 2011: The Dynamics of Strongly Stratified Estuaries. *Treatise on Estuarine and Coastal Science, Vol 2: Water and Fine Sediment Circulation***,** 37-51.

Geyer, W. R., and D. K. Ralston, 2018: A mobile pool of contaminated sediment in the Penobscot Estuary, Maine, USA. *The Science of the total environment.*, **612,** 694-707.

Geyer, W. R., D. K. Ralston, and R. C. Holleman, 2017: Hydraulics and mixing in a laterally divergent channel of a highly stratified estuary. *Journal of Geophysical Research-Oceans*, **122,** 4743-4760.

Giddings, S. N., D. A. Fong, and S. Monismith, 2011: Role of straining and advection in the intratidal evolution of stratification, vertical mixing, and longitudinal dispersion of a shallow, macrotidal, salt wedge estuary. *Journal of geophysical research.*

Glysson, G. D., 1987: Sediment transport curves. *USGS Open File Report*, **87,** 218-247.

Grabemann, I., R. J. Uncles, G. Krause, and J. A. Stephens, 1997: Behaviour of Turbidity Maxima in the Tamar (U.K.) and Weser (F.R.G.) Estuaries. *Estuarine, coastal and shelf science.*, **45,** 235-246.

Hansen, D. V., and M. Rattray, 1966: New dimensions in estuary classification. *Limnol. Oceanogr.*, **11,** 319-&.

Harleman, D. R. F., 1961: Stratified flow. *HDB FLUID DYNAMICS.*

Harper-Owes, 1981: *Duwamish Waterways navigation improvement study : analysis of impacts on water quality and salt wedge characteristics.* Seattle : publisher not identified. Springfield, Va. : available from the National Technical Information Service.

——, 1983: Water quality assessment of the Duwamish Estuary, Washington. Seattle : METRO.

Hayter, E. J., and A. J. Mehta, 1986: Modelling cohesive sediment transport in estuarial waters. *Applied mathematical modelling.*, **10,** 294-303.

Jaeger, J. M., and C. A. Nittrouer, 1995: Tidal controls on the formation of fine-scale sedimentary strata near the Amazon river mouth. *Marine geology.*, **125,** 259-281.

Jay, D. A., 1987: Residual circulation in shallow stratified estuaries. *Residual circulation in shallow stratified estuaries*.

Jay, D. A., and J. D. Smith, 1990a: Residual circulation in shallow estuaries. 1. Highly stratified, narrow estuaries. *Journal of Geophysical Research-Oceans*, **95,** 711-731.

——, 1990b: Circulation, density, distribution, and neap-spring transitions in the Columbia River Estuary. *Progress in Oceanography*, **25,** 81-112.

Jay, D. A., and J. D. Musiak, 1996: Internal tidal asymmetry in channel flows: Origins and consequences. *Mixing in estuaries and coastal seas /*, **50,** 211-249.

Kostaschuk, R., 2002: Flow and sediment dynamics in migrating salinity intrusions: Fraser River estuary, Canada. *Estuaries.*, **25,** 197-203.

Kostaschuk, R. A., and J. L. Luternauer, 1989: The rold of the salt-wedge in sediment trsuspension and deposition - Fraser River Estuary, Canada. *Shoreline mapping and change analysis : technical considerations and management implications /*, **5,** 93-101.

LDWG, 2003: Final Remedial Investigation Report: Phase 1. *Final Remedial Investigation Report*.

——, 2008: Final Sediment Transport Modeling Report.

——, 2009: Final Sediment Transport Analysis Report.

——, 2010: FInal Remedian Investigation Report.

——, 2014: Record of decision.

Maa, J. P. Y., L. Sanford, and J. P. Halka, 1998: Sediment resuspension characteristics in Baltimore Harbor, Maryland. *Marine geology.*, **146,** 137-145.

MacCready, P., and W. R. Geyer, 2010: Advances in Estuarine Physics. *Annual Review of Marine Science*, **2,** 35-58.

MacDonald, D. G., and A. R. Horner-Devine, 2008: Temporal and spatial variability of vertical salt flux in a highly stratified estuary. *Journal of geophysical research*, **113**.

Mathew, R., and J. C. Winterwerp, 2017: Surficial sediment erodibility from time-series measurements of suspended sediment concentrations: development and validation. *Ocean dynamics.*, **67,** 691-712.

McKeon, M. A., A. R. Horner-Devine, and S. N. Giddings, 2020: Seasonal Changes in Structure and Dynamics in an Urbanized Salt Wedge Estuary. *Estuaries and coasts.*

Mehta, A. J., E. J. Hayter, W. R. Parker, R. B. Krone, and A. M. Teeter, 1989: Cohesive Sediment Transport. I: Process Description. *Journal of hydraulic engineering.*, **115,** 1076-1093.

Migniot, C., 1971: Levolution de la Gironde ou cours des temps. *Bull. Inst. Geol. Bassin Aquitaine*, **11,** 211-281.

Miles, J. W., 1961: On the stability of heterogeneous shear flows. *J. Fluid Mech.*, **10,** 496-508.

Orton, P. M., and M. Visbeck, 2009: Variability of internally generated turbulence in an estuary, from 100 days of continuous observations. *Continental Shelf Research*, **29,** 61-77.

Parchure, T. M., and A. J. Mehta, 1985: Erosion of Soft Cohesive Sediment Deposits. *Journal of hydraulic engineering.*, **111,** 1308-1326.

Parker, W. R., and K. Lee, 1981: The behavior of fine sediment relevant to the dispersal of pollutants. *The Canary current : studies of an upwelling system : a symposium held in Las Palmas, 11-14 April 1978 /*, **181,** 28-34.

Partch, E. N., and J. D. Smith, 1978: Time-dependent mixing in a salt wedge estuary. *Estuarine and Coastal Marine Science*, **6,** 3-19.

Peters, H., 2003: Broadly distributed and locally enhanced turbulent mixing in a tidal estuary. *Journal of Physical Oceanography*, **33,** 1967-1977.

Poggioli, A. R., and A. R. Horner-Devine, 2015: The Sensitivity of Salt Wedge Estuaries to Channel Geometry. *Journal of Physical Oceanography*, **45,** 3169-3183.

Ralston, D. K., W. R. Geyer, and J. A. Lerczak, 2010a: Structure, variability, and salt flux in a strongly forced salt wedge estuary. *Journal of geophysical research.*, **115**.

Ralston, D. K., W. R. Geyer, and J. C. Warner, 2012: Bathymetric controls on sediment transport in the Hudson River estuary: Lateral asymmetry and frontal trapping. *Journal of geophysical research*, **117,** n/a-n/a.

Ralston, D. K., W. R. Geyer, J. A. Lerczak, and M. Scully, 2010b: Turbulent mixing in a strongly forced salt wedge estuary. *Journal of geophysical research*, **115**.

Rattray, M., and E. Mitsuda, 1974: Theoretical analysis of conditions in a salt wedge. *Estuarine and coastal marine science*, **2,** 375-394.

Ross, D. A., 1995: *Introduction to oceanography.* HarperCollins College Publishers.

Ryan, S. E., and L. S. Porth, 2007: A Tutorial on the Piecewise Regression Approach Applied to Bedload Transport Data. *General Technical Report RMRS-GTR-189*.

Sanford, L. P., 2008: Modeling a dynamically varying mixed sediment bed with erosion, deposition, bioturbation, consolidation, and armoring. *Computers & geosciences.*, **34,** 1263-1283.

Santos, J., and J. Stoner, 1972: Physical, chemical, and biological aspects of the Duwamish River estuary. *Physical, chemical, and biological aspects of the Duwamish River estuary***,** 1963-1967.

Schijf, J. B., and J. C. Schonfeld, 1953: Theoretical Considerations on the Motion of Salt and Fresh Water. *P MINN INT HYDR CONV***,** 321-333.

Schoellhamer, D. H., 2011: Sudden Clearing of Estuarine Waters upon Crossing the Threshold from Transport to Supply Regulation of Sediment Transport as an Erodible Sediment Pool is Depleted: San Francisco Bay, 1999. *Estuaries and coasts.*, **34,** 885-899.

Scully, M. E., and C. T. Friedrichs, 2007: Sediment pumping by tidal asymmetry in a partially mixed estuary. *Journal of geophysical research*, **112**.

Senter, C. A., K. Conn, E. , R. W. Black, N. Peterson, A. Vanderpool-Kimura, and J. Foreman, 2018: Suspended-Sediment Transport from the Green-Duwamish River to the Lower Duwamish Waterway, Seattle, Washington, 2013-17. *U.S. Department of the Interior and U.S. Geological Survey; Open-File Report 2018-2019*.

Shields, A., 1936: Mitteilungen preussi. *MITTEILUNGEN PREUSSI*.

Stenstrom, P., 2004: Hydraulics and mixing in the Hudson River estuary: A numerical model study of tidal variations during neap tide conditions. *Journal of Geophysical Research-Oceans*, **109**.

Stoner, J., 1967: Prediction of salt-water intrusion in the Duwamish River estuary, King County, Washington. *Geological Survey research.***,** D253-D255.

Templeton, W. J., and D. A. Jay, 2013: Lower Columbia River Sand Supply and Removal: Estimates of Two Sand Budget Components. *Journal of waterway, port, coastal, and ocean engineering /*, **139,** 383-392.

Torfs, H., H. Mitchener, H. Huysentruyt, and E. Toorman, 1996: Settling and consolidation of mud/sand mixtures. *Coastal engineering*, **29,** 27-45.

Traykovski, P., R. Geyer, and C. Sommerfield, 2004: Rapid sediment deposition and fine-scale strata formation in the Hudson estuary. *Journal of geophysical research.*, **109,** n/a-n/a.

Walling, D. E., 1974: Suspended sediment and solute yields from a small catchment prior to urbanization. *Fluvial Processes in Instrumented Watersheds*, **6,** 169-192.

Wellershaus, S., 1981: Turbidity maximum and mud shoaling in the Weser Estuary. *Archiv für Hydrobiologie*, **92,** 161-198.

Winterwerp, J. C., 2011: 2.15 - The Physical Analyses of Muddy Sedimentation Processes. Elsevier Inc, 311-360.

Woodruff, J. D., W. Geyer, C. K. Sommerfield, and N. W. Driscoll, 2001: Seasonal variation of sediment deposition in the Hudson River estuary. *Marine geology.*, **179,** 105-119.